NAS 1.60:1011

DEC 13 1977

NASA Technical Paper 1011

COMPLETED
ORIGINAL

Entry Dynamics of Space Shuttle Orbiter With Lateral-Directional Stability and Control Uncertainties at Supersonic and Hypersonic Speeds

Howard W. Stone and Richard W. Powell

DECEMBER 1977

NASA

104

NAS 1.60:1011

NASA Technical Paper 1011

Entry Dynamics of Space Shuttle Orbiter With Lateral-Directional Stability and Control Uncertainties at Supersonic and Hypersonic Speeds

Howard W. Stone and Richard W. Powell
Langley Research Center
Hampton, Virginia

National Aeronautics
and Space Administration

**Scientific and Technical
Information Office**

1977

SUMMARY

A six-degree-of-freedom simulation analysis was conducted to examine the effects of lateral-directional static aerodynamic stability and control uncertainties on the performance of the automatic (no manual inputs) entry-guidance and control systems of the space shuttle orbiter. To establish the acceptable boundaries of the uncertainties, the static aerodynamic characteristics were varied either by applying a multiplier to the aerodynamic parameter or by adding an increment. Two control-system modifications, (1) an increase in the yaw-jet augmentation of the rudder and (2) a change in the angle of attack for switching to an aircraft-type rudder-aileron control system, were identified that decreased the system sensitivity to off-nominal aerodynamics.

INTRODUCTION

A reusable Earth-to-orbit transportation system known as the space shuttle is being developed by the National Aeronautics and Space Administration. The space shuttle will be capable of inserting payloads of up to 29 484 kg (65 000 lb) into a near-Earth orbit, retrieving payloads already in orbit, and landing with a payload of up to 14 515 kg (32 000 lb). The space shuttle consists of an orbiter, an external fuel tank, and two solid rocket boosters (referred to hereinafter as SRB). The SRB's will be recovered after each launch for reuse. The external tank is designed for one use and is not recovered.

The orbiter will have the capability to enter the Earth's atmosphere, fly up to 2037 km (1100 n. mi.) cross range, and land horizontally. A closed-loop guidance system is being developed to provide the necessary roll-angle and angle-of-attack commands for either the automatic flight control system or a pilot-operated, augmented flight control system. A general description of the configuration and mission is given in reference 1.

The orbiter aerodynamic configuration has evolved through several design iterations, and wind-tunnel test data have been obtained at various conditions throughout the design evolution. There are data uncertainties due to variations in wind-tunnel conditions, instrumentation uncertainties, extrapolation of previous configuration data to the latest configuration, extrapolation of wind-tunnel data to flight, and evolutionary configuration changes from the present design to the flight hardware. Thus, to establish confidence in the overall system design it is necessary to know the range of uncertainties in the aerodynamic parameters that the guidance and control systems can tolerate.

With the aid of a six-degree-of-freedom simulation, an analysis was undertaken to establish the system tolerance to variations in the aerodynamic characteristics during entry. This report presents the portion of this analysis pertaining to results of the lateral-directional stability and control. The longitudinal stability and control part of this analysis is presented in reference 2.

The lateral-directional stability and control characteristics have been varied during a 600-second period of the entry during which the velocity decreases from 4267 m/sec (14 000 ft/sec) to 457.2 m/sec (1500 ft/sec) and the altitude decreases from 56.4 km (185 000 ft) to 21.3 km (70 000 ft). This 600 seconds represents the period during which the orbiter performs its most extreme maneuvers and where the aerodynamic parameters are undergoing significant changes as the vehicle decelerates from hypersonic to low-supersonic velocities and the angle of attack is lowered from its deorbit values of 34.25° to 10°. These results have been obtained without considering external disturbance sources such as winds. This simulation study considered the center of gravity to be located at the most forward operational center of gravity (65 percent of the fuselage reference length) and offset laterally by 0.0381 m (1.5 in.), the maximum expected lateral offset.

SYMBOLS

Values are given in both SI and U.S. Customary Units. The measurements were made in U.S. Customary Units.

All coefficients and vehicle rates are in the body axis system.

a_Y	side acceleration at center of gravity, m/sec^2 (ft/sec^2)
b	reference wing span, m
C_l	rolling-moment coefficient, Rolling moment/$q_\infty Sb$
C_{l_β}	effective-dihedral parameter, $\partial C_l/\partial\beta$, deg^{-1}
$C_{l_{\delta a}}$	rolling-moment coefficient due to aileron deflection, $\partial C_l/\partial\delta_a$, deg^{-1}
$C_{l_{\delta r}}$	rolling-moment coefficient due to rudder deflection, $\partial C_l/\partial\delta_r$, deg^{-1}
C_n	yawing-moment coefficient, Yawing moment/$q_\infty Sb$
C_{n_β}	directional-stability parameter, $\partial C_n/\partial\beta$, deg^{-1}
$\left(C_{n_\beta}\right)_{dyn}$	dynamic-stability parameter, $C_{n_\beta}\cos\alpha - (I_Z/I_X)C_{l_\beta}\sin\alpha$, deg^{-1}
$C_{n_{\delta a}}$	yawing-moment coefficient due to aileron deflection, $\partial C_n/\partial\delta_a$, deg^{-1}
$C_{n_{\delta r}}$	yawing-moment coefficient due to rudder deflection, $\partial C_n/\partial\delta_r$, deg^{-1}
C_Y	side-force coefficient, Side force/$q_\infty S$
C_{Y_β}	side-force coefficient due to sideslip, $\partial C_Y/\partial\beta$, deg^{-1}
$C_{Y_{\delta a}}$	side-force coefficient due to aileron deflection, $\partial C_Y/\partial\delta_a$, deg^{-1}
$C_{Y_{\delta r}}$	side-force coefficient due to rudder deflection, $\partial C_Y/\partial\delta_r$, deg^{-1}

E_Y	yaw RCS error signal
g	acceleration due to gravity (1g = 9.8 m/sec^2 (32.2 ft/sec^2))
I_{sp}	specific impulse, sec
I_X	moment of inertia about body roll axis, kg-m^2 (slug-ft^2)
I_Y	moment of inertia about body pitch axis, kg-m^2 (slug-ft^2)
I_Z	moment of inertia about body yaw axis, kg-m^2 (slug-ft^2)
I_{XZ}	product of inertia in body XZ-plane, kg-m^2 (slug-ft^2)
M	Mach number
P	period of oscillation, sec
p	roll rate, deg/sec
q_∞	free-stream dynamic pressure, Pa (lb/ft^2)
RCS	reaction control system
r	yaw rate, deg/sec
r'	$= r - (180g \sin \Phi \cos \theta)/\pi V_R$
S	reference area, m^2 (ft^2)
s	Laplace operator
$t_{1/2}$	time to half-amplitude, sec
t_2	time to double-amplitude, sec
V_R	Earth relative velocity, m/sec (ft/sec)
W	RCS fuel consumption, kg (lb)
α	angle of attack, deg
β	sideslip angle, deg
δ_a	aileron-deflection angle, (Left elevon - Right elevon)/2, deg
δ_r	rudder-deflection angle, deg
θ	pitch angle about body axis, deg
Φ	roll angle about body axis, deg

Subscripts:

c commanded value going to flight control system

i initial condition

The symbol G before any aerodynamic coefficient indicates a multiplicative gain.

The symbol Δ before any symbol indicates an increment.

DESCRIPTION OF SPACE SHUTTLE ORBITER

The physical characteristics of the space shuttle orbiter used in this study are summarized in table I. A sketch of the orbiter is shown in figure 1. The mission used was a once-around return from a 104° inclined orbit launched from the Space and Missile Test Center (formerly Western Test Range). Figure 2 depicts this entry on a world map, and figure 3 shows some of the trajectory parameters.

Guidance System

A guidance system has been designed to provide the necessary roll-angle and angle-of-attack commands either for the automatic flight control system or for pilot displays for an augmented manual flight control system. The entry guidance is designed to direct the orbiter from 121.9 km (400 000 ft), the atmospheric interface, down to 21.3 km (70 000 ft), the beginning of the landing phase. The entry down range and entry cross range are controlled through roll-angle modulation, whereas the angle of attack follows a preselected schedule. The guidance system is described in more detail in appendix A of reference 3.

Automatic Flight Control System

This control system compares the vehicle attitude with the guidance commands and directs aerodynamic control-surface deflections and the reaction control system (referred to hereinafter as RCS) jet firings. The aerodynamic control surfaces depicted in figure 1 include elevons, which are used as ailerons and elevators, a rudder with speed-brake capability, and a body flap for longitudinal trim. The RCS jets are used to supplement control about the roll, pitch, and yaw axes. The roll and pitch jets are used only during the early portion of the entry at low dynamic pressures. The jets have a nominal vacuum thrust of 3870 N (870 lb). To approximate the effects of thrust buildup with time and of thrust loss due to back pressure increases with decreasing altitude, an average thrust level of 3336 N (750 lb) and a specific impulse I_{sp} of 242 seconds for each jet were used in this study.

The lateral-directional portion of the control system operates in two basic modes. In the spacecraft mode ($\alpha > 18°$ or $M > 5$), the roll-angle com-

mand from the guidance system is directed to the yaw RCS channel, which produces a yawing rate and a small β, allowing the effective dihedral of the orbiter to generate a rolling moment. The ailerons are used for turn coordination. In the spacecraft mode the rudder is not engaged. The control system switches to the aircraft mode when $\alpha \leq 18^{\circ}$ and $M \leq 5$. In this mode the ailerons are used for roll control and the rudder, now activated with yaw-jet augmentation, is used for turn coordination. The speed-brake and body-flap deflections are based on a velocity schedule and the longitudinal center-of-gravity location, respectively. The control system is described in more detail in appendix B of reference 3.

DESCRIPTION OF SIMULATION

The automatic reentry flight dynamics simulator (hereinafter referred to as ARFDS) used for this study is an automatic (unmanned), nonlinear, six-degree-of-freedom, interactive, digital computer program developed at the NASA Langley Research Center that utilizes hardware developed for real-time simulations. (See ref. 4.) The ARFDS is controlled from a console where changes can be made between and during runs; such changes include multiplying aerodynamic parameters by constants or adding increments, modifying initial conditions, and altering system gains. This capability has been used to start at different points in the trajectory when flying with the guidance system or to bypass the guidance system and put in step commands to the control system at various conditions. The vehicle response is observed on time-history strip charts.

The nominal entry trajectory used in this study was for a once-around southerly launch from the Space and Missile Test Center requiring approximately 1852 km (1000 n. mi.) cross range. The trajectory included viscous interaction effects on aerodynamic longitudinal performance and control parameters at high altitudes.

The nominal aerodynamic characteristics used in this study are from the data set available as of June 1974. These data include longitudinal and lateral-directional static aerodynamic characteristics and damping derivatives. The nominal values of the lateral-directional stability and control derivatives at the trimmed angle of attack are shown in figure 4. Interference and cross-coupling effects from reaction control system (RCS) jets were also accounted for throughout the speed range. The actuators for the elevons and rudder were approximated by a first-order lag filter with rate and position limiting.

AERODYNAMIC PARAMETER VARIATION

In the simulations, each stability and control aerodynamic parameter has been varied by applying either multipliers or increments to the nominal values. These parameters were examined initially to identify any flow-field interdependencies which would affect how the parameters should be varied. Parameters that were considered to be dependent upon one another were varied by using either identical multipliers in a given run or slightly different multipliers. Parameters that were considered independent were varied together (i.e., the

same multiplier), oppositely, and randomly. The control parameters and the stability parameters were considered independent of one another.

The rudder derivatives $C_{l_{\delta r}}$, $C_{Y_{\delta r}}$, and $C_{n_{\delta r}}$ are approximately linearly dependent (fig. 4) and hence were varied together. In addition, $C_{l_{\delta r}}$ and $C_{n_{\delta r}}$ were varied independently to a small degree to simulate possible uncertainties in the geometric relationship. The multiplier values used in this study are shown in figure 5.

The aileron derivatives $C_{l_{\delta a}}$ and $C_{n_{\delta a}}$ are not linearly dependent (fig. 4(b)) and were varied independently by using the multiplier values shown in figure 6. The symbols with the flags attached represent an effective multiplier due to applying an increment to $C_{n_{\delta a}}$. The increment was used because the nominal value of $C_{n_{\delta a}}$ goes through zero for the nominal angle-of-attack schedule at a Mach number of about 2.5. Thus, the increment insures a variation in $C_{n_{\delta a}}$ over the entire trajectory. The effective multiplier for the purposes of figure 6 was defined as $\left(C_{n_{\delta a}} + \text{Increment}\right) \Big/ C_{n_{\delta a}}$. The symbols have been placed at the values of the effective multiplier at hypersonic speeds. The coefficient $C_{Y_{\delta a}}$ was also considered independent and was varied both by multipliers and increments.

The derivatives due to sideslip, roll C_{l_β}, and yaw C_{n_β} were considered independent in this study since these moments are due in large measure to different elements of the aerodynamic configuration. The derivatives C_{l_β} and C_{n_β} were varied by multipliers and, in addition, an increment was used to vary C_{n_β} as shown in figure 7. The coefficient C_{Y_β} was also considered independent and was varied by a multiplier.

Criteria for Satisfactory Flight

There are several criteria by which the simulation results can be judged. There are target conditions plus allowances for dispersions that have been used in the design of the entry-guidance algorithm. The targeting envelope boundaries, used in this study as a measure of the targeting capability of the system, were defined at a velocity of 457 m/sec (1500 ft/sec) to be $\pm$0.3 km (1000 ft) of altitude, $\pm$9.3 km (5 n. mi.) of range, and $\pm 1^\circ$ of flight-path angle. Another criterion results from the structural loading limits of the orbiter which requires that the normal acceleration not exceed 2.5g. In this

study this limit was never exceeded until after control was lost completely. A third criterion comes from the fact that when the lateral-directional controls are weak due to off-nominal aerodynamics, the orbiter may acquire a low-frequency roll-spiral oscillation. It is believed desirable from a ride-quality standpoint that this oscillation be limited to no more than $\pm 10^{o}$. A fourth criterion results from an increased RCS fuel expenditure due to variations in the aerodynamics during entry. The nominal entry that was used in this study requires about 181 kg (400 lb) of fuel. Winds or turbulence and dispersions can result in a significant increase in this fuel expenditure. Since the total fuel budget for entry is approximately 454 kg (1000 lb), a fuel consumption of 136 kg (300 lb) was allowed for off-nominal aerodynamics in this study.

Critical Combinations

In the simulations the multipliers or increments on the aerodynamic parameters were held constant throughout a run. The aerodynamic parameters were varied first independently, except for the rudder-effectiveness parameters, and then in combination to establish critical combinations. A critical combination is a set of off-nominal parameters such that if any one of the parameters is varied any more from the nominal, a criterion violation will occur; thus, the combination represents the worst case aerodynamic parameters that will allow the vehicle to fly satisfactorily. In some instances the variation of a parameter was reduced to allow a larger variation in other parameters in order to obtain parameter variation boundaries that are better balanced. These critical combinations determined the boundary values for each parameter.

DISCUSSION OF RESULTS

The results of this study are presented in the following sequence: effects of varying lateral-directional stability parameters, aileron effectiveness, rudder effectiveness, and combined stability and control (aileron and rudder) parameters. The final boundary values for each parameter come from the combined stability and control variations.

In the spacecraft mode the RCS fuel consumption is indicative of the overall system performance and is used to demonstrate the effects of varying the stability parameters, aileron effectiveness, and combined stability and control parameters. In the aircraft mode, the RCS fuel consumption and the required rudder deflection are used as a measure of the effects of stability and control parameter variations.

Lateral-Directional Stability

The effect on RCS fuel consumption of varying C_{l_β} is shown in figure 8. There is a significant increase in RCS fuel consumption when the multiplier GC_{l_β} is less than 0.6. The simulation results showed that the increase in

fuel consumption occurred while the vehicle was in the spacecraft mode. In this flight mode C_{l_β} was a source of the roll torque required to make a rolling maneuver; thus, reduced C_{l_β} required larger sideslip angles to generate the necessary torque. After switchover to the aircraft mode, the reduced C_{l_β} had little effect on either RCS fuel consumption or vehicle controllability even though the dynamic-stability parameter $C_{n_\beta\ dyn}$ became negative.

The effect of C_{n_β} variations on RCS fuel consumption for three values of GC_{Y_β} is shown in figure 9. Figure 4(a) shows that C_{n_β} is nominally negative (unstable) at $M \geq 1.7$, and some increase in fuel consumption is evident (fig. 9) as the instability is substantially increased $\left(GC_{n_\beta} \geq 1.8\right)$. The simulation time histories showed that neither increasing C_{n_β} to more than twice the nominal value nor decreasing the value to less than half with $GC_{Y_\beta} = 1.0$ resulted in any system stability or vehicle control problems. Also, for $0.6 \leq GC_{Y_\beta} \leq 1.4$, there is negligible effect on the fuel consumption when coupled with directional stability variation. Where increments have been used, the multiplier shown in the figure is the value at hypersonic speeds.

The results of combining the lateral and directional stability variations are illustrated in figure 10 where GC_{l_β} is plotted against RCS fuel consumption for various values of GC_{n_β} and GC_{Y_β}. The variation of GC_{l_β} alone $\left(GC_{n_\beta} = 1.0\right)$ is repeated for reference. For values of $GC_{n_\beta} < 1.0$ and for an increment of 0.0006 (circle and square symbols), the fuel consumption was similar to $GC_{n_\beta} = 1.0$; that is, increased directional stability over the range simulated had negligible effect on the overall system performance as indicated by the RCS fuel consumption. For decreased stability, an increment of -0.0006 (triangular and circular-sector symbols), and decreased effective dihedral $\left(GC_{l_\beta} < 1.0\right)$, there was a considerable increase in RCS fuel consumption. The simulation data showed that this increased fuel consumption occurred while the vehicle was in the spacecraft mode during and just after roll reversals.

Time histories of several 80-second vehicle-response simulations initiated at a Mach number of 8 are shown in figure 11. In these simulations step commands were substituted for the entry-guidance-system commands. Figure 11(a) presents the time histories with nominal aerodynamics. Since the lateral-trim condition is affected by the parameters being varied, the aileron deflection was initialized at zero in these simulations, and, thus, the activity during the first 10 seconds was to establish trim. When a step roll-reversal command

ϕ_c was given, the yaw jets fired resulting in a negative sideslip angle. The roll rate p built up to 4.5 deg/sec. The aileron initially deflected positively and then negatively to help achieve the proper balance between yawing rate and rolling rate for proper turn coordination. (See fig. B3(b) of ref. 4.) After about 20 seconds the roll-angle error was significantly reduced (ϕ was within $\pm 3^{\circ}$ of ϕ_c), the yaw jets fired to stop the yawing rate, β became positive, the aileron deflected more negatively to decrease the roll rate, and the motion was arrested. There was some continued activity as the system sought to hold the roll angle.

Time histories for $GC_{l_\beta} = 0.6$ and $GC_{n_\beta} = GC_{Y_\beta} = 1.4$ at $M_i = 8$ are shown in figure 11(b). Some ϕ oscillation after the rolling maneuver is evident with considerable aileron activity. The δ_a and p spikes after 30 seconds correspond to yaw-jet firings. Also, the β peak after 20 seconds is higher than the nonimal (fig. 11(a)). With this increased difficulty in controlling the roll angle ϕ, the fuel consumption was expected to increase as is evident in figure 10. A further decrease in effective dihedral, to $GC_{l_\beta} = 0.2$, results in much larger angles of β and noticeably higher roll rates as is shown in figure 11(c).

The bare-airframe characteristic modes with the aforementioned variations revealed that the dynamic character changed radically with the multipliers as can be seen in table II. For nominal aerodynamics and $GC_{l_\beta} = 0.6$ and $GC_{n_\beta} = 1.4$ at $M_i = 8$, $\left(C_{n_\beta}\right)_{dyn}$ was positive and there were two lateral-directional oscillations. For $GC_{l_\beta} = 0.2$ and $GC_{n_\beta} = 1.4$, $\left(C_{n_\beta}\right)_{dyn}$ was slightly negative and there were two aperiodic modes and one oscillatory mode. As C_{n_β} was further degraded $\left(GC_{n_\beta} = 2.2\right)$, the modes were made up of two oscillations or all aperiodic modes depending upon whether $\left(C_{n_\beta}\right)_{dyn}$ was positive or negative. Figures 11(d) and 11(e) show the vehicle-response simulation results for $GC_{n_\beta} = 2.2$ which are very similar to the results for $GC_{n_\beta} = 1.4$. (Compare with figs. 11(b) and 11(c).) Thus, the vehicle response appears more dependent on $\left(C_{n_\beta}\right)_{dyn}$ than on C_{n_β}.

The effects of varying GC_{Y_β} on vehicle response and the characteristic modes were also examined. Figure 11(f) shows the vehicle response for $GC_{Y_\beta} = 0.6$, and figure 11(g) shows the results for $GC_{l_\beta} = 0.2$, $GC_{n_\beta} = 2.2$, and $GC_{Y_\beta} = 0.6$. Comparing figures 11(b) and 11(g) with 11(a) and 11(e) shows that no significant effect on vehicle response was evident for decreased C_{Y_β} with both positive and negative $\left(C_{n_\beta}\right)_{dyn}$ while in the spacecraft control

mode. As expected, varying GC_{Y_β} from 0.6 to 1.4 had negligible effect on the bare-airframe mode for both positive and negative values of $\left(C_{n_\beta}\right)_{dyn}$.

Some vehicle-response simulations were also conducted at $M_i = 4$, just after switchover to the aircraft mode. The results are shown in figure 12. The nominal case (fig. 12(a)) handled the roll reversal well. Figures 12(b) to 12(d) show the effect of varying GC_{Y_β} from 0.4 to 1.8. Although the differences are not large, there is a tendency for the damping to decrease as GC_{Y_β} decreases. In the aircraft mode the control system has a side-acceleration feedback loop to the rudder which acts to decrease the yawing rate. Since $C_{n_{\delta_a}}$ was nominally negative (adverse) at a Mach number of 4 (fig. 4(b)), a positive roll-angle command resulted in a positive β which produced a negative rolling moment (negative C_{l_β}, fig. 4(a)) which was opposite to the desired. Increasing GC_Y effectively increased the feedback signal, and the yawing rate and β were more effectively controlled. With degraded effective dihedral $\left(GC_{l_\beta} = 0.2\right)$, decreased directional stability $\left(GC_{n_\beta} = 2.2\right)$, and increased C_{Y_β} $\left(GC_{Y_\beta} = 2.2\right)$, the vehicle response was satisfactory as is shown in figure 12(e). The combination had a negative $\left(C_{n_\beta}\right)_{dyn}$ with bare-airframe characteristics of four aperiodic roots, two of which were divergent and one of these doubled in about 0.7 second. (See table III.) Figure 12(f) shows that for the same combination with the nominal GC_{Y_β} there was significant difficulty handling the roll angle, which indicated a high sensitivity to C_{Y_β} when lateral-directional stability was degraded after switchover.

From the previous discussion it appears desirable to keep $\left(C_{n_\beta}\right)_{dyn}$ positive; thus, some tentative boundary values are $GC_{l_\beta} \geq 0.6$ and $GC_{n_\beta} \leq 1.4$ or $GC_{n_\beta} \leq \left(C_{n_\beta} - 0.0006\right)/C_{n_\beta}$.

Aileron Effectiveness

The effect of $C_{l_{\delta_a}}$ variation is shown in figure 13. Increased effectiveness resulted in some increased fuel consumption. Most of this increase took place while the control system was tracking small roll-angle changes in the spacecraft mode. For small changes, the aileron was producing considerably more roll torque than desired; that is, some system gains were inappropriate. The results of a vehicle-response simulation at $M_i = 8$ with $GC_{l_{\delta_a}} = 1.8$ are shown in figure 14. Comparing figures 11(a) (nominal) and 14 shows that more

aileron activity occurred during and after the roll reversal, particularly between 30 and 40 seconds, with increased aileron effectiveness.

As $GC_{l_{\delta a}}$ was decreased, figure 13 shows that the fuel consumption increased rapidly below $GC_{l_{\delta a}} = 0.4$. Again, the increased fuel consumption occurred prior to switchover. As the control authority was decreased, the system had more difficulty providing turn coordination and trimming at a given roll angle as can be seen in the vehicle-response results at $M_i = 8$ for $GC_{l_{\delta a}} = 0.4$ and 0.2 (figs. 15(a) and 15(b), respectively).

Although the increased fuel consumption occurred prior to switchover, the effects of decreased aileron effectiveness were also felt after switchover. Figure 15(c) shows the vehicle response at $M_i = 4$ for $GC_{l_{\delta a}} = 0.4$. A comparison with the nominal case (fig. 12(a)) shows that considerably larger aileron angles were required to achieve the roll reversal and an overshoot followed by long-period oscillation occurred. For $GC_{l_{\delta a}} = 0.2$ at $M_i = 4$, the severity of the overshoot and oscillation amplitude were increased; however, the entry-simulation results with the guidance commands going to the flight control system showed that the oscillation following switchover was eventually damped and the vehicle was within the targeting envelope.

Wide variations in $C_{Y_{\delta a}}$ alone had negligible effect on RCS fuel consumption, and the results are not presented herein.

The effects of varying $C_{n_{\delta a}}$ are shown in figure 16. A positive increment of 0.0004 made $C_{n_{\delta a}}$ nearly zero down to $M = 7$, and then it became positive, reaching 0.0004 at $M = 2$. An increment of -0.0002 or less made the yaw due to aileron-deflection adverse over the entire portion of the trajectory considered. (See fig. 4.) Figure 16 shows that the fuel consumption increased as $C_{n_{\delta a}}$ became more adverse. The simulation data showed that the increased fuel consumption occurred prior to switchover for $\Delta C_{n_{\delta a}} > -0.0003$ and both before and after switchover for more negative values of $\Delta C_{n_{\delta a}}$. Figure 17 shows the vehicle response at $M_i = 8$ for $\Delta C_{n_{\delta a}} = -0.0006$. Comparing figure 17 with the nominal case (fig. 11(a)) does not reveal any significant differences.

Vehicle-response results at $M_i = 4.0$ are shown in figure 18. For $\Delta C_{n_{\delta a}} = -0.0002$ the simulation results were similar to the nominal case (fig. 12(a)) except for some ϕ overshoot following the reversal. For $\Delta C_{n_{\delta a}} = -0.0004$ (fig. 18(b)) there was an oscillation following the roll

reversal which became more severe for $\Delta C_{n_{\delta a}} = -0.0006$ (fig. 18(c)). Another simulation was performed at $M_i = 4$ for $\Delta C_{n_{\delta a}} = -0.0006$ in which the command was to hold a constant roll angle (fig. 18(d)). The orbiter has a lateral center-of-gravity offset, which was not initially trimmed and resulted in a small initial disturbance. The simulation results (fig. 18(d)) show there was a significant oscillation with small values of β. For the nominal conditions at a Mach number of 4 the bare-airframe dynamic characteristics (table III) consisted of a lightly damped Dutch-roll oscillation and a long-period (133 sec) roll-spiral oscillation. This latter oscillation was damped with a time to half-amplitude $t_{1/2}$ of 31.6 seconds. With the adverse $C_{n_{\delta a}}$, an aileron deflection induced a yawing moment in the wrong direction as the aileron was trying to control roll angle and roll rate. The rudder was unable to contain the yawing motion at this level of $\Delta C_{n_{\delta a}}$, which apparently allowed the roll-spiral oscillation to be driven; that is, the control system introduced some negative damping into this oscillation.

The effects on fuel consumption of combined variation of the aileron-effectiveness parameters are shown in two plots: first as a function of $GC_{l_{\delta a}}$ (fig. 19(a)) and second as a function of $\Delta C_{n_{\delta a}}$ (fig. 19(b)). As $GC_{l_{\delta a}}$ was increased to 1.8, the change in fuel consumption with the range of $\Delta C_{n_{\delta a}}$ shown was approximately 50 kg (110 lb) ($\Delta C_{n_{\delta a}} = -0.0002$). As $GC_{l_{\delta a}}$ was decreased to 0.4, large increases in fuel consumption were evident for both more adverse and more favorable yaw due to aileron deflection.

The high fuel consumption for the more favorable yaw due to aileron deflection $\left(\Delta C_{n_{\delta a}} = 0.0004\right)$ was the result of difficulty in trimming the lateral center-of-gravity offset through the use of the yaw- and roll-jet counter circuit while in the spacecraft mode. This circuit, which "increments" the aileron for asymmetric jet firing, is described in detail in reference 3. The lateral trim was limited to $\delta_a = \pm 5^\circ$; with $GC_{l_{\delta a}} = 0.4$, this limit was reached at $M = 6$, forcing the yaw RCS to handle the excess lateral trim down to switchover. When $GC_{l_{\delta a}}$ was increased to 0.6, the maximum δ_a for trim did not exceed 5° and there was little effect on fuel consumption. When $GC_{Y_{\delta a}}$ was allowed to vary between 0.4 and 1.8 for $GC_{l_{\delta a}} = 0.4$ there was negligible effect on the results. Following switchover the vehicle handled well and negligible fuel was consumed.

The high fuel consumption for the more adverse yaw due to aileron deflection, $\Delta C_{n_{\delta a}} = -0.0002$, occurred both before and after switchover with

$GC_{l_{\delta a}} = 0.4$. Prior to switchover, the control system had some difficulty tracking the roll-angle command. Vehicle-response results at $M_i = 8$ for $GC_{l_{\delta a}} = 0.4$ and $\Delta C_{n_{\delta a}} = -0.0002$ (fig. 20(a)) show that the system had difficulty terminating the roll reversal. The increased adverse yaw coupled with more aileron deflection due to degraded effectiveness resulted in substantial sideslip angles ($\beta \approx 1.4^o$). The same parameters were simulated at $M_i = 4$ and the results are shown in figure 20(b). Although the sideslip was small, the roll-angle overshoot reached about 23^o and a severe oscillation ensued which had not damped out after 80 seconds. The entry simulations, using the guidance commands, indicated that an oscillation occurred around $M = 4$ following switchover with small commanded roll-angle changes. The oscillation did damp out, however, as Mach number and angle of attack decreased but the vehicle missed the target envelope slightly. For $GC_{Y_{\delta a}} = 1.8$, fuel consumption decreased; whereas for $GC_{Y_{\delta a}} = 0.4$ the fuel consumption increased slightly. Vehicle-response results at $M_i = 8$ and $M_i = 4$ did not show any significant differences between $GC_{Y_{\delta a}} = 1.8$ and 1.4.

The foregoing discussion has suggested a tentative lower boundary value for $GC_{l_{\delta a}}$, namely, 0.6. Smaller values have been shown to result in questionable flight performance: for example, the lack of aerodynamic lateral trim around a Mach number of 6 for $\alpha > 18^o$, and roll-angle overshoot and oscillation problems for $\alpha < 18^o$. By using this possible boundary value, the increment on $C_{n_{\delta a}}$ was varied (fig. 19(b)). A large increase in fuel consumption is evident for a positive increment of 0.0006. The reason for this increase is again a lack of aerodynamic lateral trim, because the $\delta_a = -5^o$ limit was reached around a Mach number of 6. Thus, an increment of 0.0004 was selected as a tentative upper boundary value for $C_{n_{\delta a}}$. The negative increment on $C_{n_{\delta a}}$ of -0.0004 resulted in ϕ errors greater than 40^o after switchover and resulted in poor targeting. An increment of -0.0003 resulted in ϕ errors of 14^o with a large amount of RCS fuel consumed after switchover. Therefore, a negative boundary value for $C_{n_{\delta a}}$ after switchover was tentatively selected to be -0.0002.

Rudder Effectiveness

The rudder effectiveness (applicable only after switchover) was varied by using multipliers. An indicator of the impact of rudder-effectiveness variation is the rudder deflection required to coordinate a roll maneuver. This rudder deflection is shown in figure 21. As rudder-derivative multipliers were varied from 0.4 to 1.8 the rudder deflection for turn coordination varied linearly and the fuel consumed by the yaw jets augmenting the rudder was negligible. At multipliers of 0.2 and less, the augmentation due to the yaw RCS was adequate to maintain sufficient control to achieve the target conditions. With

four jets per side (the maximum available), the RCS propellant consumed following the guidance-commanded roll angle, including roll reversals between $M = 4$ and $M = 1.5$, was 45 kg (100 lb), 83 kg (183 lb), and 243 kg (536 lb) for multiplier values of 0.2, 0.1, and 0.0, respectively. With two jets per side, control was maintained with multipliers of 0.1, but with a cost of 86 kg 190 lb) of propellant. Thus, while control is maintained, the fuel consumption is heavy for multipliers less than 0.4.

Combined Stability and Control Effects

The results discussed up to this point can be summarized as follows:

(1) Prior to switchover to the aircraft mode, a $C_{n_{\delta a}}$ increment greater than 0.0004 with $GC_{l_{\delta a}} \leq 0.6$ made lateral trim with the ailerons alone impossible with a lateral center-of-gravity offset of 0.0381 m (1.5 in.) and required heavy use of the yaw jets.

(2) After switchover, roll-angle control problems became severe with $C_{n_{\delta a}}$ increments less than -0.0002 with $GC_{l_{\delta a}} \leq 0.6$.

(3) Increasing $GC_{l_{\delta a}}$ and/or the rudder multipliers ($GC_{n_{\delta r}}$, $GC_{l_{\delta r}}$, and $GC_{Y_{\delta r}}$) to 1.8 presented no problem. Values of $GC_{Y_{\delta a}}$ from 0.4 to 1.8 did not significantly affect system performance.

(4) Rudder multipliers less than 0.4 required significant yaw RCS fuel consumption for augmentation to maintain control.

(5) Negative values of $\left(C_{n_\beta}\right)_{dyn}$ tend to produce ϕ control problems after switchover with $GC_{Y_\beta} \leq 1.0$. Thus, tentative boundary values are $GC_{l_\beta} > 0.6$ and $GC_{n_\beta} \leq 1.4$ or $\Delta C_{n_\beta} \geq -0.0006$ (whichever is greater). This results in a near-zero value of $\left(C_{n_\beta}\right)_{dyn}$ at $M \leq 4$. A value of $GC_{Y_\beta} \geq 0.6$ was assumed as a tentative boundary value.

With this background, the stability and control characteristics were combined to determine the critical combinations that would result in the boundary values for each aerodynamic parameter. To determine the critical combinations, some previously determined apparent boundary values were held and other parameters were varied until the critical combinations were determined. Therefore, several of the aforementioned values were assumed to be boundary values while the rudder derivatives and negative increments on $C_{n_{\delta a}}$ were varied. The assumed boundary values were $GC_{l_{\delta a}} = 0.6$, $GC_{l_\beta} = 0.6$, and $\Delta C_{n_\beta} = -0.0006$.

The RCS fuel consumption for $C_{n_{\delta a}} = -0.0002$ and -0.0003 is shown in figure 22 as a function of the rudder multipliers. Variation of the rudder multipliers did not change the fuel consumption prior to switchover since the rudder was not used in this flight regime. Thus, figure 22 shows that for values of the rudder multipliers greater than 1.0, the fuel consumption after switchover was unchanged or reduced. The simulation data also showed that control was improved with increased rudder effectiveness. Thus, for the purposes of this study, rudder multipliers of 1.8 have been assumed to be the upper boundary value. This level is believed sufficient to encompass the aerodynamic uncertainties.

As rudder effectiveness was decreased (rudder multipliers less than 1.0) with the aforementioned assumed boundary values, the fuel consumption after switchover increased significantly (fig. 22). For rudder multipliers of 0.6, this RCS fuel-consumption limit specified earlier as 135 kg (approximately 300 lb) was exceeded for $\Delta C_{n_{\delta a}} = -0.0003$ and was close to the limit for $\Delta C_{n_{\delta a}} = 0.0002$. The reason for the large fuel consumption in these cases is shown in figure 23(a). The results at $M_i = 4$ for a constant $\phi_c = -30^\circ$ show that an apparent divergent oscillation occurs. With $GC_{l_\beta} = 0.6$ and $\Delta C_{n_\beta} = -0.0006$, $\left(C_{n_\beta}\right)_{dyn}$ is zero or slightly negative for $M < 4$ and the bare-airframe characteristic modes consisted of a Dutch-roll and a roll-spiral oscillation. The roll-spiral oscillation was divergent with a time to double of 41.1 seconds. (See table III.) In spite of this condition, the system handled the instability and targeted properly in entry simulations where the system followed the guidance command. Figure 23(b) shows the vehicle-response results with the same aerodynamics but commanding a roll reversal. The oscillation following the reversal does not appear to be divergent, but it is larger in amplitude than the assumed limits of $\pm 10^\circ$ specified earlier. This should result in a definition of a smaller value for $\Delta C_{n_{\delta a}}$ or require larger rudder multipliers as a boundary value; however, later discussion will demonstrate control-system software modifications that reduce these oscillations to within the specified limits.

A further look at the effects of $\Delta C_{n_{\delta a}}$ is shown in figure 24 where the increment was varied from -0.0004 to 0.0004. It has been shown previously that $GC_{l_{\delta a}}$ must be greater than 0.6 and $\Delta C_{n_{\delta a}}$ must be less than 0.0004 because of aerodynamic lateral-trim limits prior to switchover. Figure 24 shows that several parameter combinations exceed the 135 kg (300 lb) fuel-consumption limit with $\Delta C_{n_{\delta a}} < 0$. On the basis of this limit and with $GC_{l_{\delta a}} = 0.6$, $GC_{l_\beta} = 0.6$, and $\Delta C_{n_\beta} = -0.0006$, apparent boundary values of $\Delta C_{n_{\delta a}}$ and the rudder multipliers are -0.0002 and 0.6, respectively.

The entry-simulation results showed that some combinations with large overall fuel consumption performed adequately prior to switchover. The combination $GC_{l_{\delta a}} = GC_{l_\beta} = 0.6$, $C_{n_\beta} = -0.0006$, and $C_{n_{\delta a}} = -0.0004$ performed adequately and consumed about 100 kg (221 lb) of fuel prior to switchover, but the total fuel consumption with rudder multipliers at 0.6 was more than 250 kg (551 lb). The vehicle-response results for this combination at $M_i = 8$ shown in figure 25 indicate that although β was large, the roll-reversal performance was satisfactory. Thus, the system was more tolerant of adverse $C_{n_{\delta a}}$ prior to switchover than afterwards.

Finally, the effects of C_{l_β} and C_{n_β} are shown in figure 26. For $\Delta C_{n_\beta} = -0.0006$, fuel consumption was high for all values of GC_{l_β} and the combination of parameters shown. As GC_{l_β} was decreased to 0.4, the fuel consumption increased to the limiting value. As GC_{l_β} was increased, the total fuel consumption decreased, but the fuel consumed after switchover increased. With the adverse yaw due to aileron deflection tending to yaw the orbiter out of the turn, more roll torque out of the turn was generated by the increased positive dihedral effect, thus requiring more aileron deflection and more yaw-jet firing. Figure 27 shows the vehicle-response results for $GC_{l_\beta} = 1.4$. Figures 27(a) and (b) show the roll-reversal and roll-angle-hold results, respectively, at $M_i = 4$. With these off-nominal aerodynamics there was considerable oscillation and control activity, more than was acceptable. The bare-airframe characteristics for $GC_{l_\beta} = 1.4$ and $\Delta C_{n_\beta} = 0.0006$ consisted of two rather well-behaved oscillatory roots as $\left(C_{n_\beta}\right)_{dyn}$ was positive. Nevertheless, with degraded control authority and adverse yaw due to aileron deflection the motions were unacceptable. Figure 27(c) shows the vehicle-response results for $GC_{l_\beta} = 1.4$ and the aforementioned degraded characteristics for $M_i = 8$. Although β went beyond 1°, no undue oscillations occurred. Once again, it appears that the system tolerance to off-nominal aerodynamics and the boundary values was dependent upon whether switchover had occurred. Figure 26 also indicates little improvement was gained by increasing ΔC_{n_β} to -0.0005 in terms of fuel consumption; however, increasing ΔC_{n_β} to 0.0006 had a significantly favorable effect on the system.

Up to this point in establishing the flyable combinations of parameters, the side-force derivatives C_{Y_β} and $C_{Y_{\delta a}}$ have been assumed to be nominal. Since the effects of C_{Y_β} discussed earlier show decreased damping with decreased C_{Y_β} after switchover, GC_{Y_β} was varied primarily for the combinations that result in ϕ control difficulties. A vehicle-response simulation

at $M_i = 4$ (no figure) with $GC_{l_\beta} = 1.4$, $\Delta C_{n_\beta} = 0.0006$, $GC_{l_{\delta a}} = 0.6$, $\Delta C_{n_{\delta a}} = -0.0002$, $GC_{n_{\delta r}} = GC_{l_{\delta r}} = GC_{Y_{\delta r}} = 0.6$, and $GC_{Y_\beta} = 0.9$ resulted in a severe roll-angle oscillation with a roll-angle overshoot of 40°. The oscillation after the roll reversal was still severe with $GC_{n_{\delta r}} = GC_{l_{\delta r}} = GC_{Y_{\delta r}} = 0.7$. Thus, to accommodate variations in C_{Y_β} less than nominal requires several other parameters to be upgraded. Figure 28(a) presents the vehicle-response results at $M_i = 4$ for $GC_{l_\beta} = 1.3$, $GC_{l_{\delta a}} = 0.7$, $GC_{Y_\beta} = 0.7$, $\Delta C_{n_{\delta a}} = -0.0002$, $\Delta C_{n_\beta} = -0.0006$, and $GC_{n_{\delta r}} = GC_{l_{\delta r}} = GC_{Y_{\delta r}} = 0.7$. The response was very similar to that shown in figure 27(a). These results were not satisfactory, and further parameter changes would be required or appropriate control-system software modifications should be incorporated as will be shown later. The vehicle-response results at $M_i = 8$ for the aforementioned combination, shown in figure 28(b), are satisfactory. Decreasing GC_{l_β} from 1.3 to 0.6 with this combination improved the roll-response results. (See figs. 28(c) and (d).) A value of GC_{Y_β} of 1.8 significantly improved the flight characteristics as is shown in figure 29.

The nominal value of $C_{Y_{\delta a}}$ changes sign as the entry Mach number varies (see fig. 4(d)), and, thus, several entries were simulated by using increments in $C_{Y_{\delta a}}$ in combination with the other parameter variations that gave the poorest system performance. An increment range from -0.0004 to 0.0006 in $C_{Y_{\delta a}}$ had negligible effect on the system prior to switchover for $GC_{l_\beta} = 0.6$ or 1.3, $\Delta C_{n_\beta} = -0.0006$, $GC_{Y_\beta} = 0.7$, $GC_{l_{\delta a}} = 0.7$, and $\Delta C_{n_{\delta a}} = -0.0002$. After switchover with $GC_{n_{\delta r}} = GC_{l_{\delta r}} = GC_{Y_{\delta r}} = 0.7$, an increment of -0.0006 in $C_{Y_{\delta a}}$ improved control and fuel consumption as the side-force feedback (see earlier discussion of GC_{Y_β}) caused the rudder to maintain tighter control on β. An increment of only 0.0001 in $C_{Y_{\delta a}}$, however, resulted in increased fuel consumption and degraded controllability. The vehicle-response results for a roll-angle step command at $M_i = 4$ for $\Delta C_{Y_{\delta a}} = 0.0001$ are shown in figures 30(a) and (b) for $GC_{l_\beta} = 1.3$ and 0.6, respectively. Comparing these figures with figures 28(a) and (c) shows that control is degraded, particularly for $GC_{l_\beta} = 1.3$. Figures 30(c) and (d) are the vehicle-response results for

$\Delta C_{Y_{\delta a}} = -0.0004$ for $GC_{l_\beta} = 1.3$ and 0.6, respectively. The controllability improvement is very evident. (Compare with figs. 28(a) and (c).)

The vehicle-response results at $M_1 = 8$ for various combinations of $\Delta C_{Y_{\delta a}}$ and GC_{l_β} are shown in figure 31. Comparing appropriate figures with figures 28(b) and (d) shows that there is no apparent effect of $\Delta C_{Y_{\delta a}}$ on the hypersonic vehicle response.

The effect of decreased C_{Y_β} (with $GC_{Y_\beta} = 0.7$) and an increment range of -0.0004 to 0.0006 in $C_{Y_{\delta a}}$ was included with positive increments in $C_{n_{\delta a}}$ and C_{n_β} prior to switchover. The δ_a trim limit was approached with a combination of $GC_{l_{\delta a}} = 0.7$, $GC_{l_\beta} = 0.6$, $GC_{Y_\beta} = 0.7$, $\Delta C_{n_{\delta a}} = 0.00035$, $\Delta C_{n_\beta} = 0.0005$, and a range of $\Delta C_{Y_{\delta a}}$ from -0.0004 to 0.0006.

Figure 32 shows the block diagram of the yaw jets for augmenting the rudder after switchover and also two modified schedules designed to increase this augmentation. Both of these modifications were examined in simulations with the aforementioned parameter combinations. The worst case in terms of roll-angle control is shown in figure 30(a). Figure 33(a) shows the same combination with yaw-jet-augmentation modification I. The amplitude of the roll-angle oscillation following the commanded roll reversal was significantly reduced but still severe. Figure 33(b) shows the results for the aforementioned and other parameter combinations with yaw-jet-augmentation modification II. The vehicle overshot initially, but after 40 seconds the roll angle was within a few degrees of the commanded value. Notice that the system had excellent control of β. The control system with modification II was able to handle a larger increment in $C_{Y_{\delta a}}$ satisfactorily $\left(\Delta C_{Y_{\delta a}} = 0.0003\right)$ as figure 34 shows. Larger increments, however, resulted in poorer control of β and, thus, the increment $\Delta C_{Y_{\delta a}} = 0.0003$ was an upper limit for these combinations. Both of these yaw-jet channel modifications had either a negligible effect or reduced the fuel consumption for the entry simulations with these combinations. The fuel consumption for the nominal aerodynamics with modification II was slightly higher than without modification II.

Another system modification examined was to delay the switch to the aircraft mode until $\alpha = 15^\circ$ which occurred at about $M = 3.1$. The roll-reversal response for the worst combination with $\Delta C_{Y_{\delta a}} = 0.0001$ and 0.0003 at $M = 3.1$ is shown in figures 35(a) and (b), respectively. There was no oscillation following the reversal; β was controlled, but the response to the command was a little sluggish for $\Delta C_{Y_{\delta a}} = 0.0001$. The effect of the adverse feedback to the rudder was evident for $\Delta C_{Y_{\delta a}} = 0.0003$ as there was difficulty establishing the initial roll rate.

The critical combinations of aerodynamic parameters resulting from the forgoing analyses, including the benefits of yaw-jet-augmentation modification II, are summarized in table IV.

The upper boundary for $GC_{l_{\delta a}}$, GC_{Y_β}, and the rudder derivatives was 1.8 since these parameters were not examined above this value. Generally, the system response and fuel consumption improved as this value was approached. The upper boundaries for $\Delta C_{n_{\delta a}}$ and ΔC_{n_β} were critical prior to switchover because of the aileron trim limit. Also, the lower boundary for $\Delta C_{n_{\delta a}}$ was reduced to -0.0004 and the upper boundary for $\Delta C_{Y_{\delta a}}$ was increased to 0.0006 with the other parameters in a worst combination prior to switchover. This combination (see bottom line of table IV) resulted in a fuel consumption down to $M = 4$ of about 91 kg (200 lb) more than the nominal case. The vehicle-response results at $M_j = 8$ for this combination are shown in figure 36. The entry simulations also showed that the aforementioned combinations would meet the targeting envelope requirements. These combinations are presented as boundary values in figures 37 to 40.

SUMMARY OF RESULTS

A six-degree-of-freedom simulation analysis was conducted to examine the effects of lateral-directional static aerodynamic stability and control uncertainties on the performance of the automatic (no manual inputs) entry-guidance and control systems of the space shuttle orbiter with a small lateral center-of-gravity offset. To establish the acceptable boundaries of the uncertainties, the static aerodynamic characteristics were varied either by applying a multiplier to the aerodynamic parameter or by adding an increment. Two control-system modifications were identified that decrease the sensitivity to off-nominal aerodynamics, and they are as follows:

1. Increase the yaw-reaction control-system augmentation of the rudder.

2. Delay the control-system switching so that it occurs at an angle of attack of 15° instead of the 18° currently proposed.

With increased yaw-reaction control-system augmentation, the space shuttle orbiter was found to fly satisfactorily within the following boundaries:

1. The rudder characteristics (yaw due to rudder deflection, roll due to rudder deflection, and side force due to rudder deflection) can be reduced to 0.70 or increased to 1.8 times their nominal values.

2. The roll due to aileron deflection can be from 0.7 to 1.8 times its nominal value.

3. The yaw due to aileron deflection can be incremented by values between -0.0002 (-0.0004 until the angle of attack is reduced to 18°) and 0.00035.

4. The effective dihedral (roll due to sideslip) can be between 0.6 and 1.3 times its nominal value.

5. The directional stability (yaw due to sideslip) can be incremented by values between -0.0006 and 0.0005.

6. The side force due to sideslip can be between 0.7 and 1.8 times its nominal value.

7. The side force due to aileron deflection can be incremented by values between -0.0004 and 0.0003 (0.0006 until the angle of attack is reduced to 18°).

Langley Research Center
National Aeronautics and Space Administration
Hampton, VA 23665
September 30, 1977

REFERENCES

1. Malkin, M. S.: Space Shuttle/The New Baseline. Astronaut. & Aeronaut., vol. 12, no. 1, Jan. 1974, pp. 62-68.

2. Stone, Howard W.; and Powell, Richard W.: Entry Dynamics of Space Shuttle Orbiter With Longitudinal Stability and Control Uncertainties at Supersonic and Hypersonic Speeds. NASA TP-1084, 1977.

3. Powell, Richard W.; Stone, Howard W.; and Rowell, Lawrence F.: Effects of Modifications to the Space Shuttle Entry Guidance and Control Systems. NASA TN D-8273, 1976.

4. Kaylor, Jack T.; Rowell, Lawrence F.; and Powell, Richard W.: A Real-Time Digital Computer Program for the Simulation of Automatic Spacecraft Reentries. NASA TM X-3496, 1977.

TABLE I.- PHYSICAL CHARACTERISTICS OF SPACE SHUTTLE ORBITER

Mass properties:	
Mass, kg (lb)	83 001 (182 986)
Moments of inertia:	
I_X, kg-m^2 (slug-ft^2)	1 029 066 (759 000)
I_Y, kg-m^2 (slug-ft^2)	7 816 290 (5 765 000)
I_Z, kg-m^2 (slug-ft^2)	8 015 596 (5 912 000)
I_{XZ}, kg-m^2 (slug-ft^2)	177 612 (131 000)
Wing:	
Reference area, m^2 (ft^2)	249.91 (2690.0)
Chord, m (ft)	12.06 (39.57)
Span, m (ft)	23.79 (78.06)
Elevon:	
Reference area, m^2 (ft^2)	19.51 (210.0)
Chord, m (ft)	2.30 (7.56)
Rudder.	
Reference area, m^2 (ft^2)	9.30 (100.15)
Chord, m (ft)	1.86 (6.1)
Body flap:	
Reference area, m^2 (ft^2)	12.54 (135.0)
Chord, m (ft)	2.06 (6.75)

TABLE II.- BARE-AIRFRAME CHARACTERISTICS AT M = 8

GC_{l_β}	GC_{n_β}	$(C_{n_\beta})_{dyn}$	Oscillatory modes		Aperiodic modes			
			1	2	1	2	3	4
1.0	1.0	0.35	P = 4.7 sec $t_{1/2}$ = 30.1 sec	P = 835 sec $t_{1/2}$ = 87.5 sec				
.6	1.4	.16	P = 6.9 sec $t_{1/2}$ = 25.4 sec	P = 454 sec $t_{1/2}$ = 184 sec				
.2	1.4	-.006	P = 33.4 sec $t_{1/2}$ = 5.2 sec ϕ/β = 29		t_2 = 66.7 sec	t_2 = 3.6 sec		
.6	2.2	.10	P = 8.3 sec $t_{1/2}$ = 19.7 sec	P = 334 sec t_2 = 166 sec				
.2	2.2	-.06			t_2 = 108 sec	$t_{1/2}$ = 7.8 sec	t_2 = 1.3 sec	$t_{1/2}$ = 1.4 sec

TABLE III.- BARE-AIRFRAME CHARACTERISTICS AT M = 4

GC_{l_β}	GC_{n_β}	$(C_{n_\beta})_{dyn}$	Oscillatory modes		Aperiodic modes			
			1	2	1	2	3	4
1.0	1.0	0.11	P = 7.2 sec $t_{1/2}$ = 9.8 sec	p = 133 sec $t_{1/2}$ = 31.6 sec				
.6	1.4	.0005	P = 23.1 sec $t_{1/2}$ = 2.9 sec ϕ/β = 31.5		t_2 = 15.4 sec	t_2 = 2.7 sec		
.2	1.4	-.08			t_2 = 63.5 sec	$t_{1/2}$ = 4.6 sec	t_2 = 0.98 sec	$t_{1/2}$ = 0.93 sec
.6	2.2	-.07			t_2 = 37.9 sec	$t_{1/2}$ = 3.3 sec	t_2 = 1.0 sec	$t_{1/2}$ = 1.0 sec
.2	2.2	-.14			t_2 = 82.8 sec	$t_{1/2}$ = 5.1 sec	t_2 = 0.71 sec	$t_{1/2}$ = 1.0 sec
1.4	ΔC_{n_β} = -0.0006	.19	P = 5.6 sec $t_{1/2}$ = 10.9 sec	P = 174 sec $t_{1/2}$ = 24.3 sec				
.6	ΔC_{n_β} = -0.0006	.035	P = 13.2 sec $t_{1/2}$ = 6.3 sec	P = 84.3 sec t_2 = 41.1 sec				

TABLE IV.- CRITICAL COMBINATIONS

$GC_{l_{\delta a}}$	$\Delta C_{n_{\delta a}}$	$\Delta C_{Y_{\delta a}}$	$GC_{l_{\delta r}} = GC_{n_{\delta r}} = GC_{Y_{\delta r}}$	$GC_{l_{\beta}}$	$\Delta C_{n_{\beta}}$	$GC_{Y_{\beta}}$
0.7	-0.0002	0.0003	0.7	1.3	-0.0006	0.7
.7	-.0002	.0003	.7	.6	-.0006	.7
.7	-.0002	-.0004	.7	1.3	-.0006	.7
.7	-.0002	-.0004	.7	.6	-.0006	.7
[a].7	.00035	.0006		.6	.0005	.7
[a].7	.00035	-.0004		.6	.0005	.7
[a].7	-.0004	.0006		.6	-.0006	.7

[a]Before switchover only.

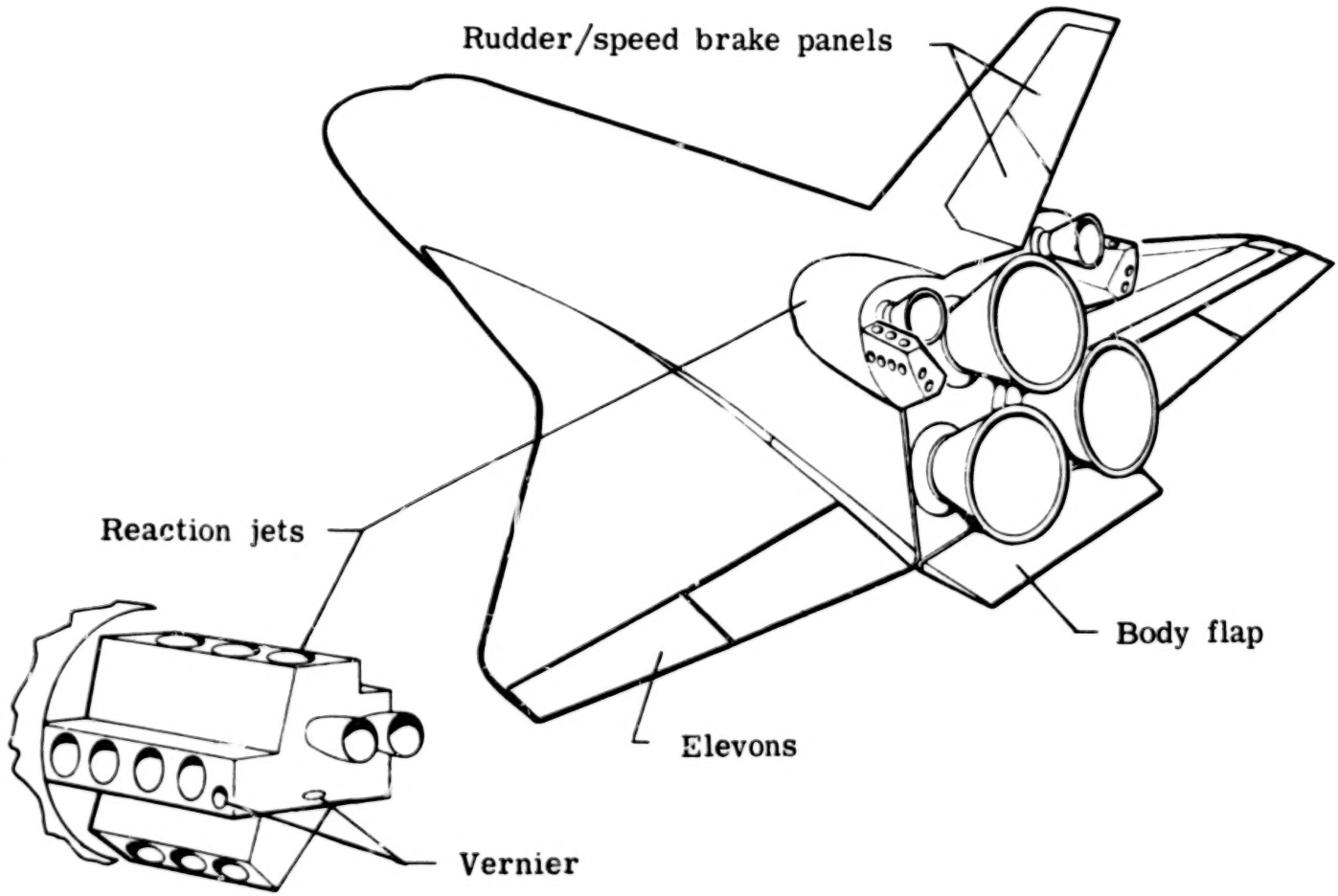

Figure 1.- Sketch of space shuttle orbiter.

Figure 2.- Entry of space shuttle orbiter.

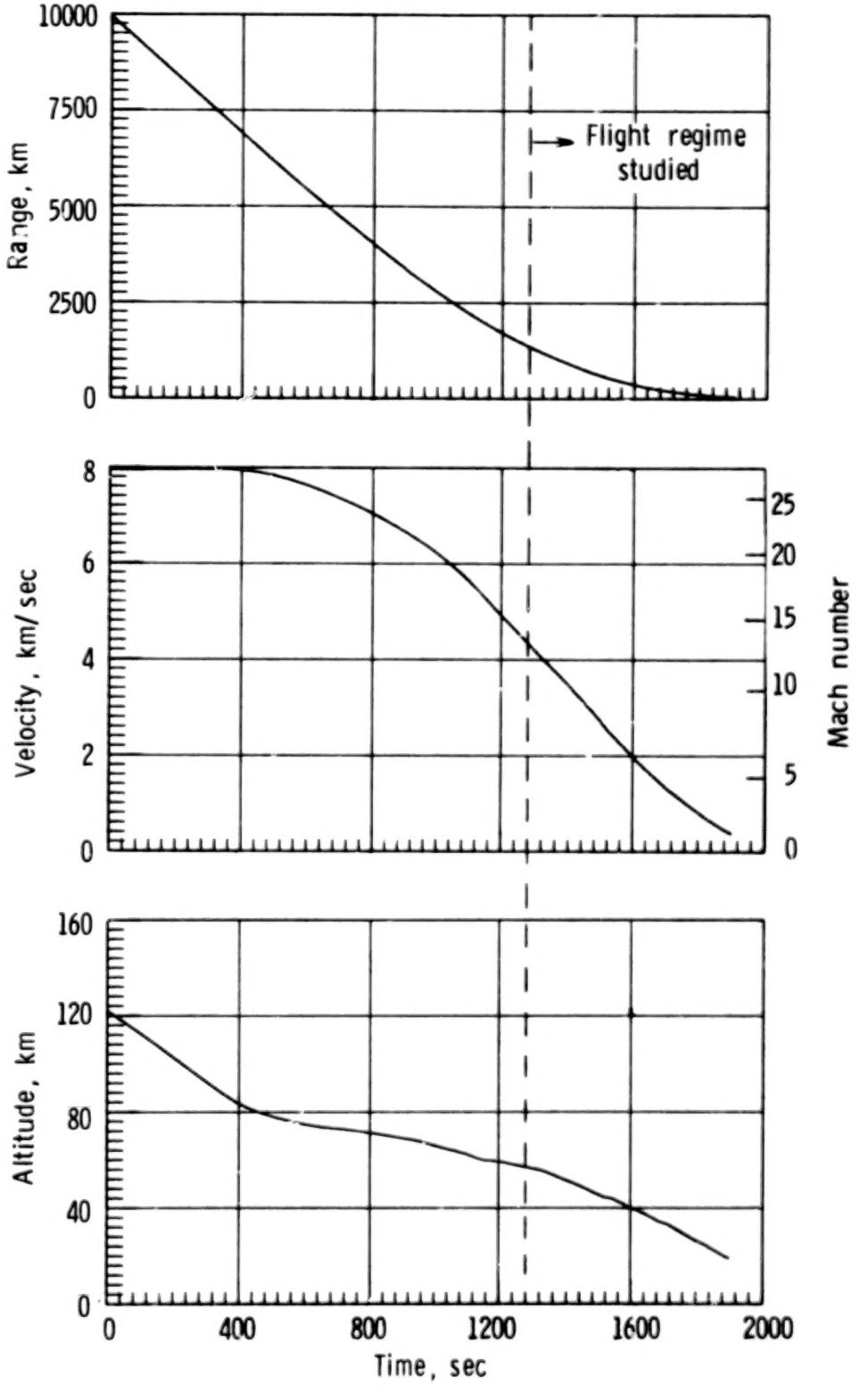

Figure 3.- Entry trajectory parameters of space shuttle orbiter.

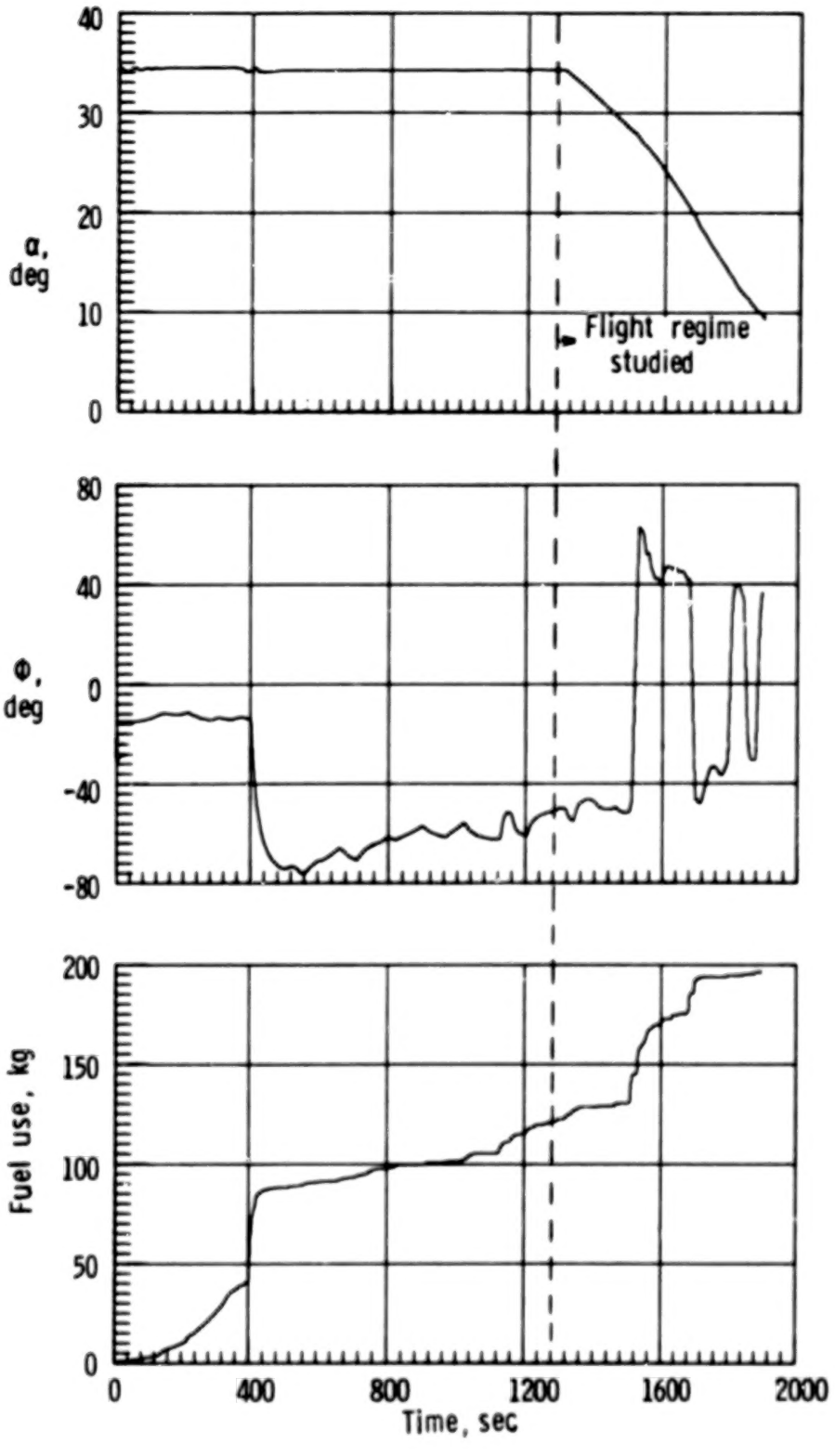

Figure 3.- Concluded.

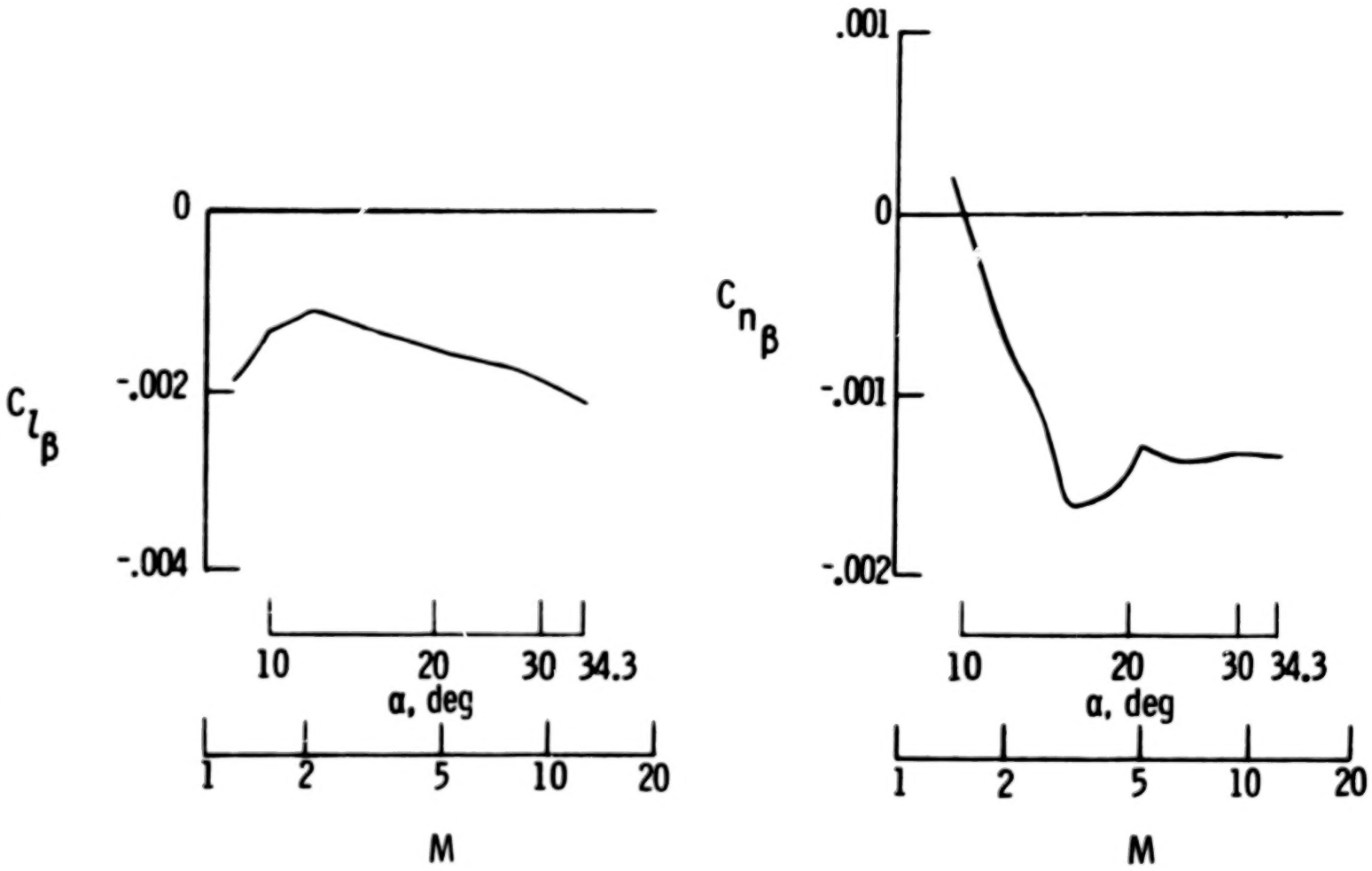

(a) Stability derivatives.

Figure 4.- Nominal lateral-directional stability and control derivatives of space shuttle orbiter.

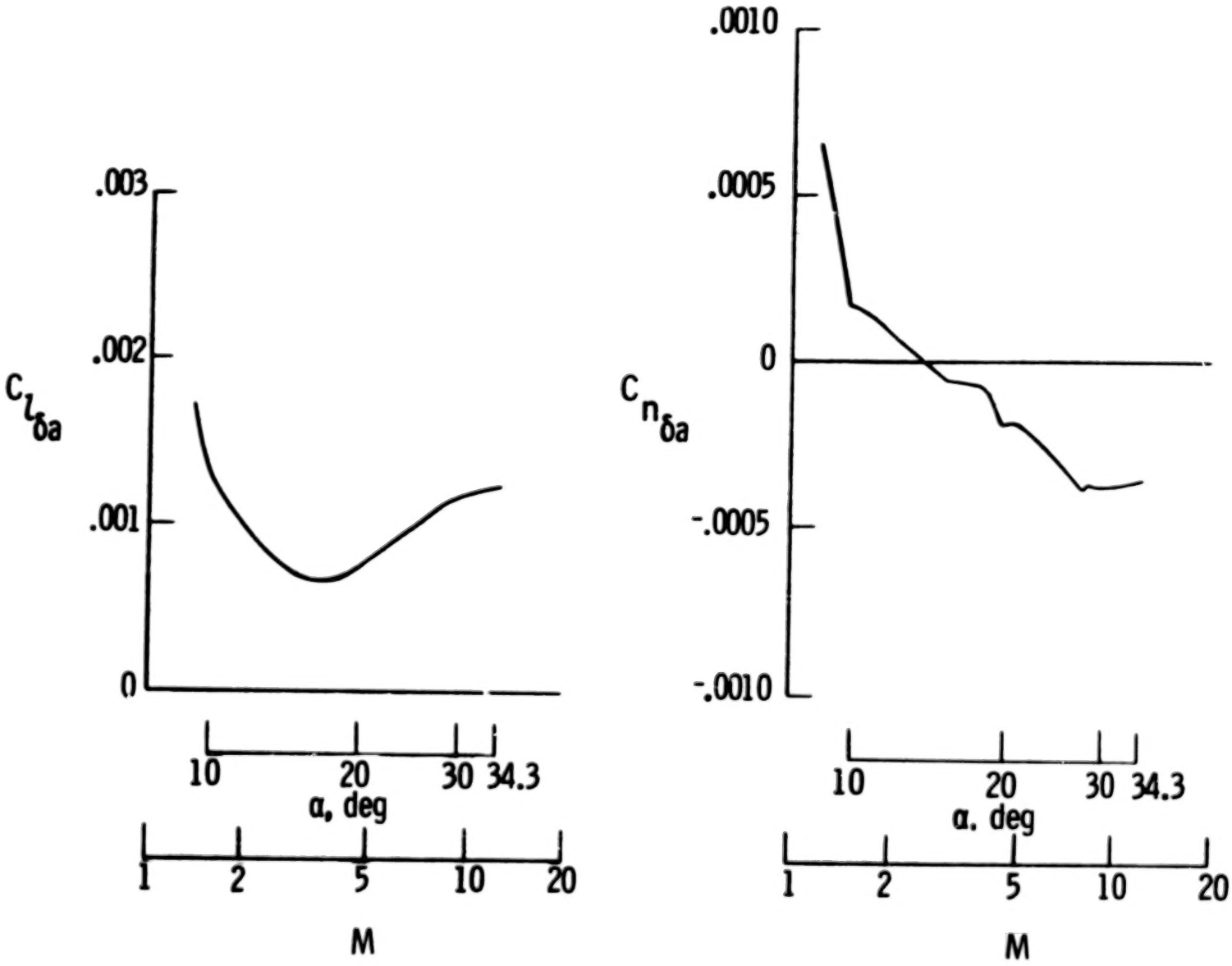

(b) Aileron derivatives.

Figure 4.- Continued.

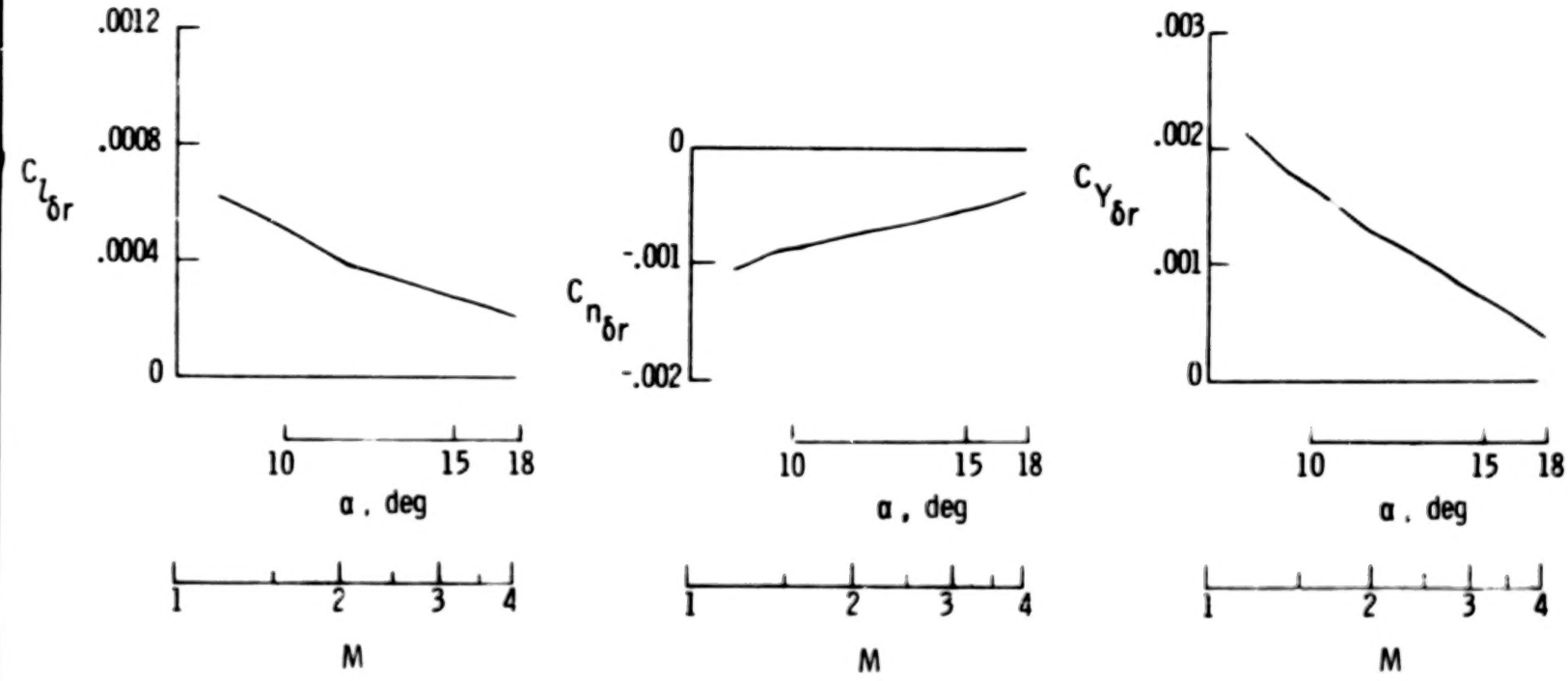

(c) Rudder derivatives.

Figure 4.- Continued.

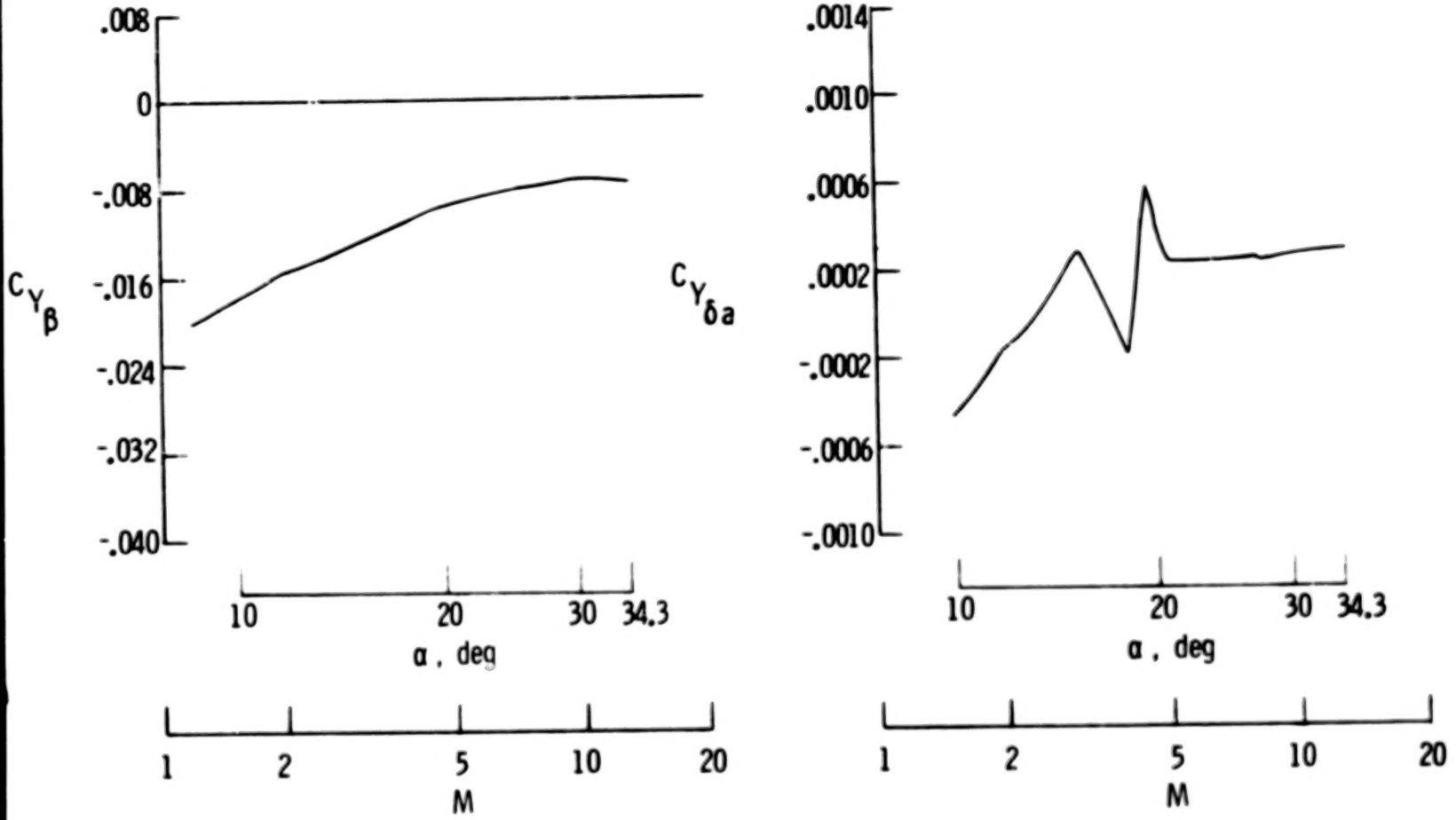

(d) Side force due to β and δ_a.

Figure 4.- Concluded.

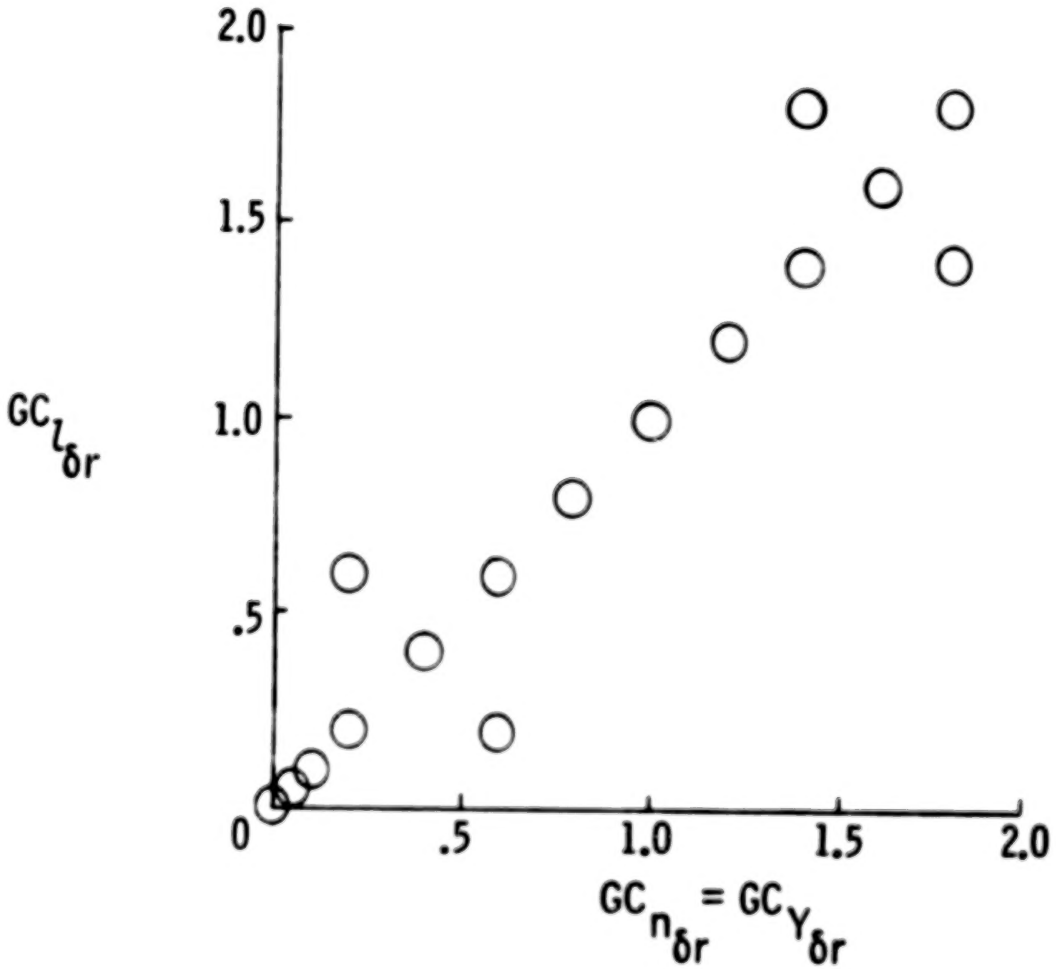

Figure 5.- Rudder-effectiveness variations.

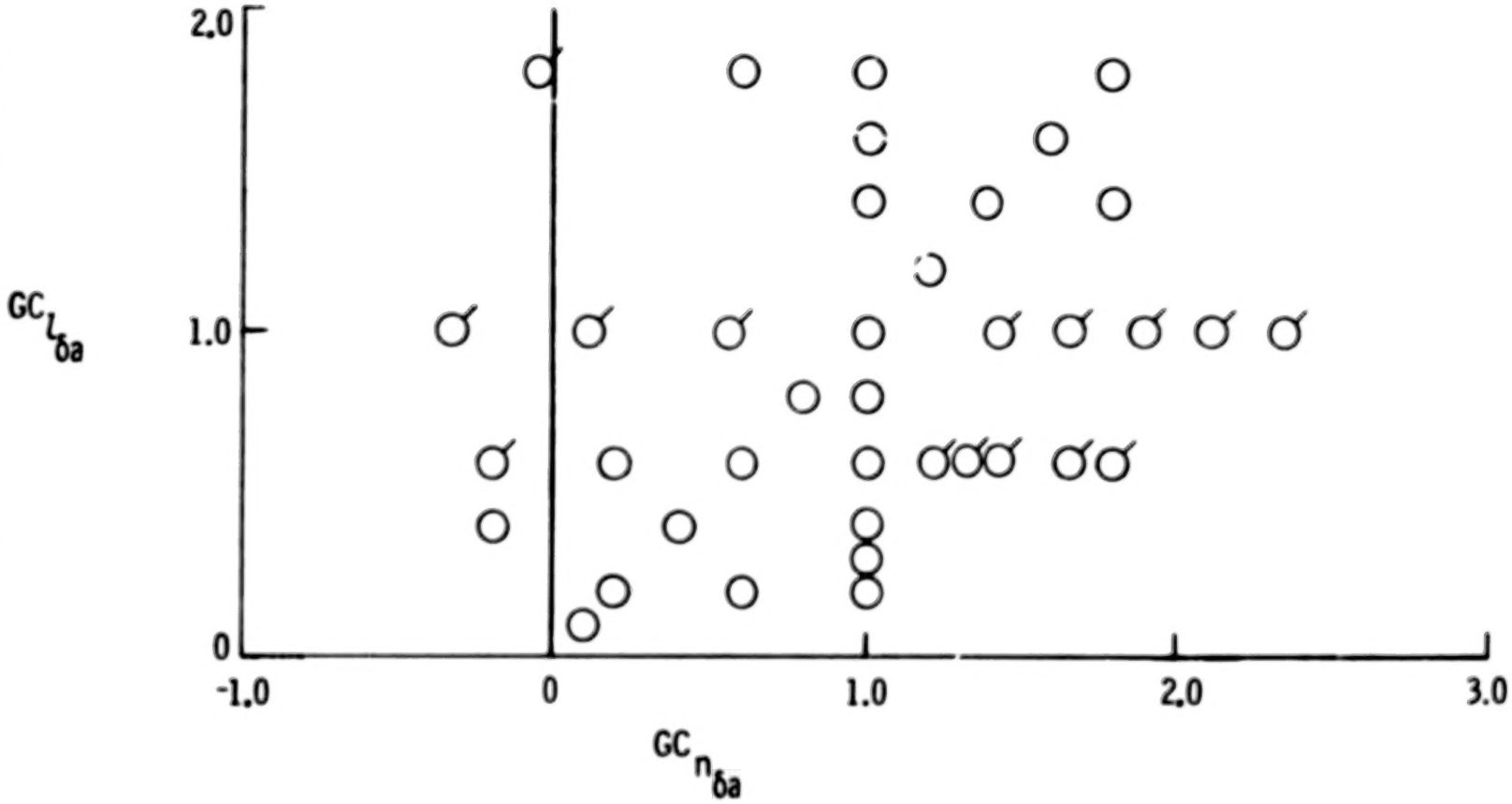

Figure 6.- Aileron-effectiveness variations. Flagged symbols denote $GC_{n_{\delta a}} = \frac{C_{n_{\delta a}} + \Delta C_{n_{\delta a}}}{C_{n_{\delta a}}}$.

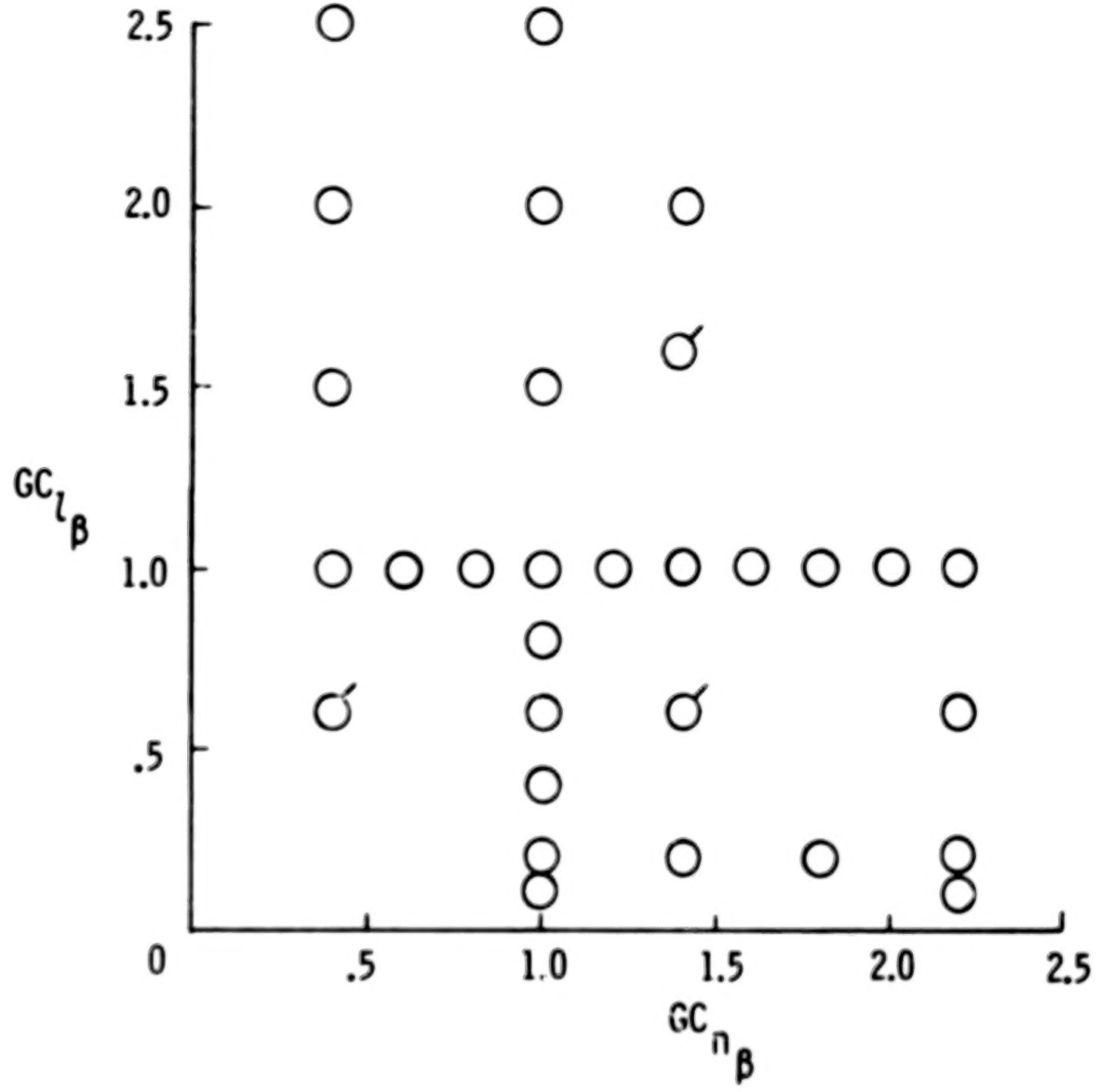

Figure 7.- Lateral-directional stability variations. Flagged symbols denote $GC_{n_\beta} = \frac{C_{n_\beta} + \Delta C_{n_\beta}}{C_{n_\beta}}$.

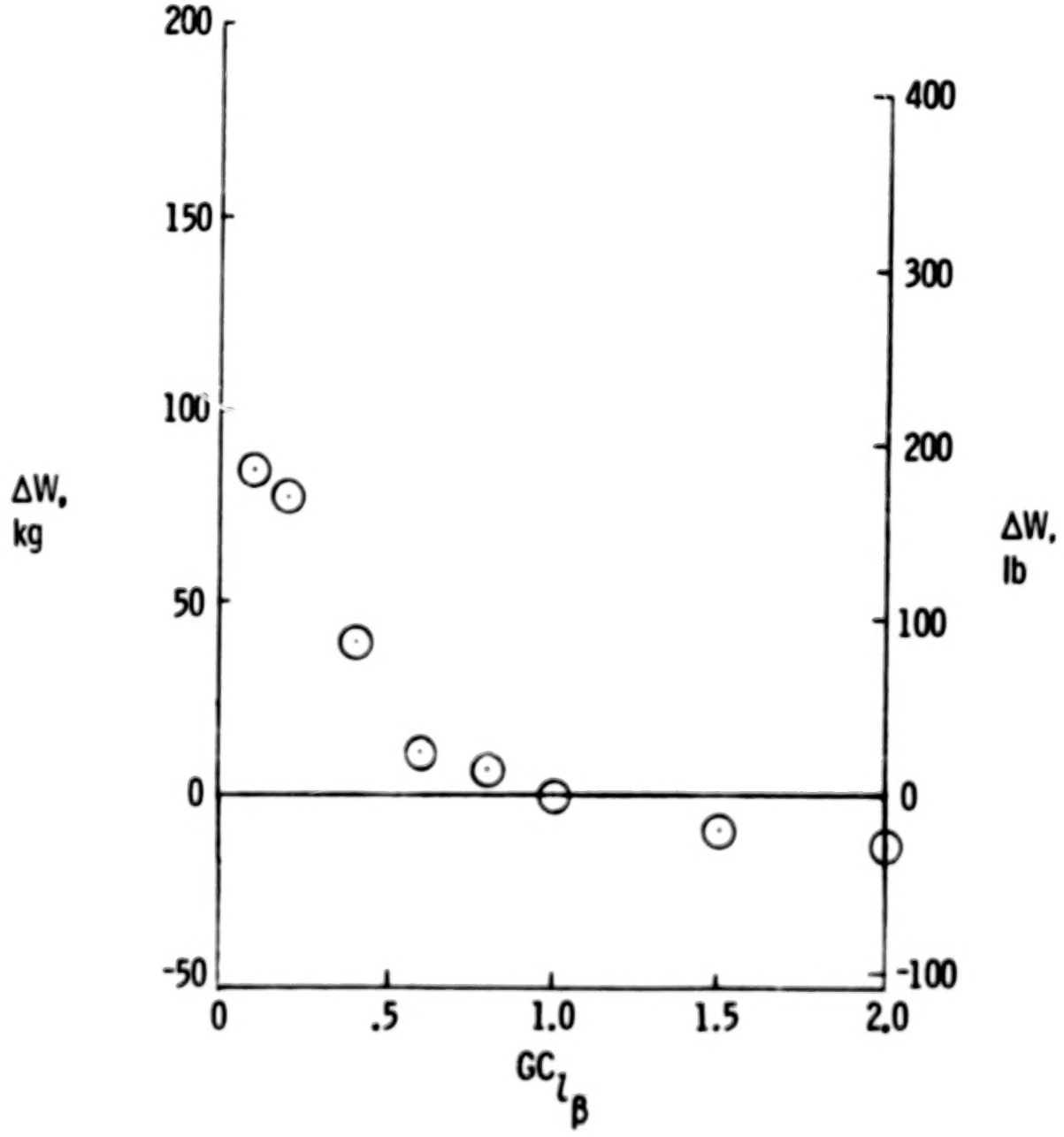

Figure 8.- Result of effective-dihedral variation C_{l_β} on RCS fuel consumption W.

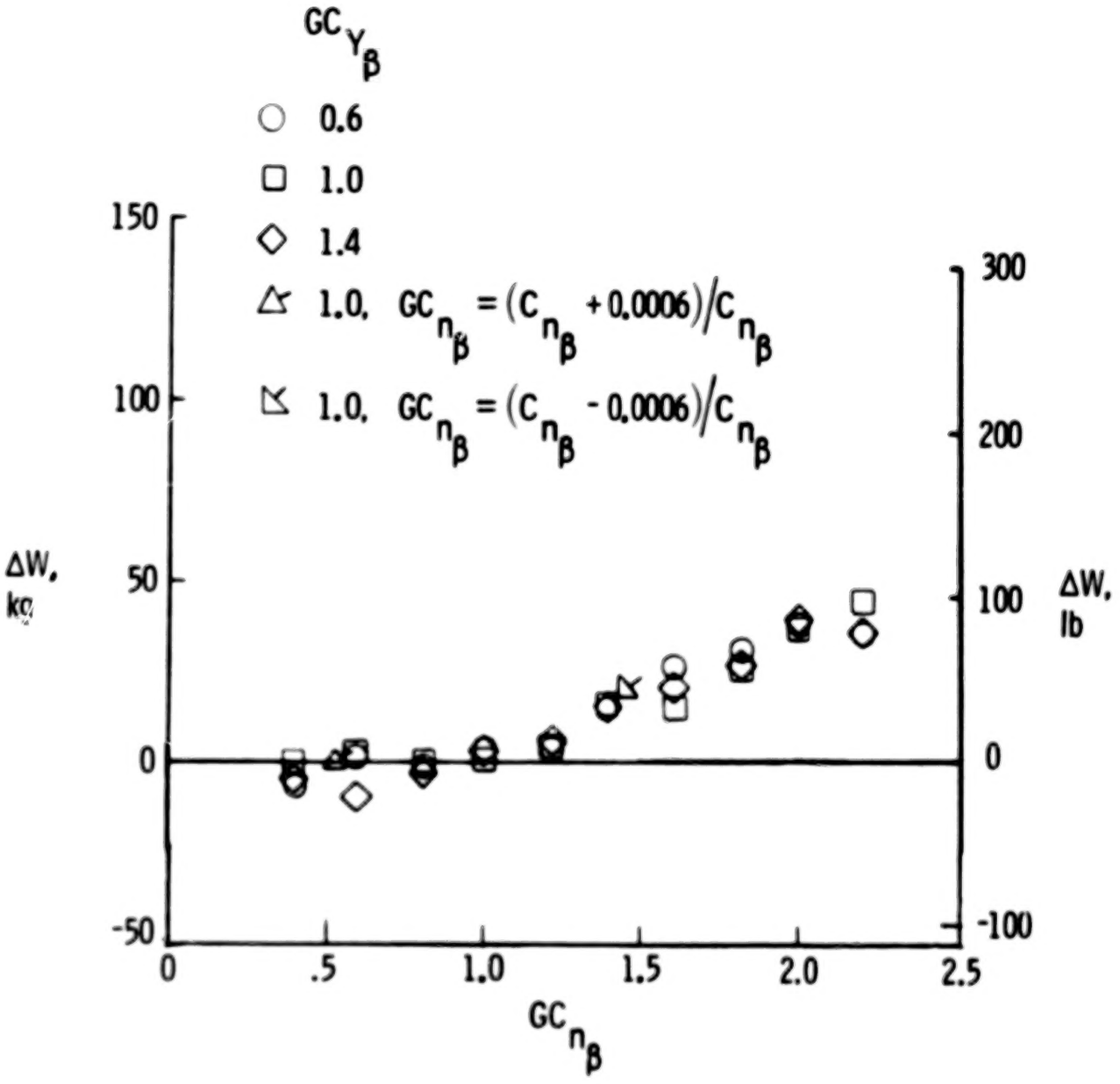

Figure 9.- Effect of directional stability variation C_{n_β} on RCS fuel consumption W.

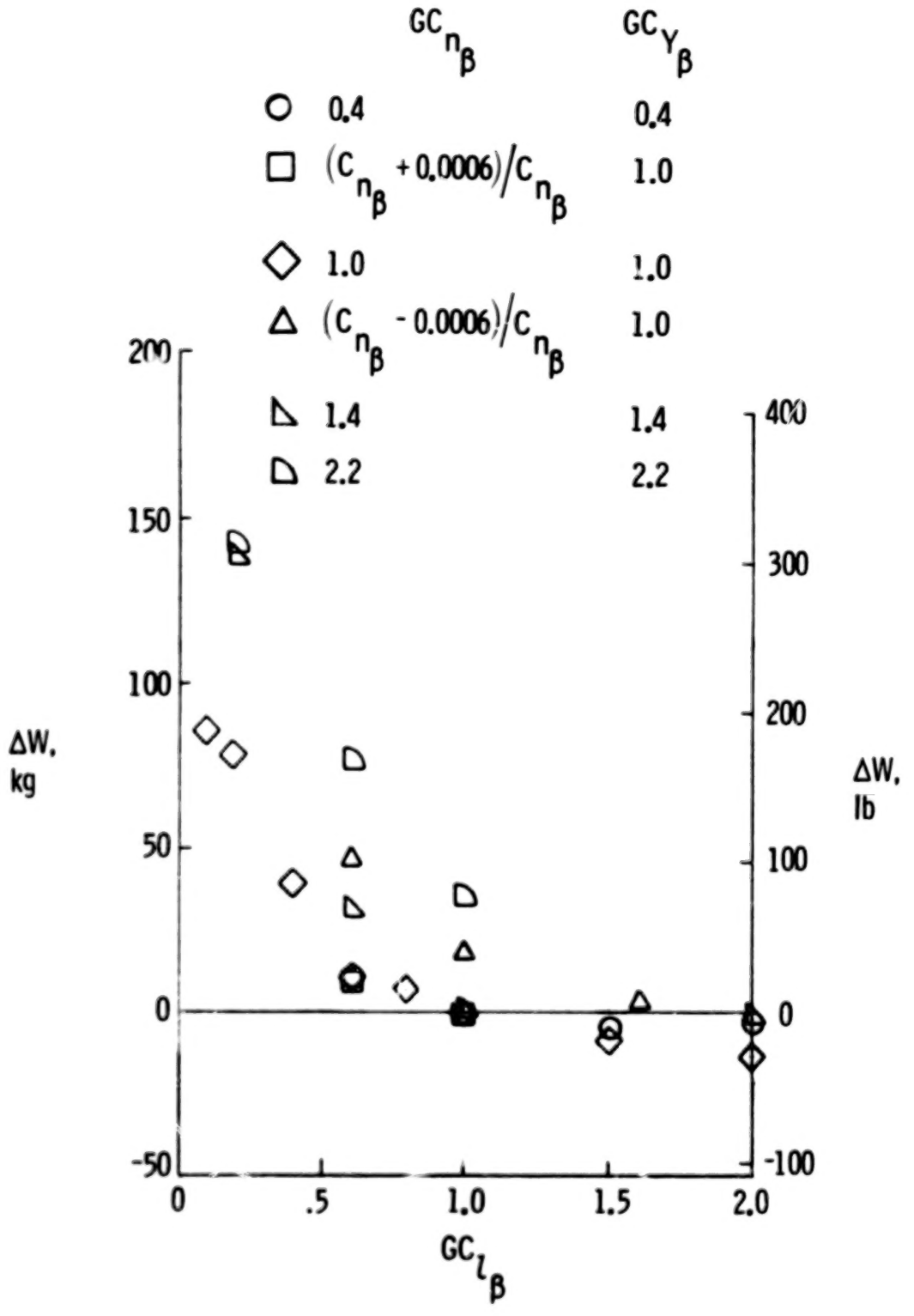

Figure 10.- Effect of combined lateral-directional stability variations on RCS fuel consumption W.

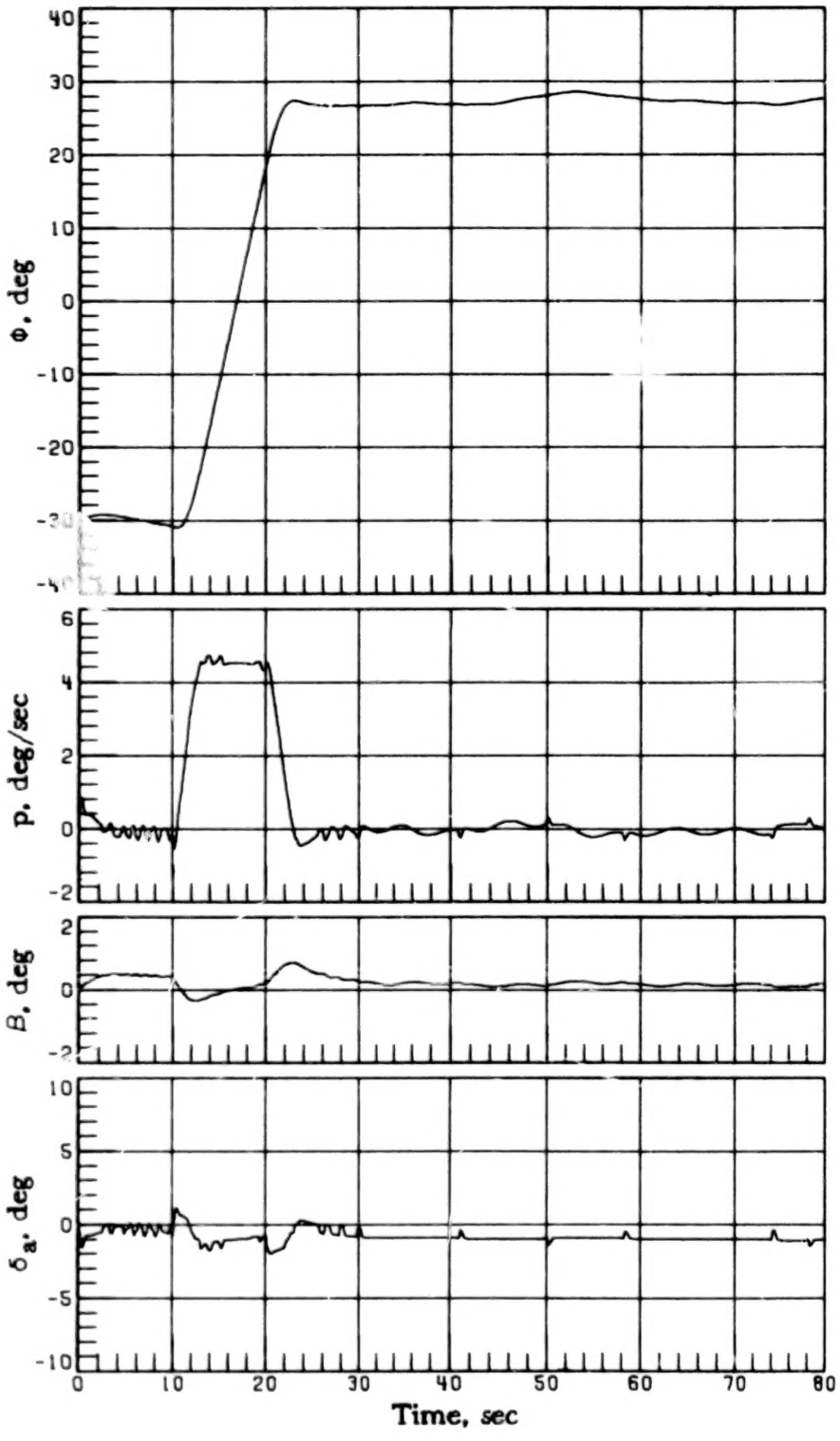

(a) Nominal case.

Figure 11.- Vehicle-response simulations at $M_i = 8$ for various lateral-directional stability characteristics. $\alpha_c = 30^o$; $\phi_c = -30^o$ for time < 10 sec; $\phi_c = 30^o$ for time ≥ 10 sec.

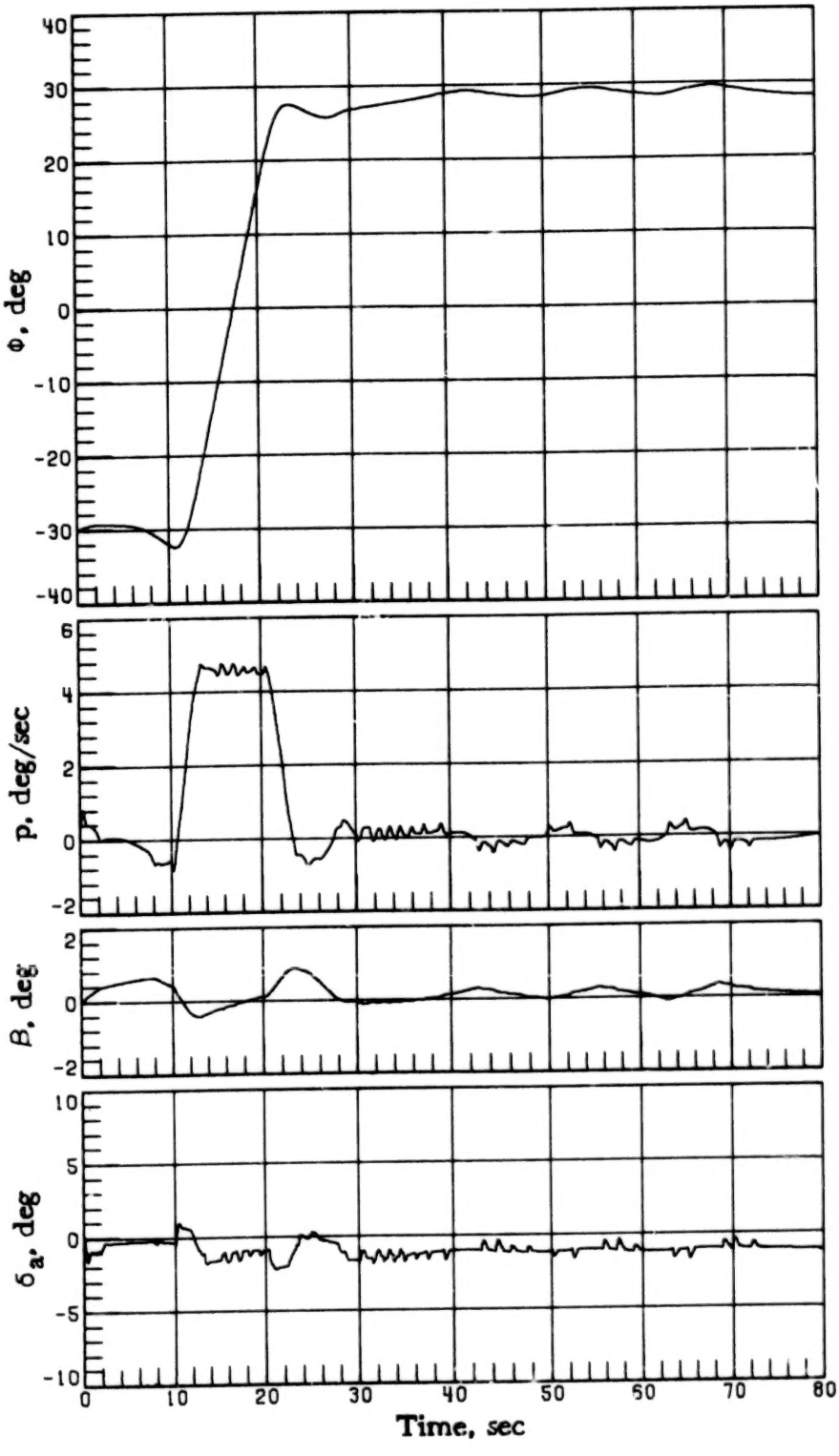

(b) $GC_{l_\beta} = 0.6$; $GC_{n_\beta} = GC_{Y_\beta} = 1.4$.

Figure 11.- Continued.

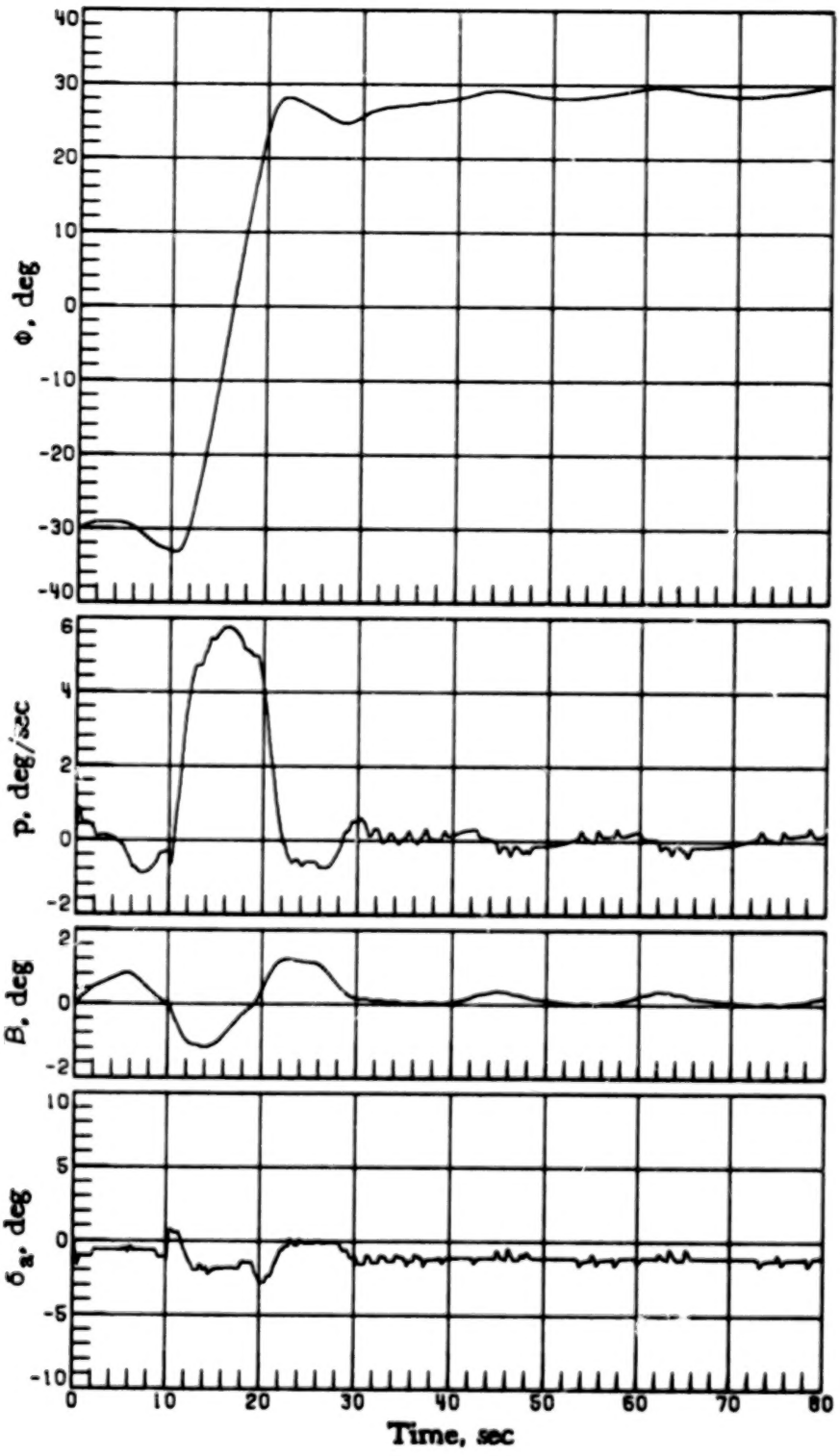

(c) GC_{l_β} = 0.2; GC_{n_β} = GC_{Y_β} = 1.4.

Figure 11.- Continued.

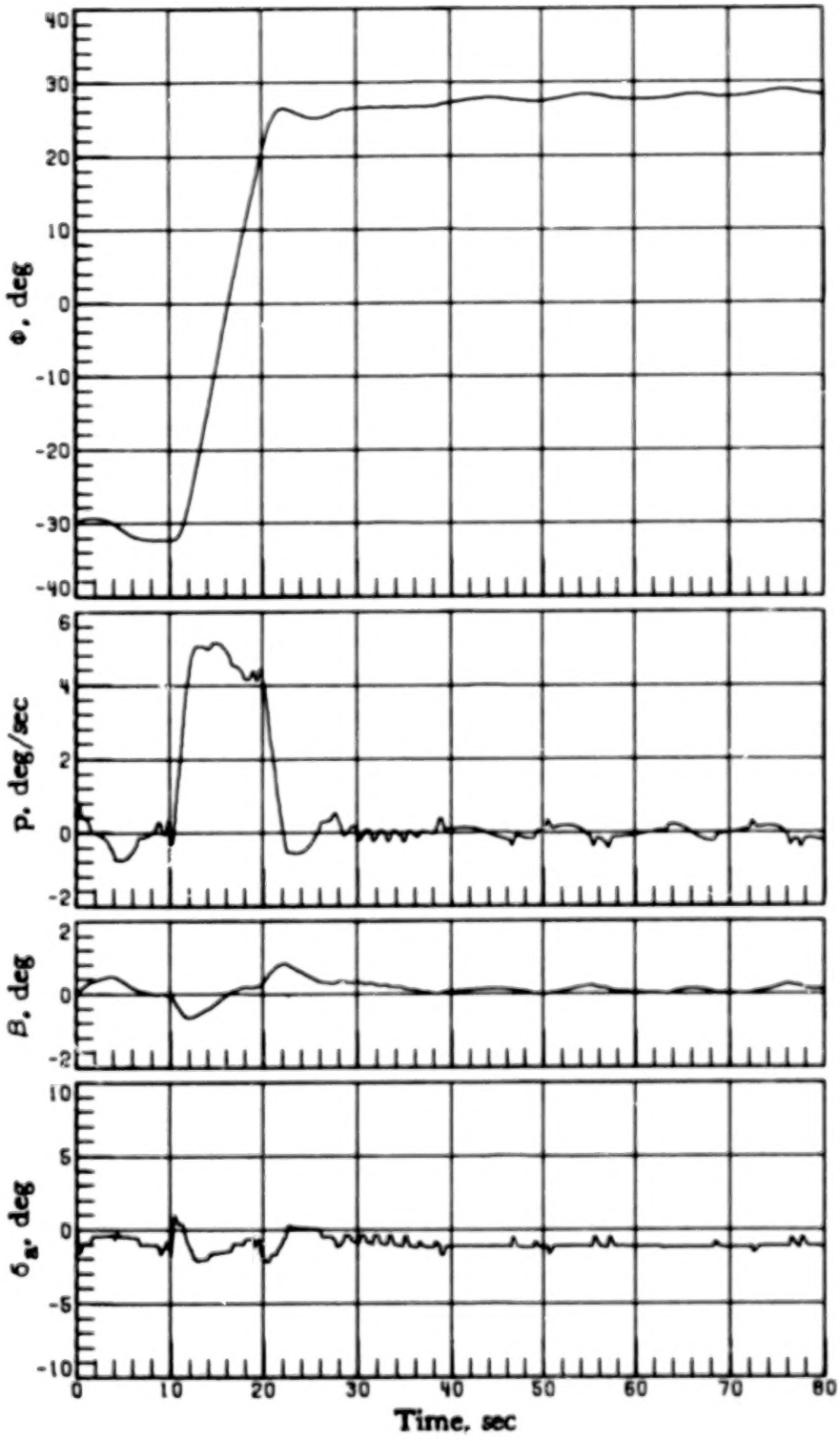

(d) $GC_{l_\beta} = 0.6$; $GC_{n_\beta} = GC_{Y_\beta} = 2.2$.

Figure 11.- Continued.

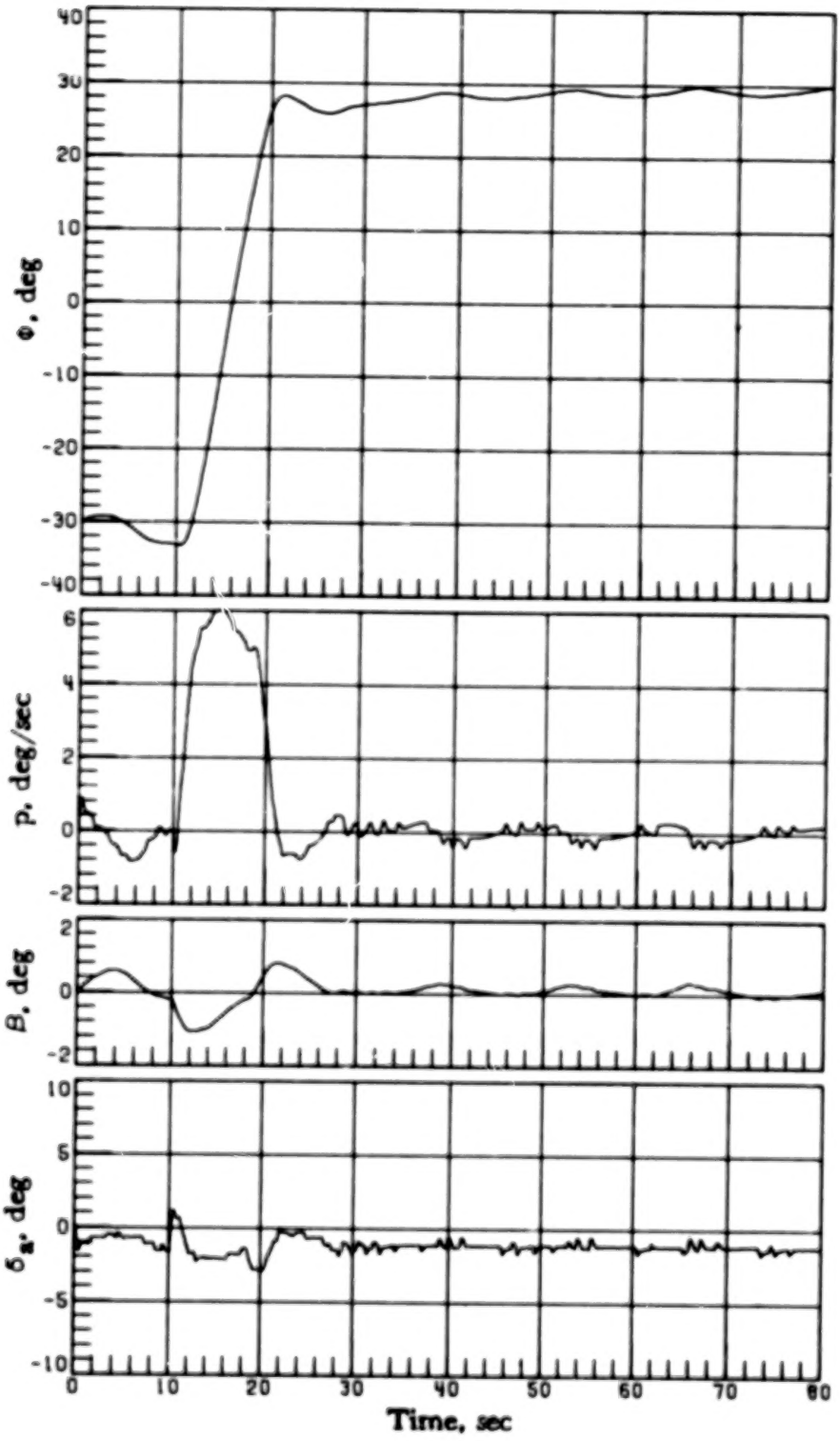

(e) $GC_{l_\beta} = 0.2$; $GC_{n_\beta} = GC_{Y_\beta} = 2.2$.

Figure 11.- Continued.

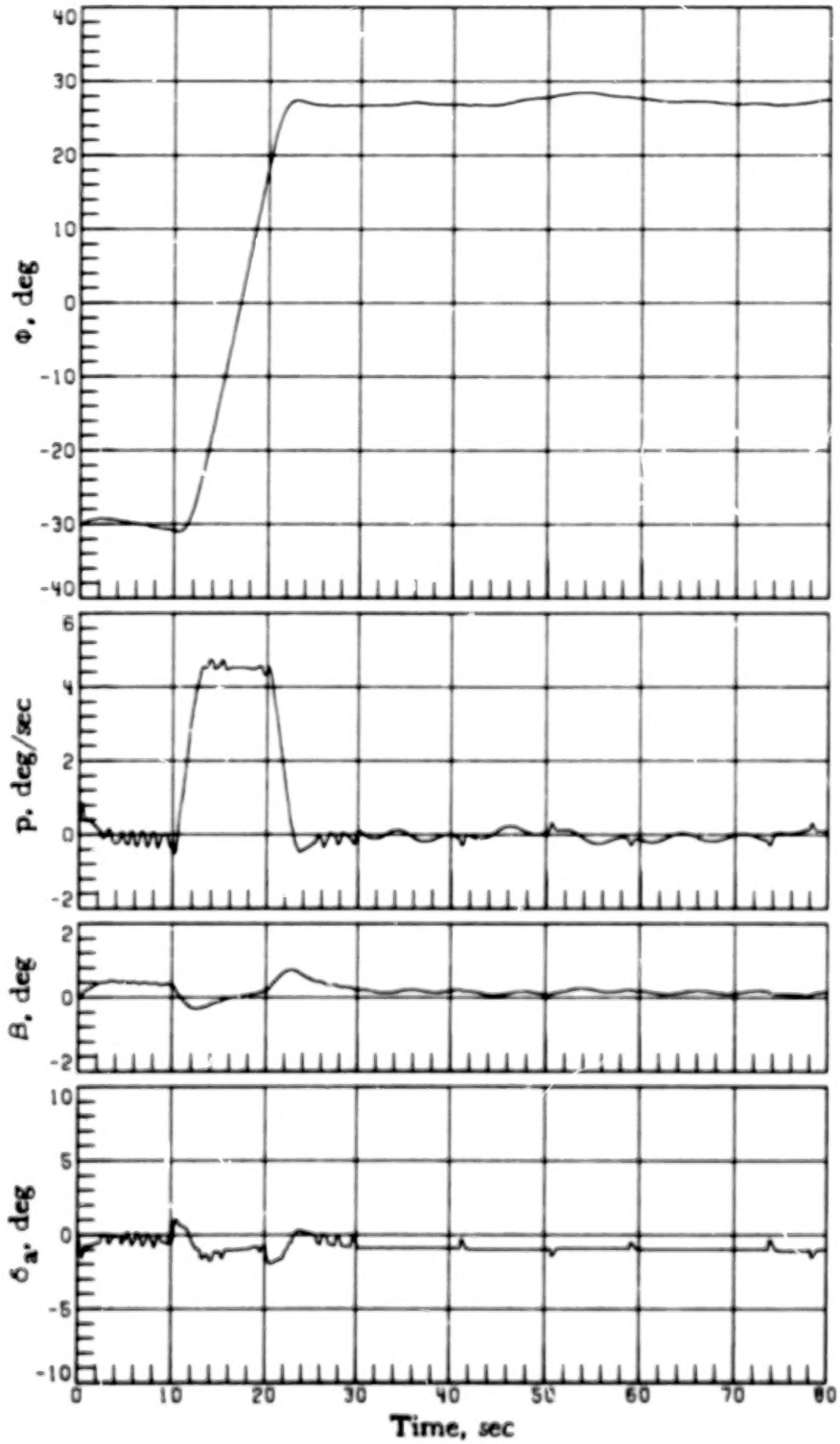

(f) $GC_{l_\beta} = 1.0$; $GC_{n_\beta} = 1.0$; $GC_{Y_\beta} = 0.6$.

Figure 11.- Continued.

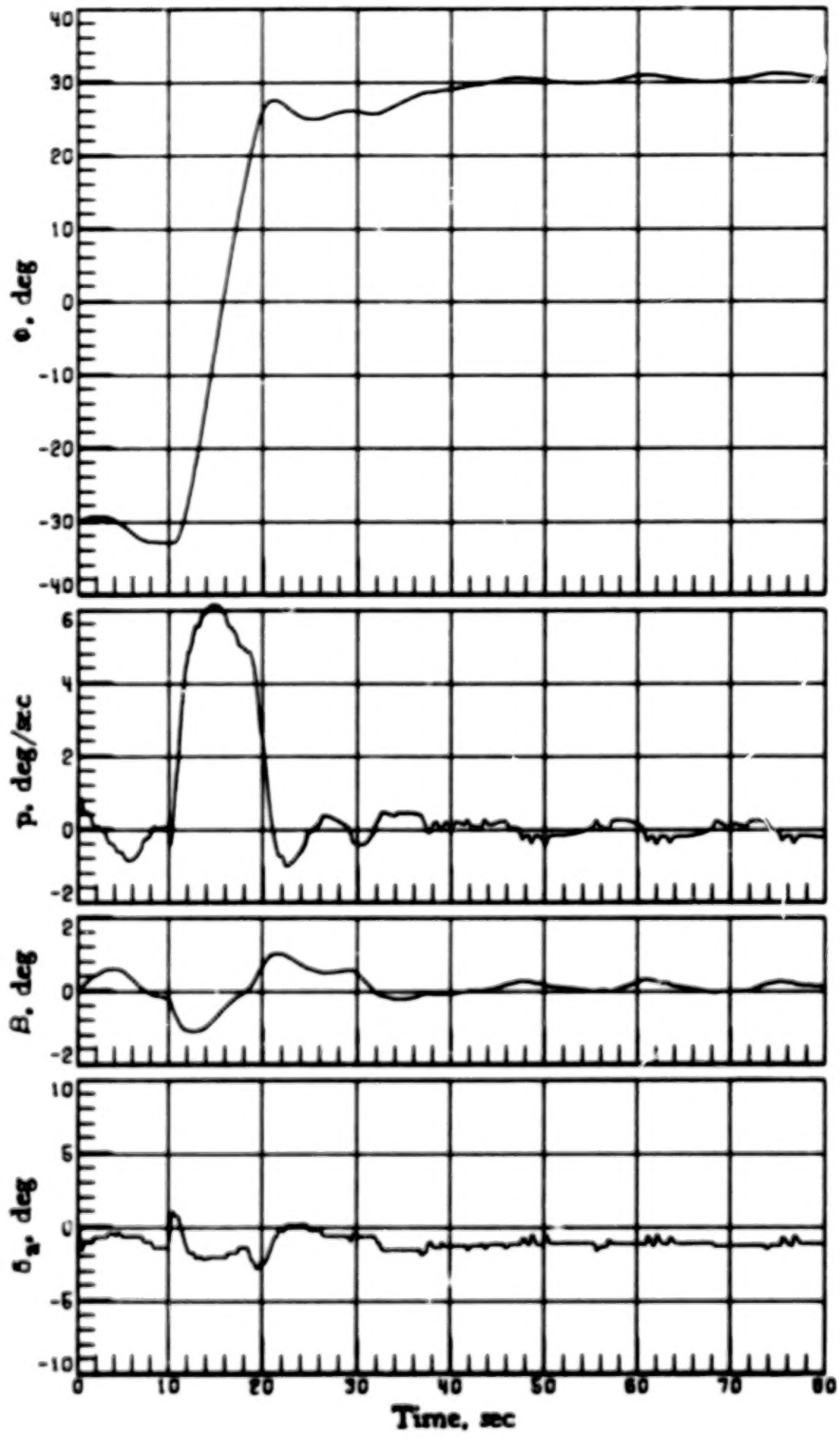

(g) $GC_{l_\beta} = 0.2$; $GC_{n_\beta} = 2.2$; $GC_{Y_\beta} = 0.6$.

Figure 11.- Concluded.

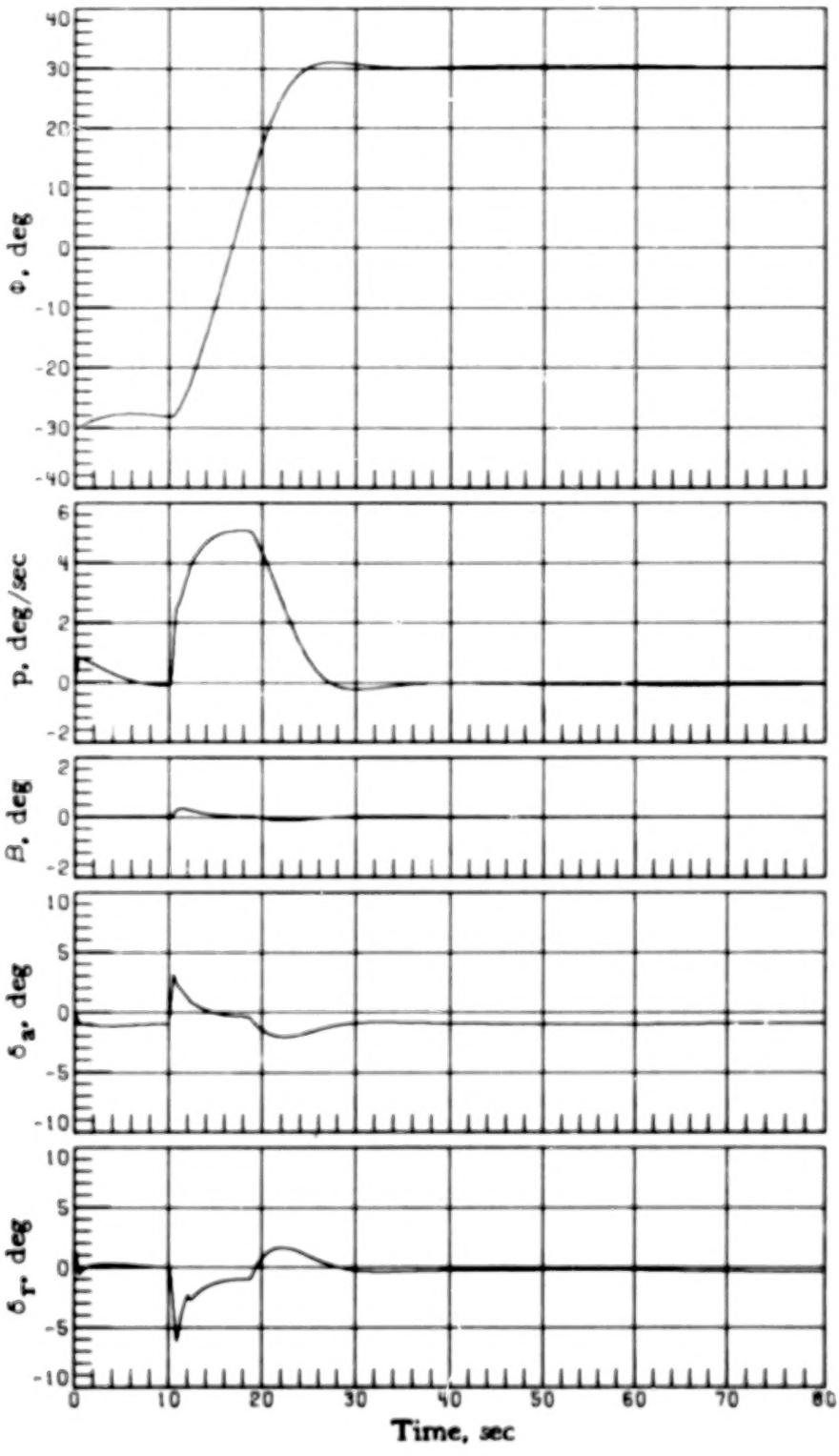

(a) Nominal case.

Figure 12.- Vehicle-response simulations at $M_i = 4$ for various lateral-directional and rudder-control parameter characteristics. $\alpha_c = 17.6^\circ$; $\phi_c = -30^\circ$ for time < 10 sec; $\phi_c = 30^\circ$ for time ≥ 10 sec.

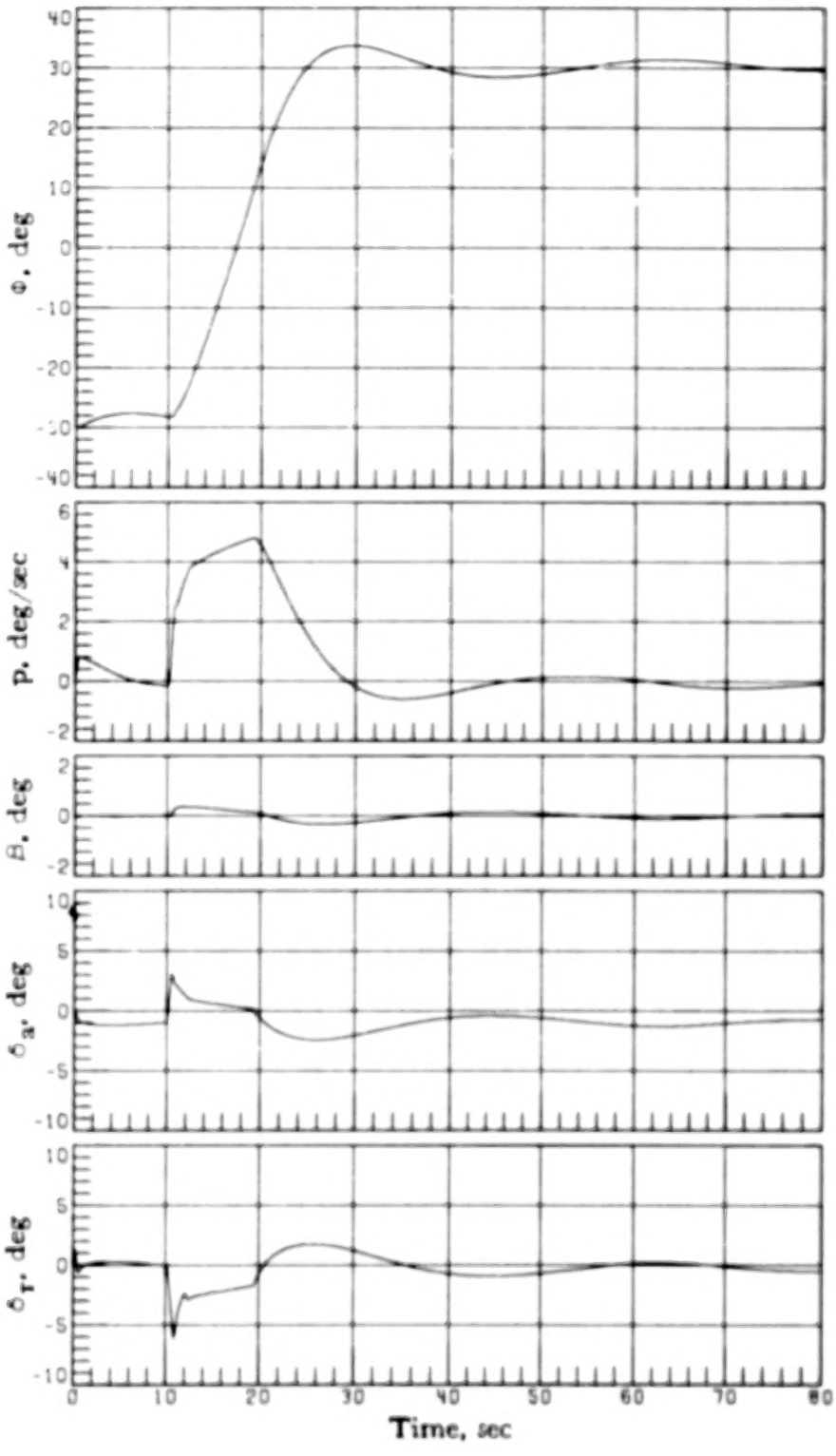

(b) $GC_{Y_\beta} = 0.4$.

Figure 12.- Continued.

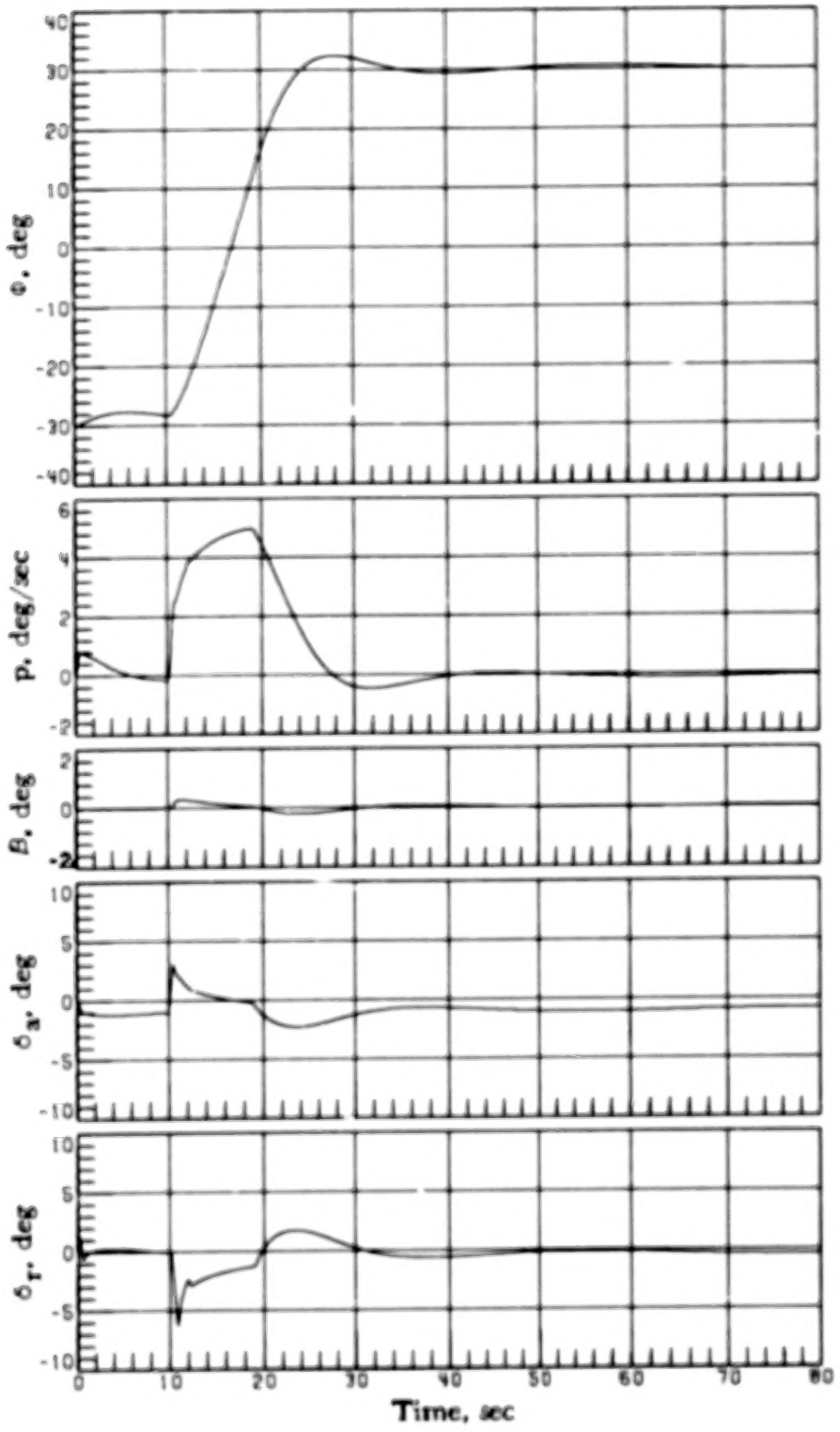

(c) $GC_{Y_\beta} = 0.6$.

Figure 12.- Continued.

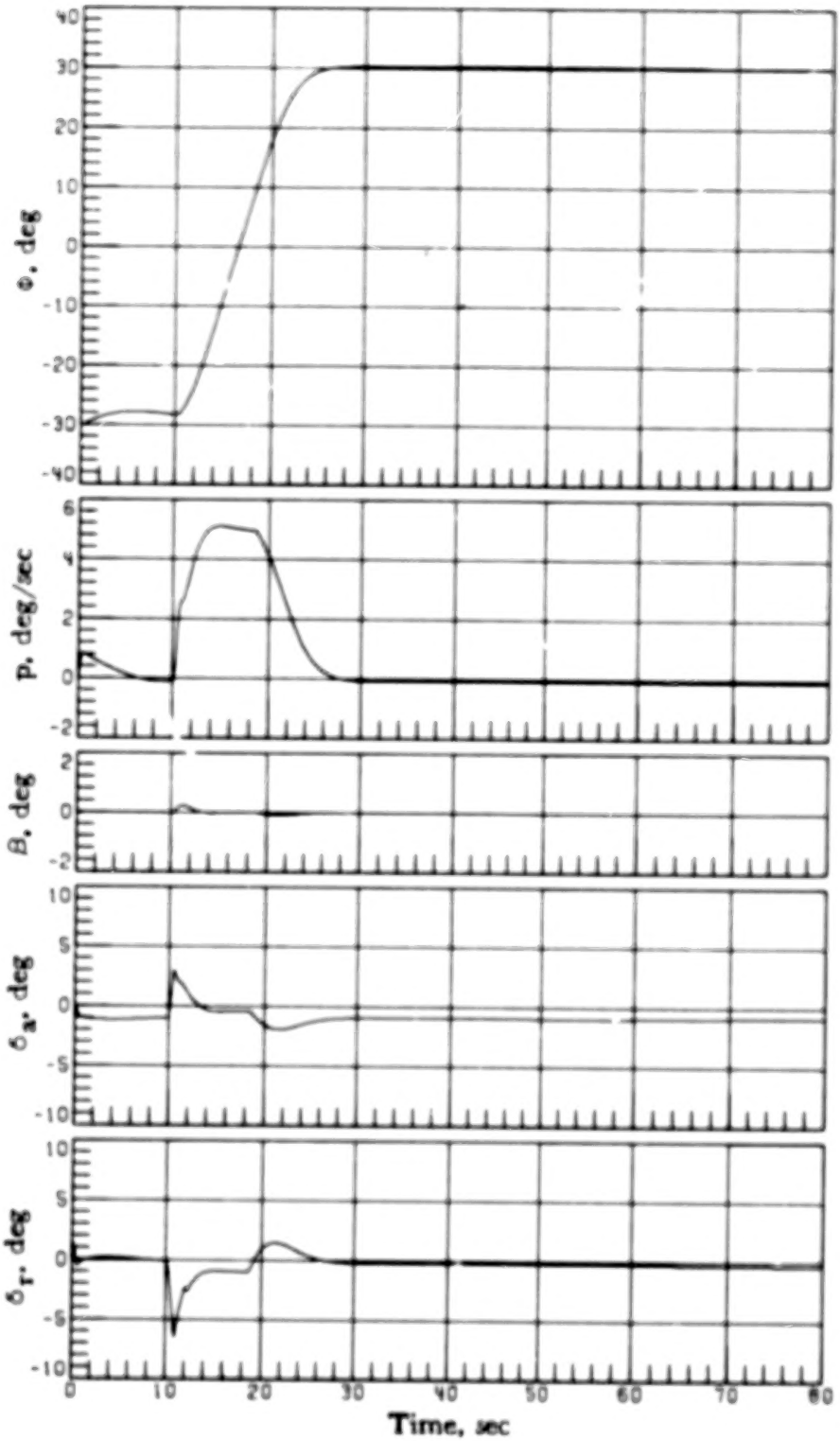

(d) $GC_{Y_\beta} = 1.8$.

Figure 12.- Continued.

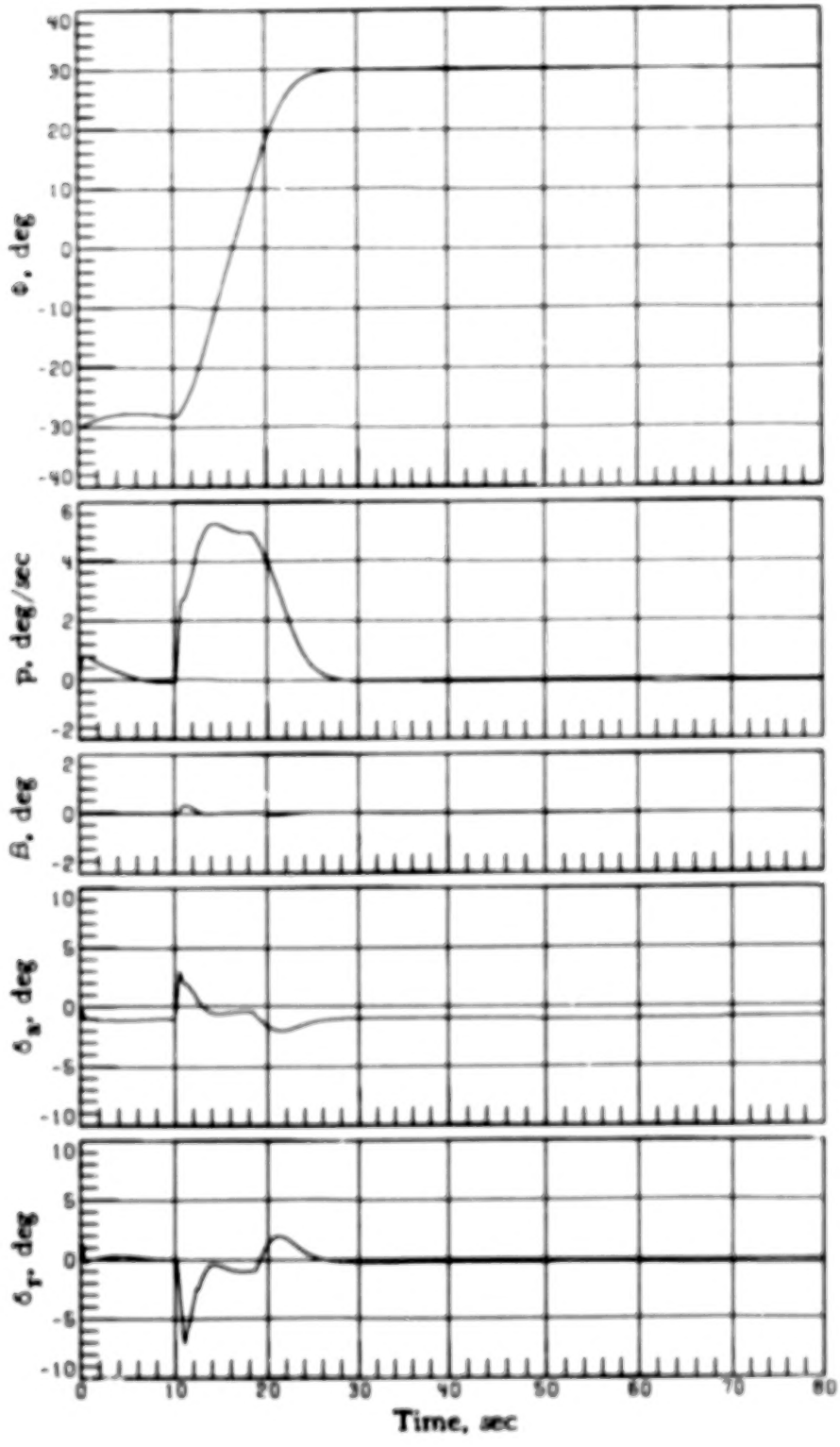

(e) $GC_{l_\beta} = 0.2$; $GC_{n_\beta} = GC_{Y_\beta} = 2.2$.

Figure 12.- Continued.

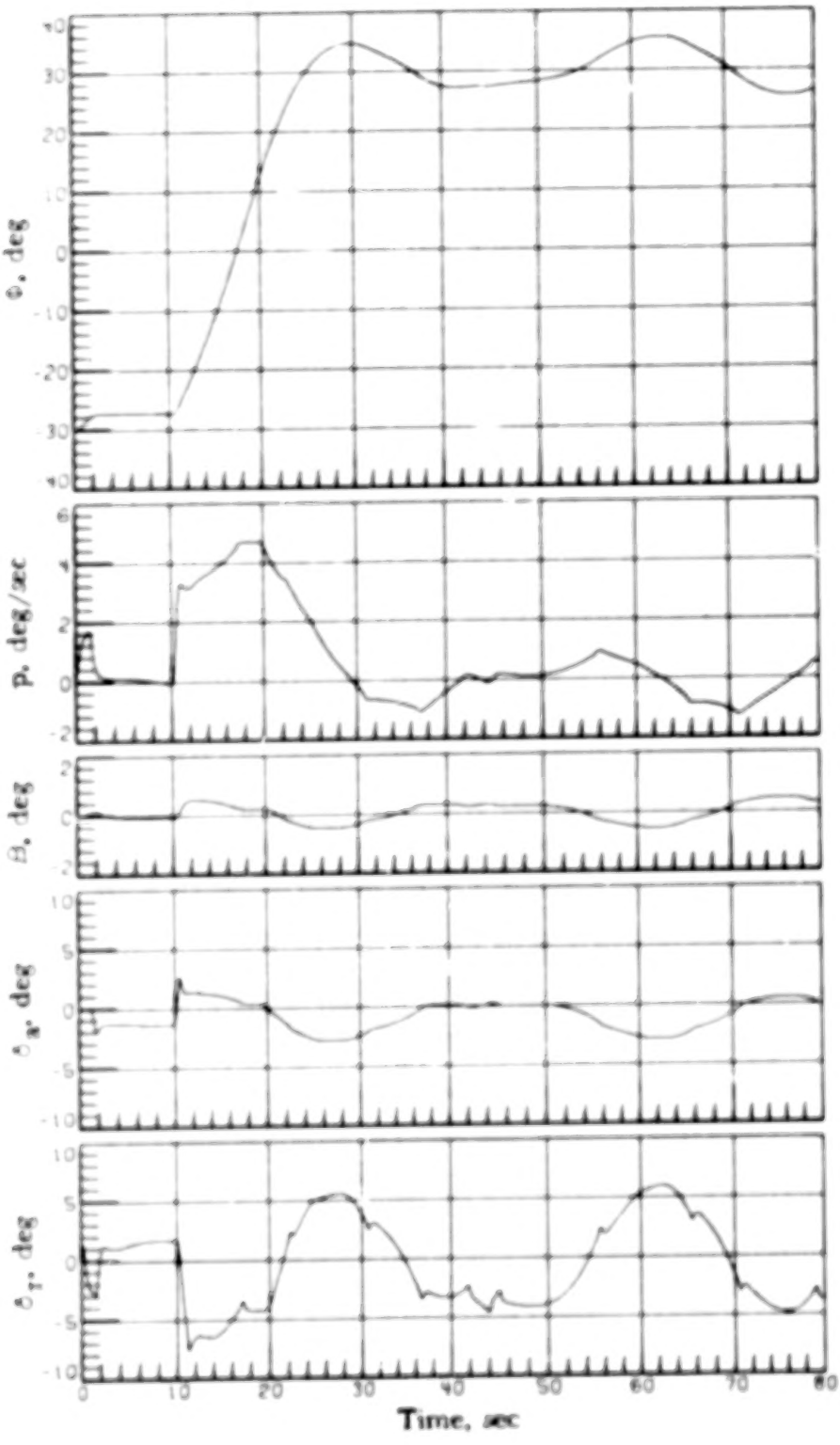

(f) GC_{l_β} = 0.2; GC_{n_β} = 2.2; GC_{Y_β} = 1.0.

Figure 12.- Concluded.

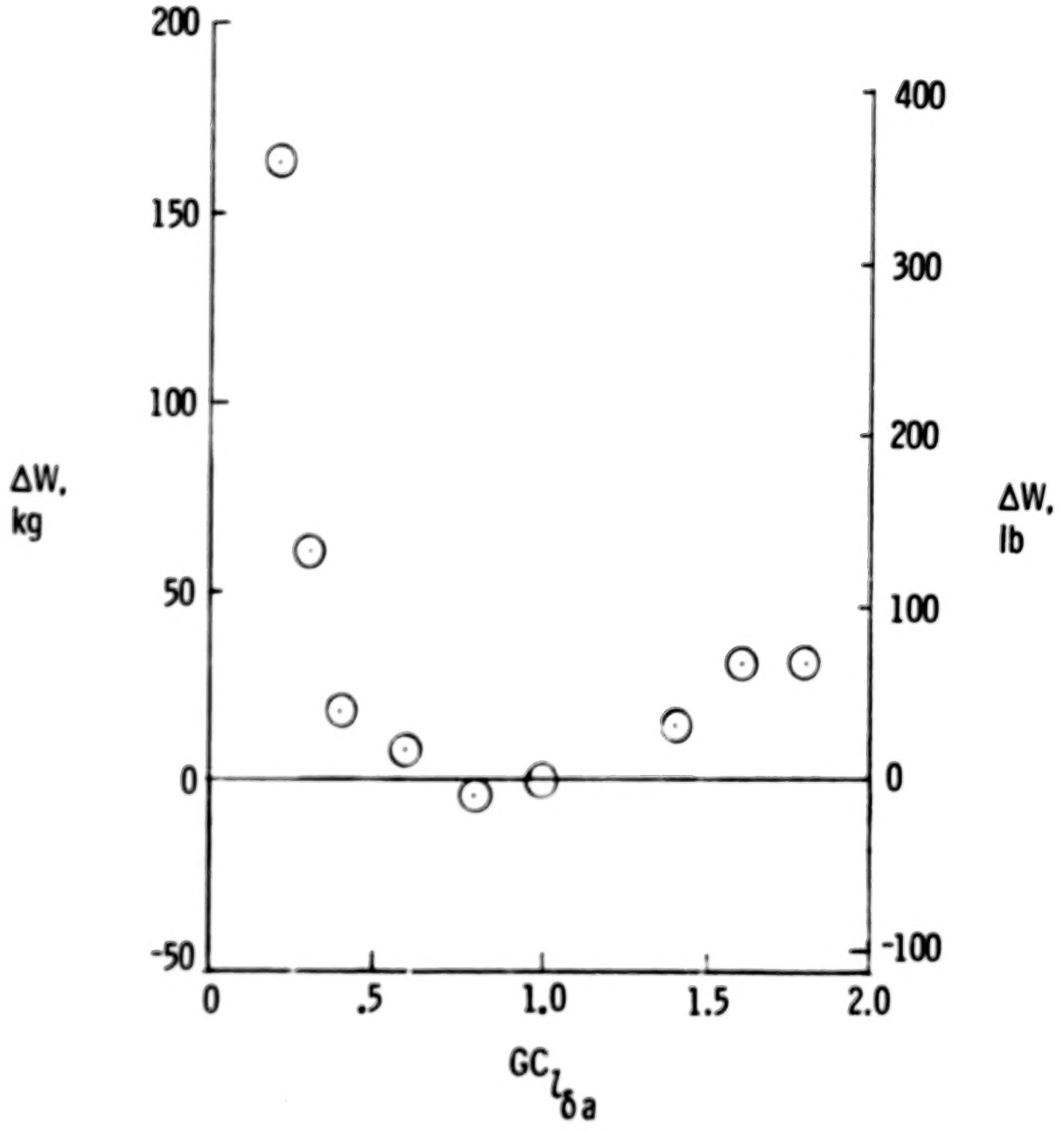

Figure 13.- Effect of roll due to aileron variation $C_{l_{\delta a}}$ on RCS fuel consumption W.

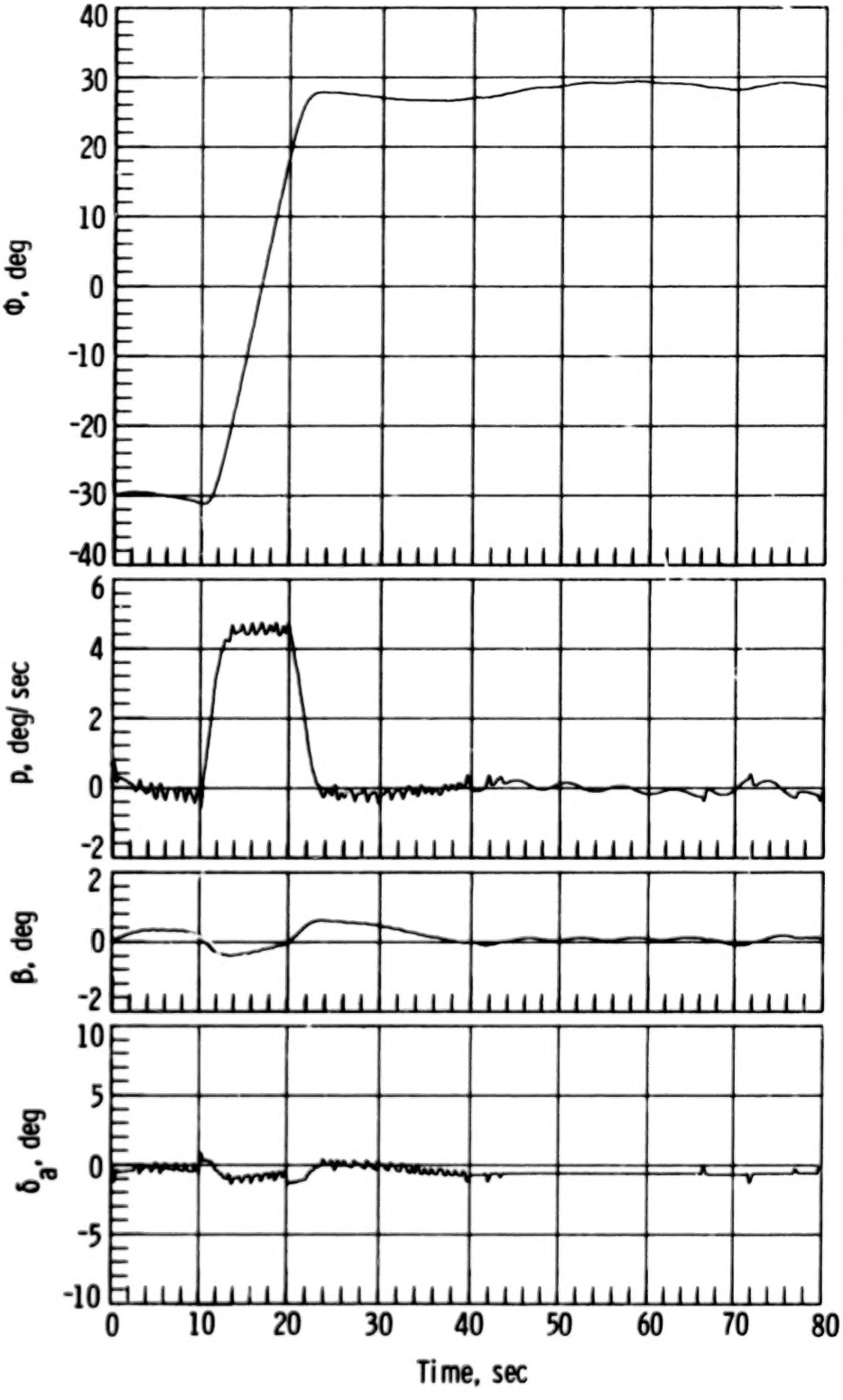

Figure 14.- Vehicle-response simulations at $M_i = 8$ with $GC_{l_{\delta a}} = 1.8$.

$\alpha_c = 30^\circ$; $\phi_c = -30^\circ$ for time < 10 sec; $\phi_c = 30^\circ$ for time ≥ 10 sec.

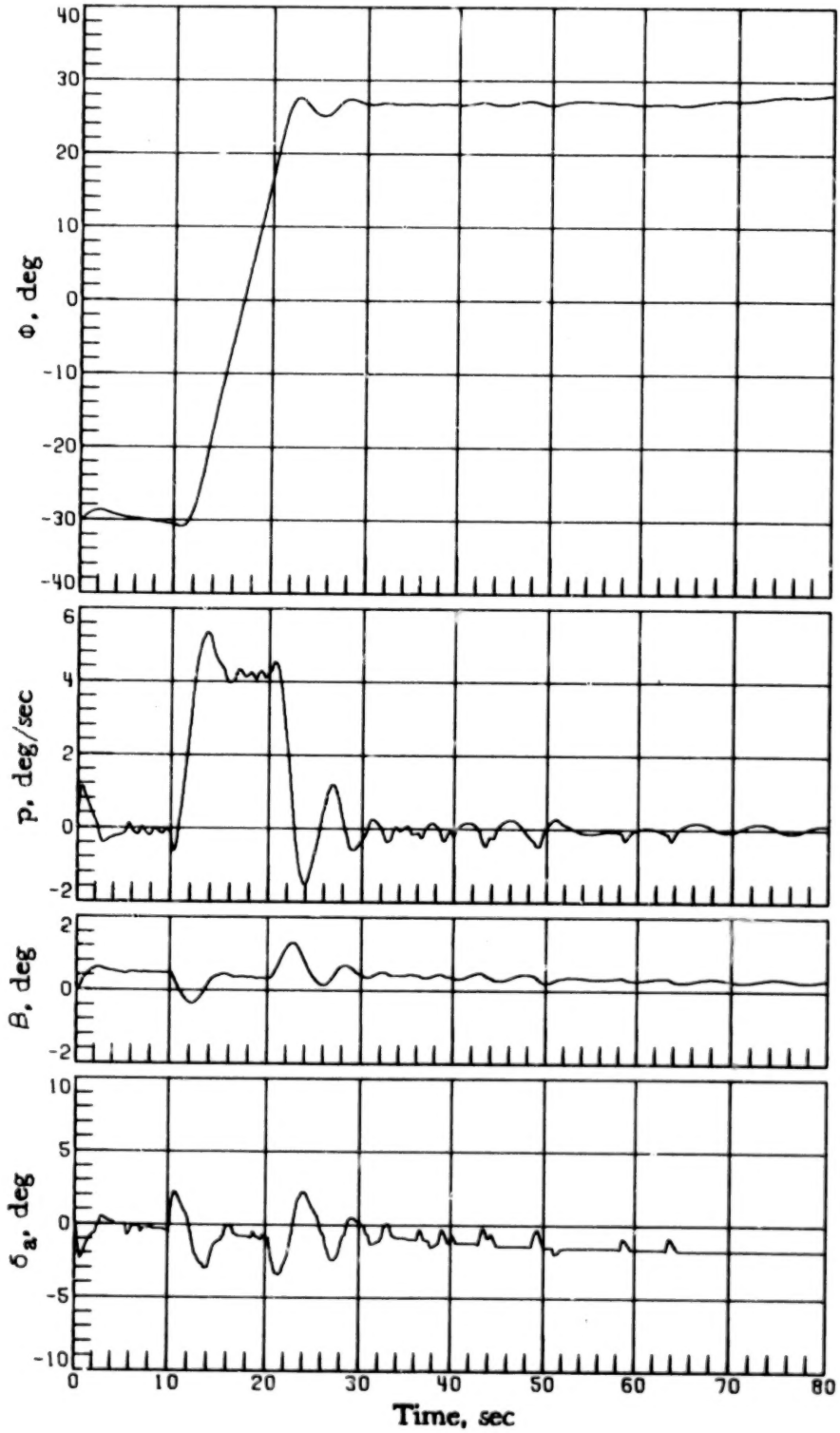

(a) $M_i = 8$; $GC_{l_{\delta a}} = 0.4$.

Figure 15.- Vehicle-response simulations with varying $GC_{l_{\delta a}}$. $\alpha_c = 30^o$; $\phi_c = -30^o$ for time < 10 sec; $\phi_c = 30^o$ for time ≥ 10 sec.

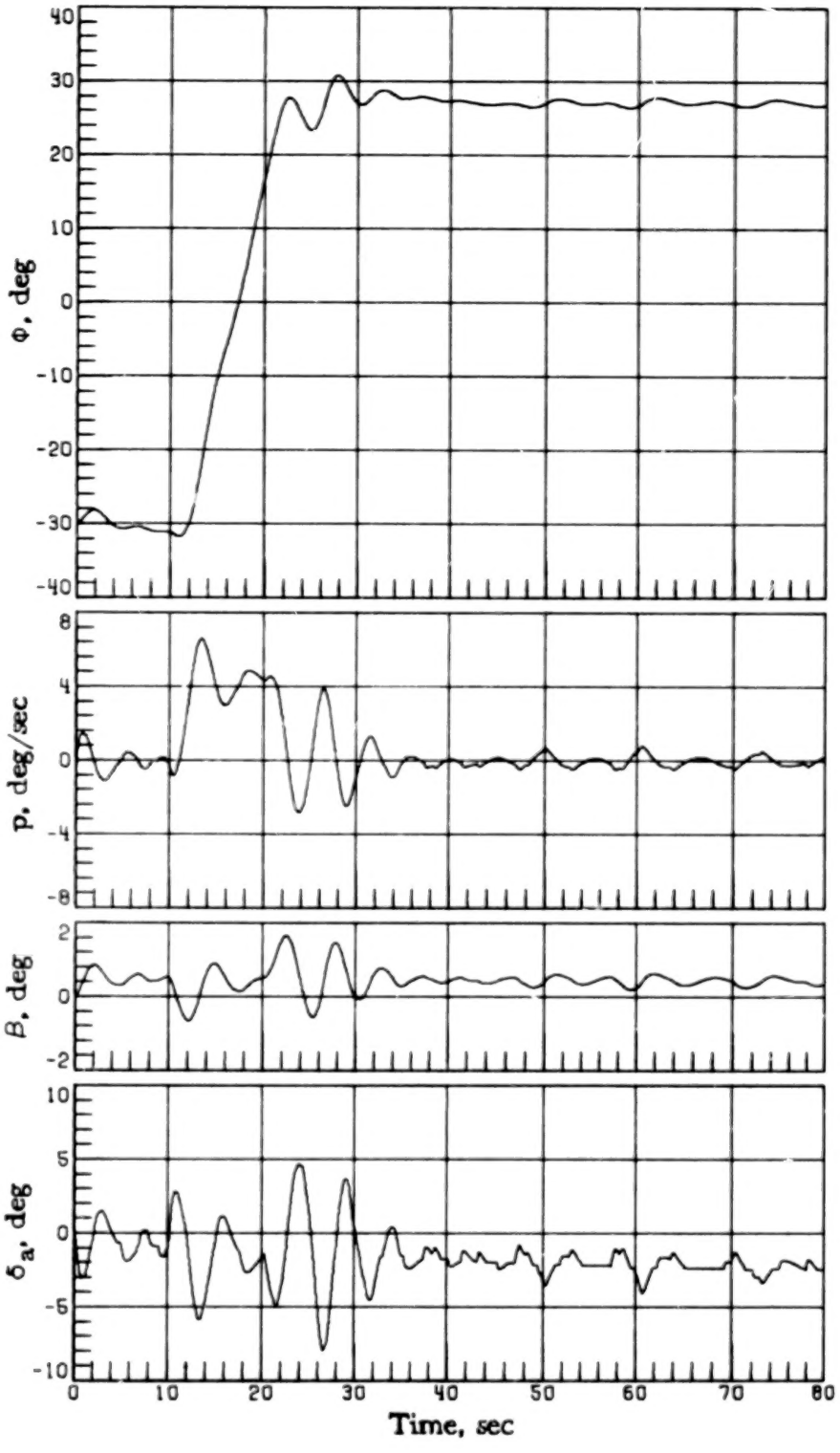

(b) $M_i = 8$; $GC_{l_{\delta a}} = 0.2$.

Figure 15.- Continued.

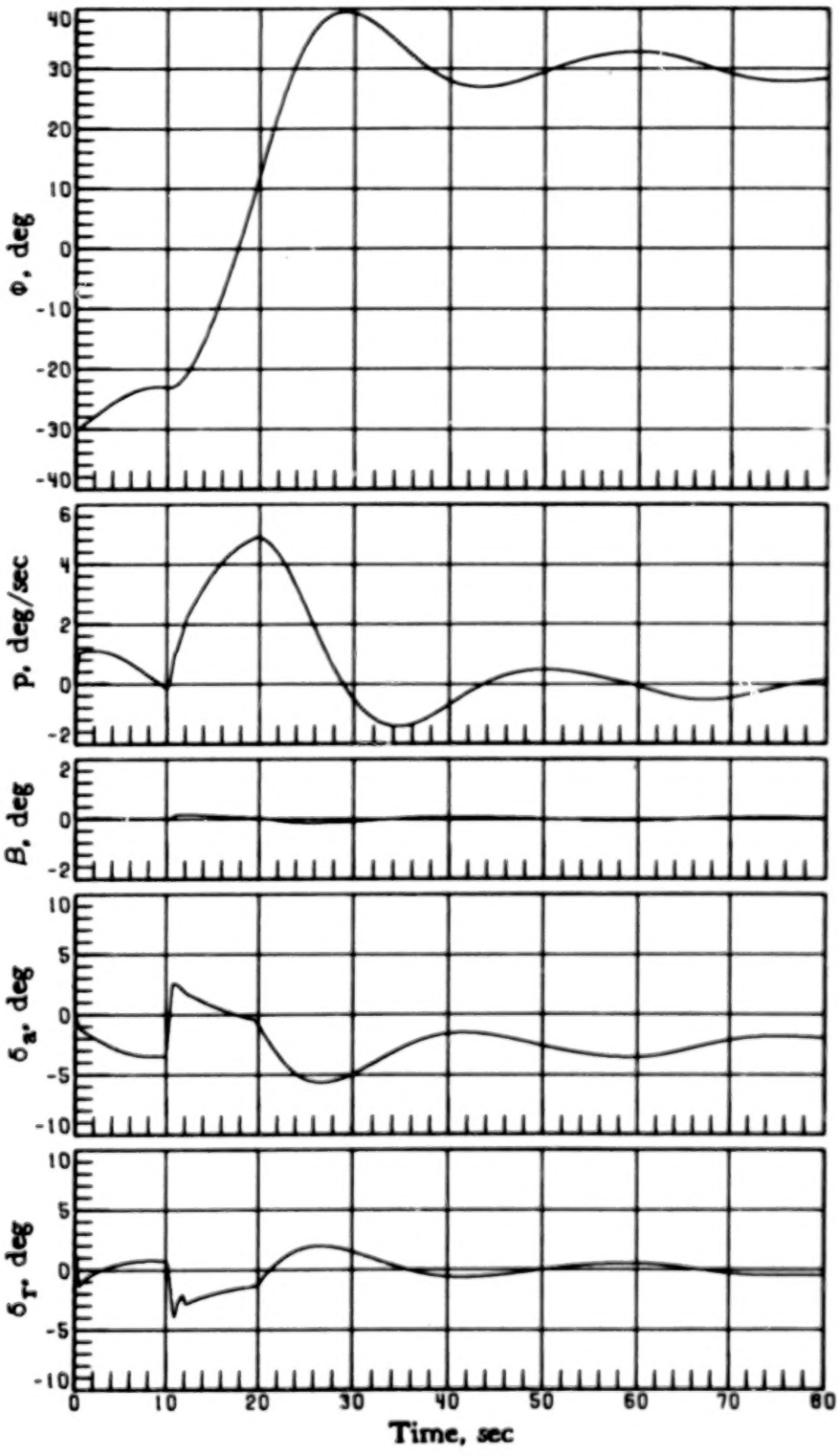

(c) $M_i = 4$; $GC_{l_{\delta a}} = 0.4$.

Figure 15.- Concluded.

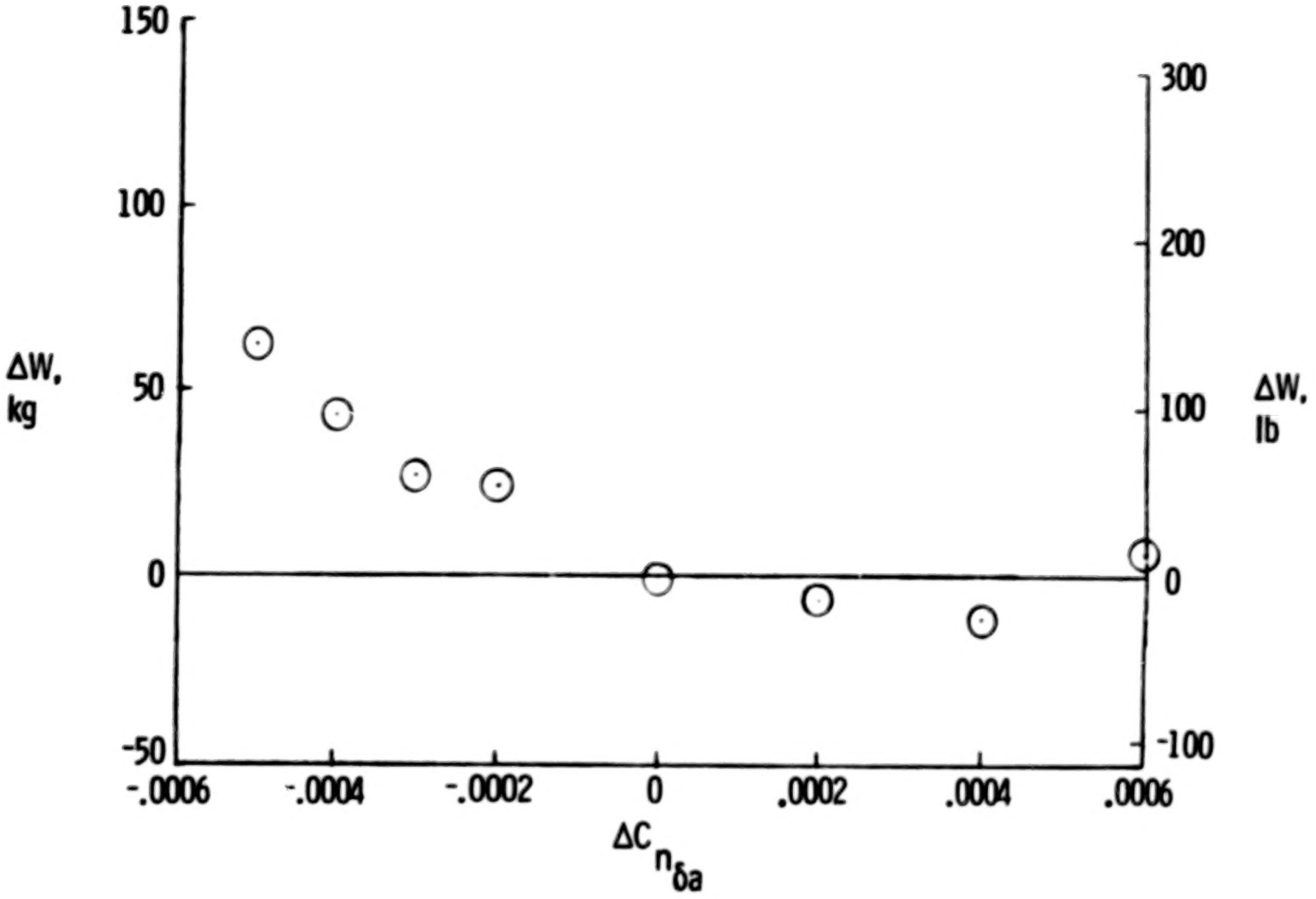

Figure 16.- Effect of yaw due to aileron variation $C_{n_{\delta a}}$ on RCS fuel consumption W.

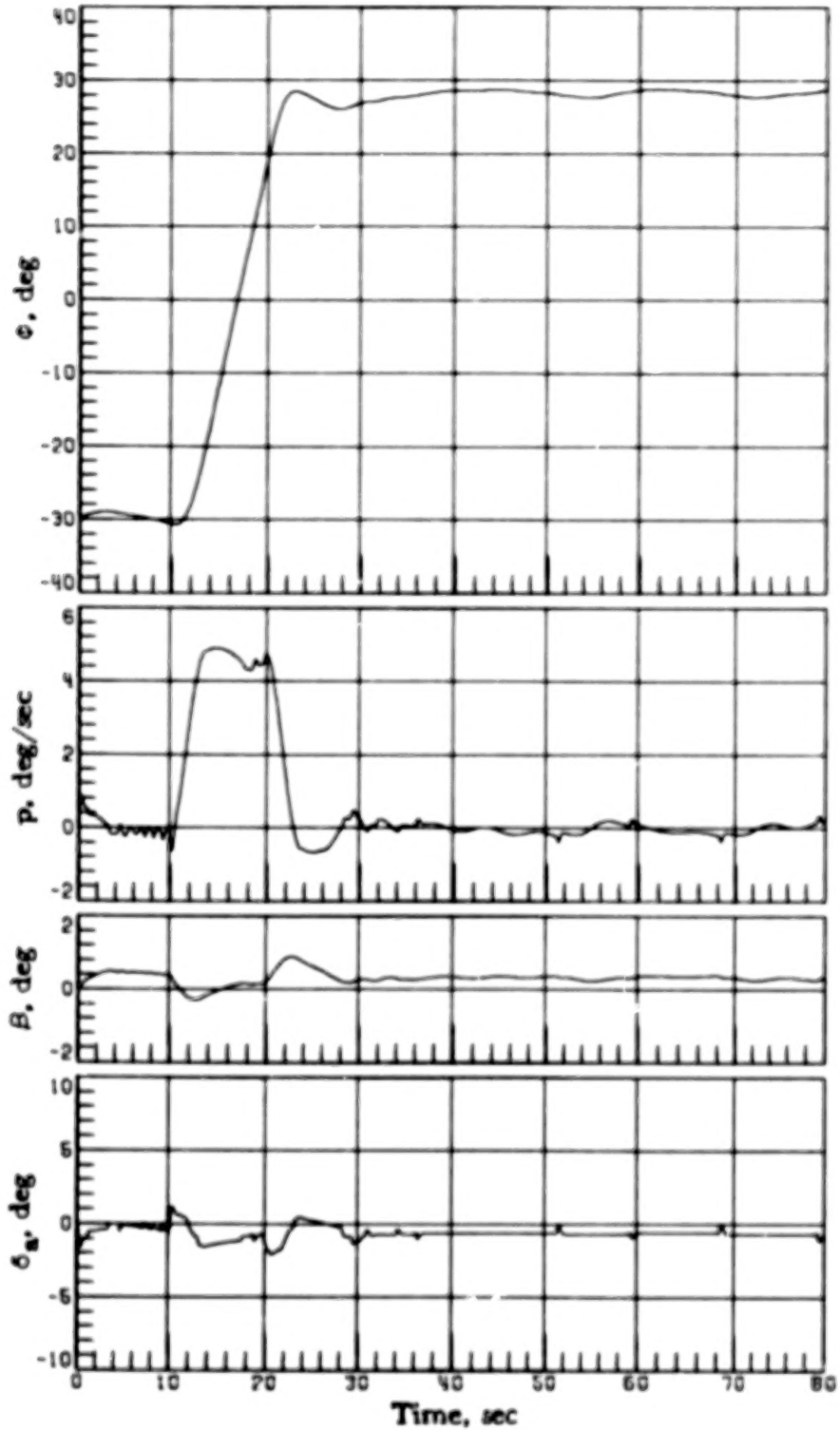

Figure 17.- Vehicle-response simulations at $M_i = 3$ with $\Delta C_{n_{\delta a}} = -0.0006$. $\alpha_c = 30^\circ$; $\phi_c = -30^\circ$ for time < 10 sec; $\phi_c = 30^\circ$ for time ≥ 10 sec.

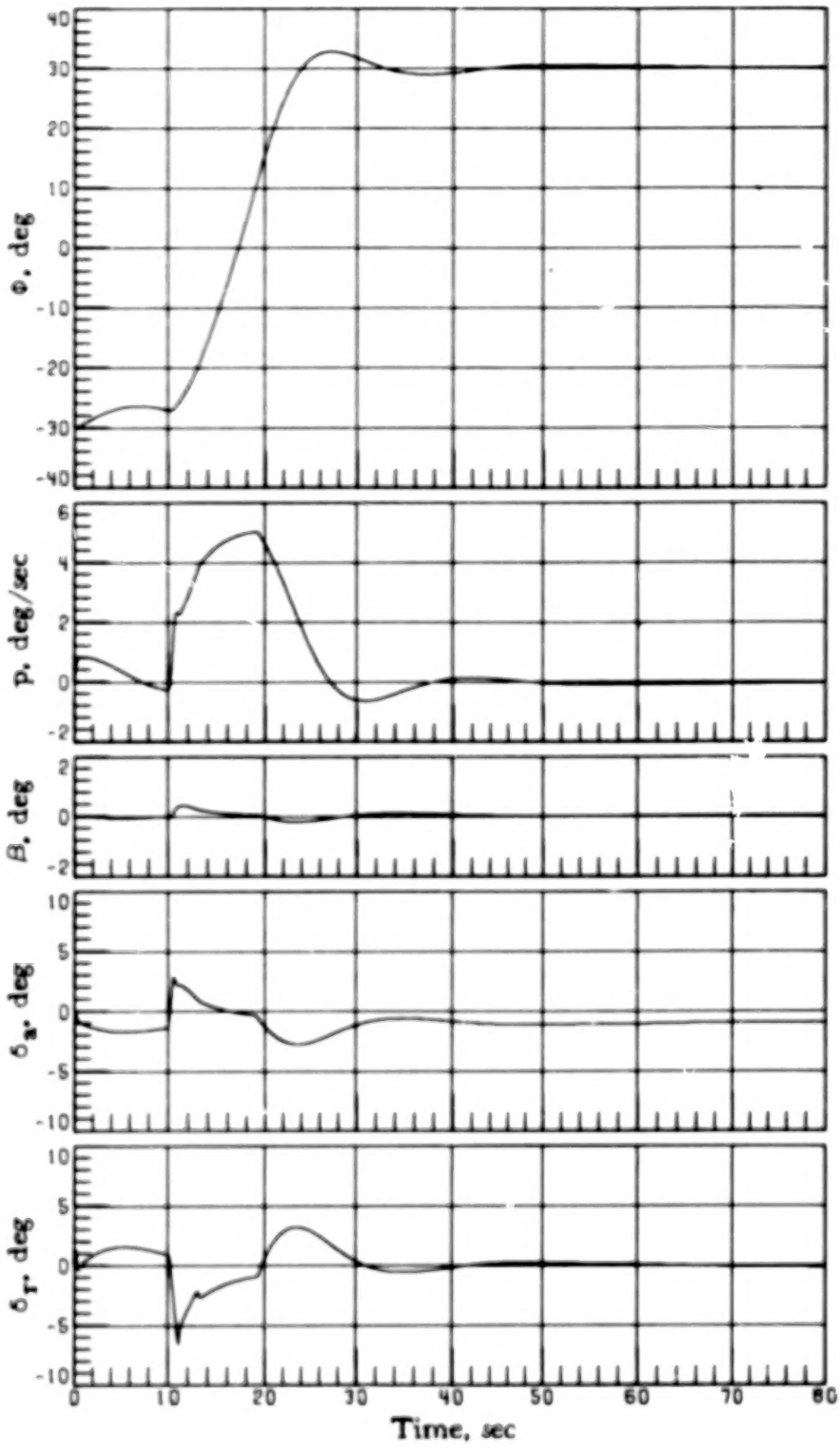

(a) $\Delta C_{n_{\delta a}} = -0.0002$; $\Phi_c = -30^\circ$ for time < 10 sec; $\Phi_c = 30^\circ$ for time ≥ 10 sec.

Figure 18.- Vehicle-response simulations at $M_i = 4$ with varying $\Delta C_{n_{\delta a}}$. $\alpha_c = 17.6^\circ$.

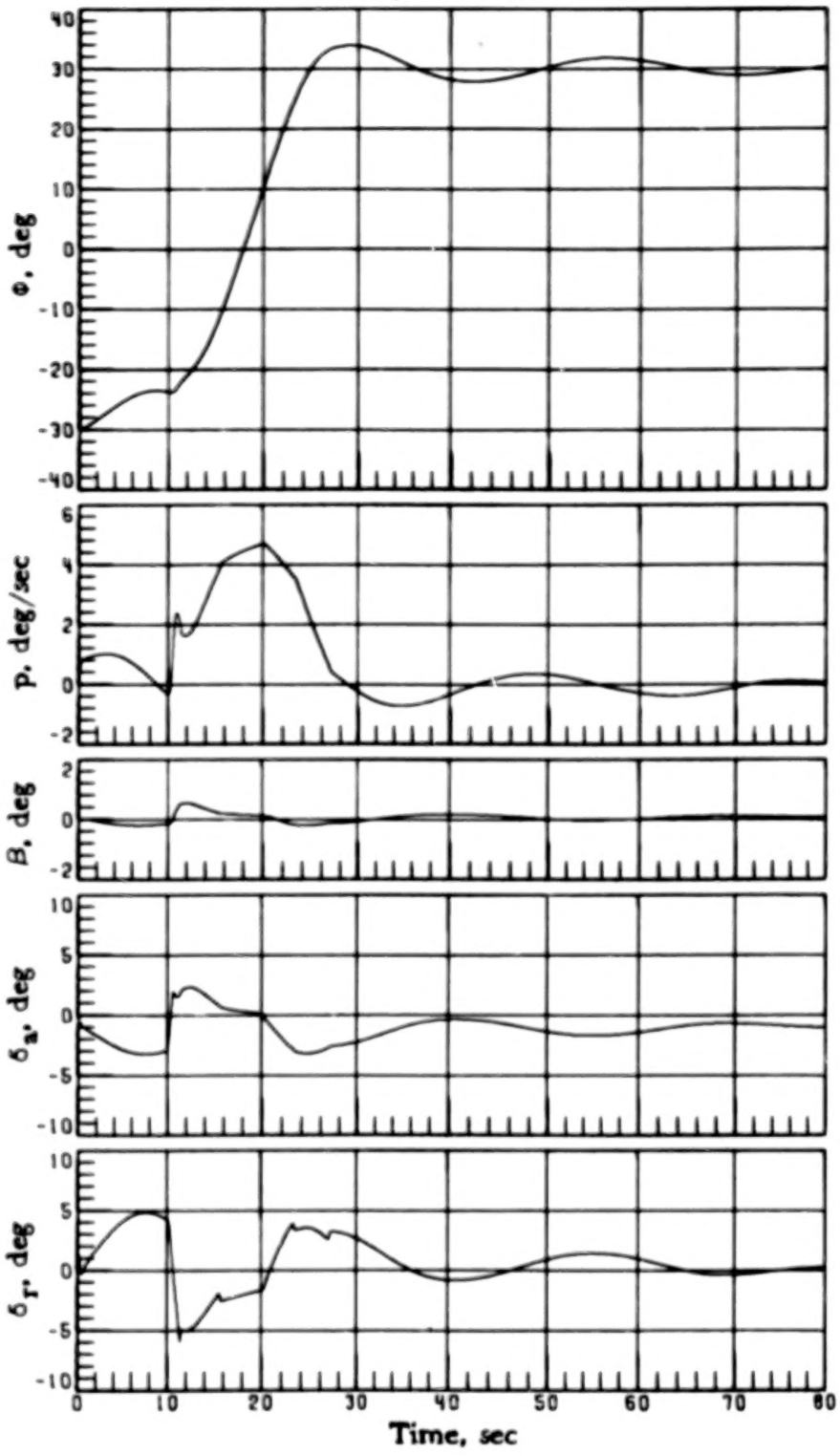

(b) $\Delta C_{n_{\delta a}} = -0.0004$; $\phi_c = -30^\circ$ for time < 10 sec; $\phi_c = 30^\circ$ for time ≥ 10 sec.

Figure 18.- Continued.

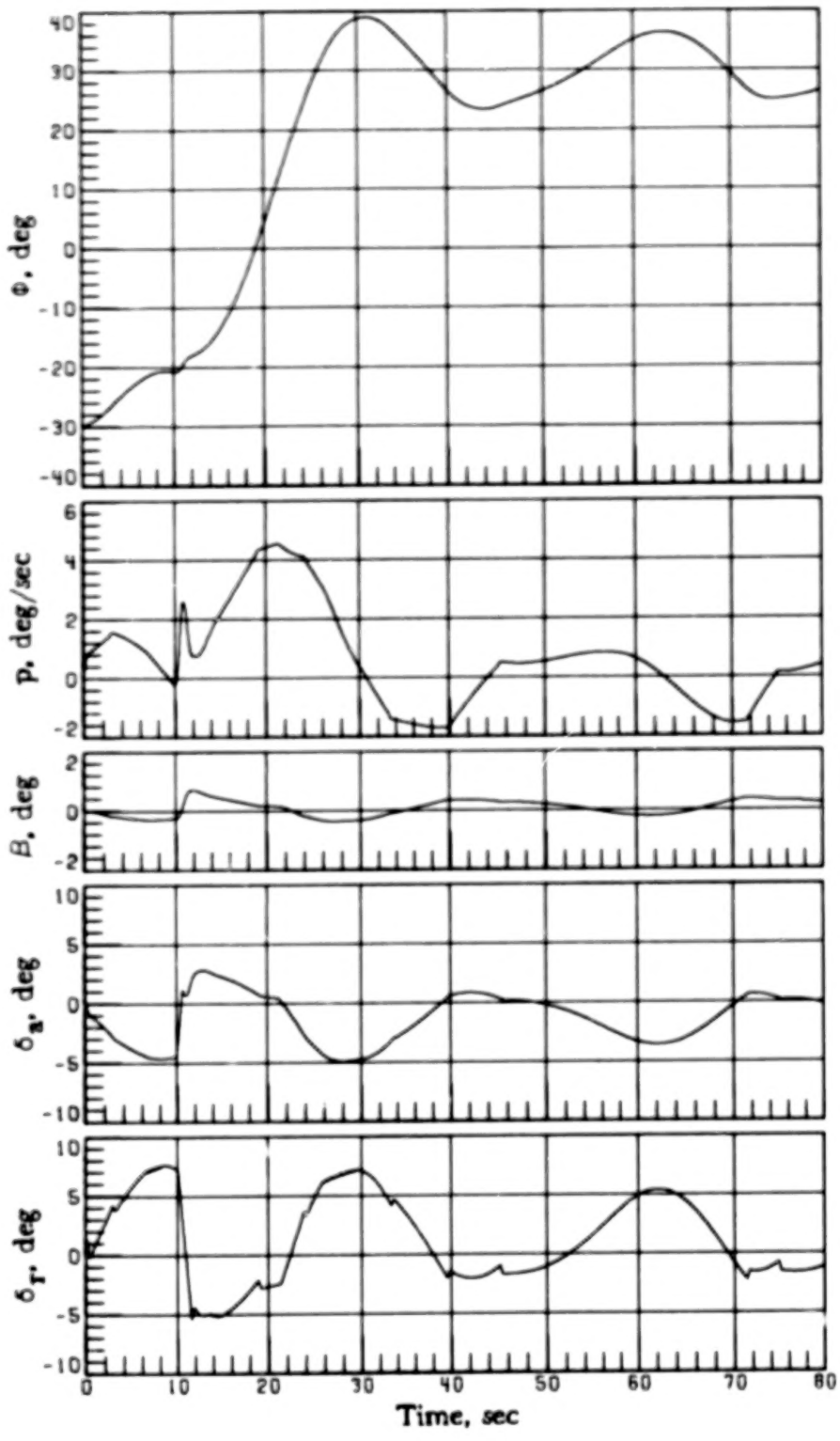

(c) $\Delta C_{n_{\delta a}} = -0.0006$; $\phi_c = -30^\circ$ for time < 10 sec; $\phi_c = 30^\circ$ for time ≥ 10 sec.

Figure 18.- Continued.

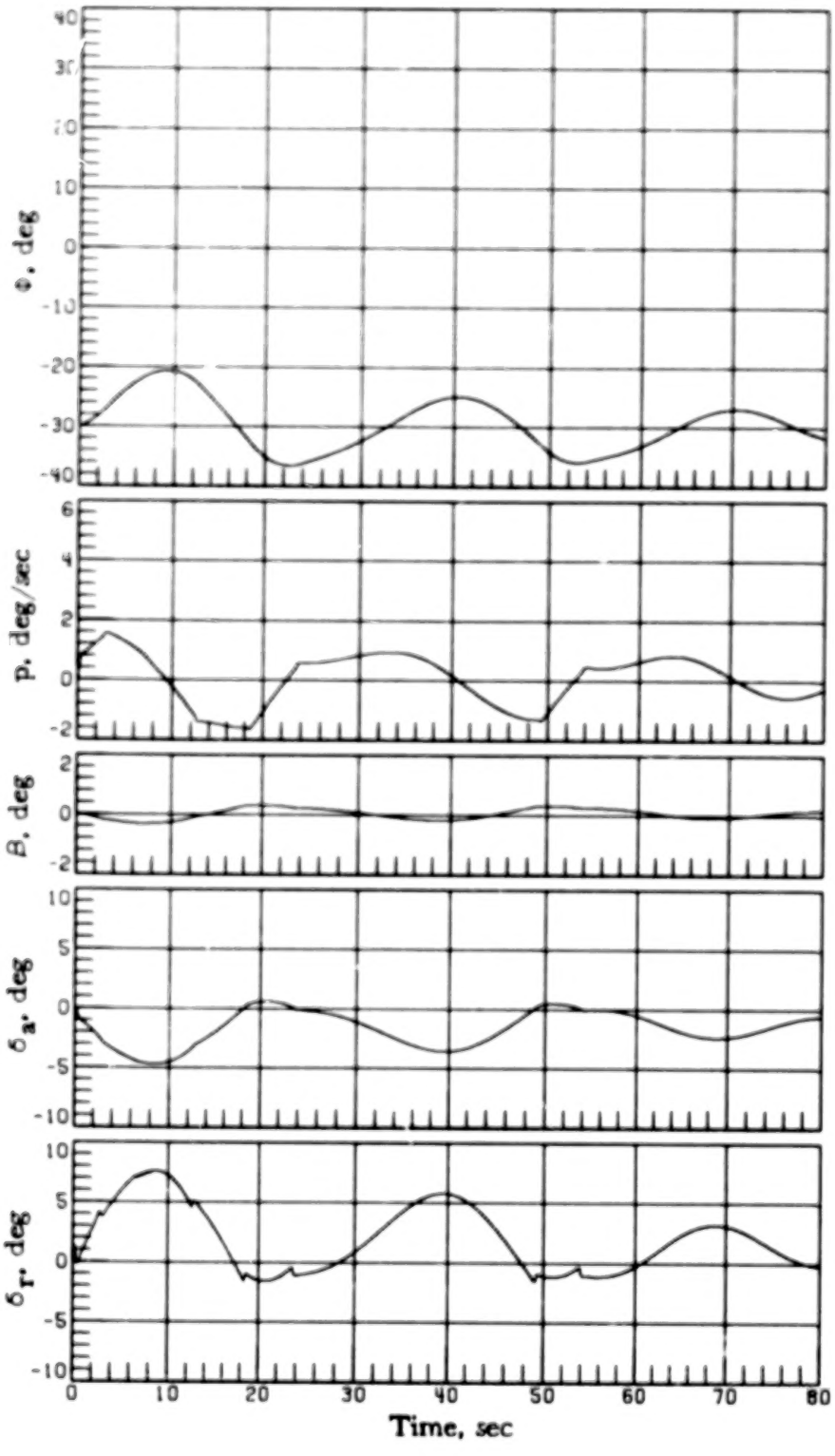

(d) $\Delta C_{n\delta_a} = -0.0006$; $\Phi_c = -30°$.

Figure 18.- Concluded.

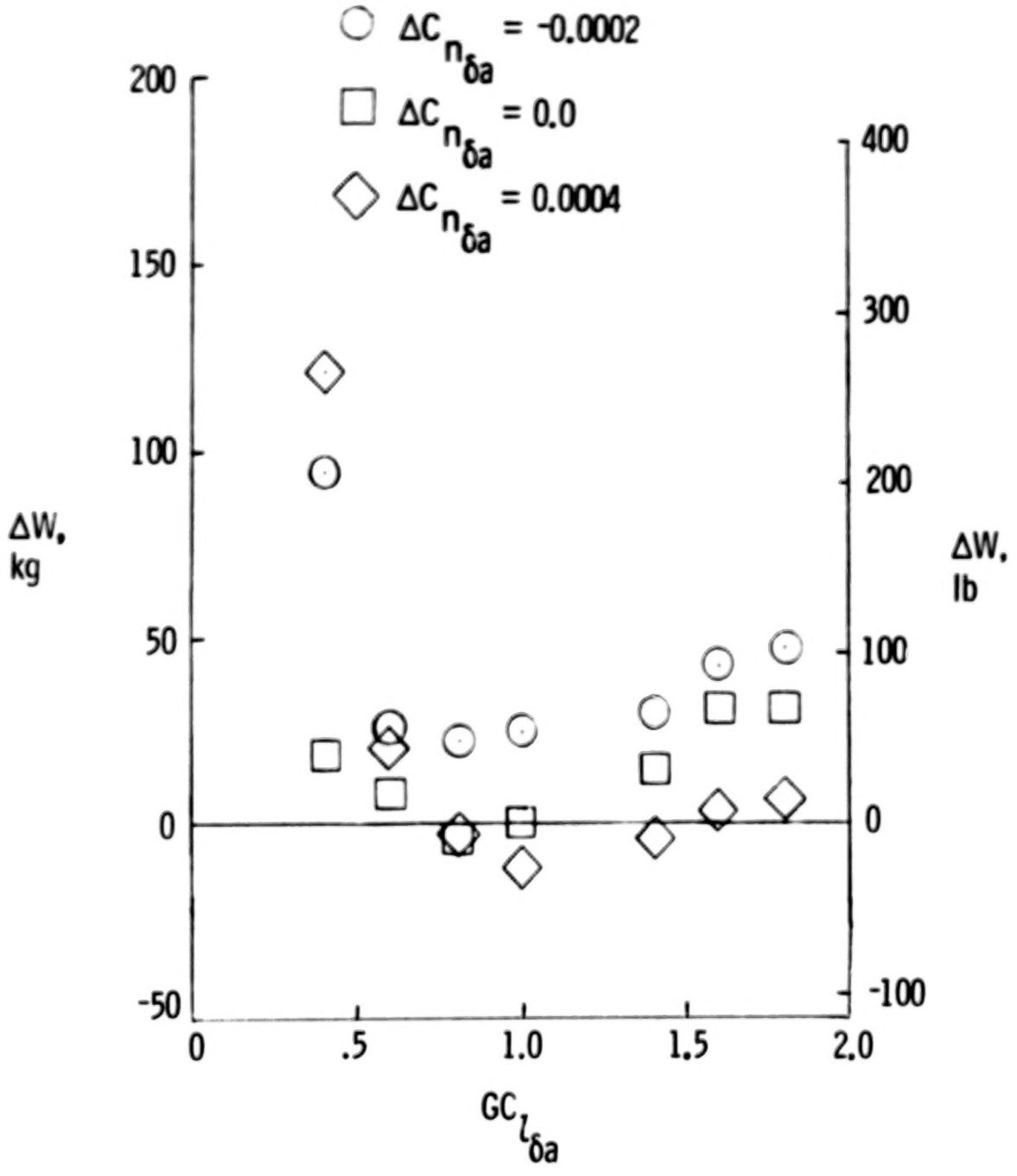

(a) Function of roll due to aileron deflection $C_{l_{\delta a}}$.

Figure 19.- Effect of combined aileron-control-parameter variation $C_{l_{\delta a}}$ and $C_{n_{\delta a}}$ on RCS fuel consumption W.

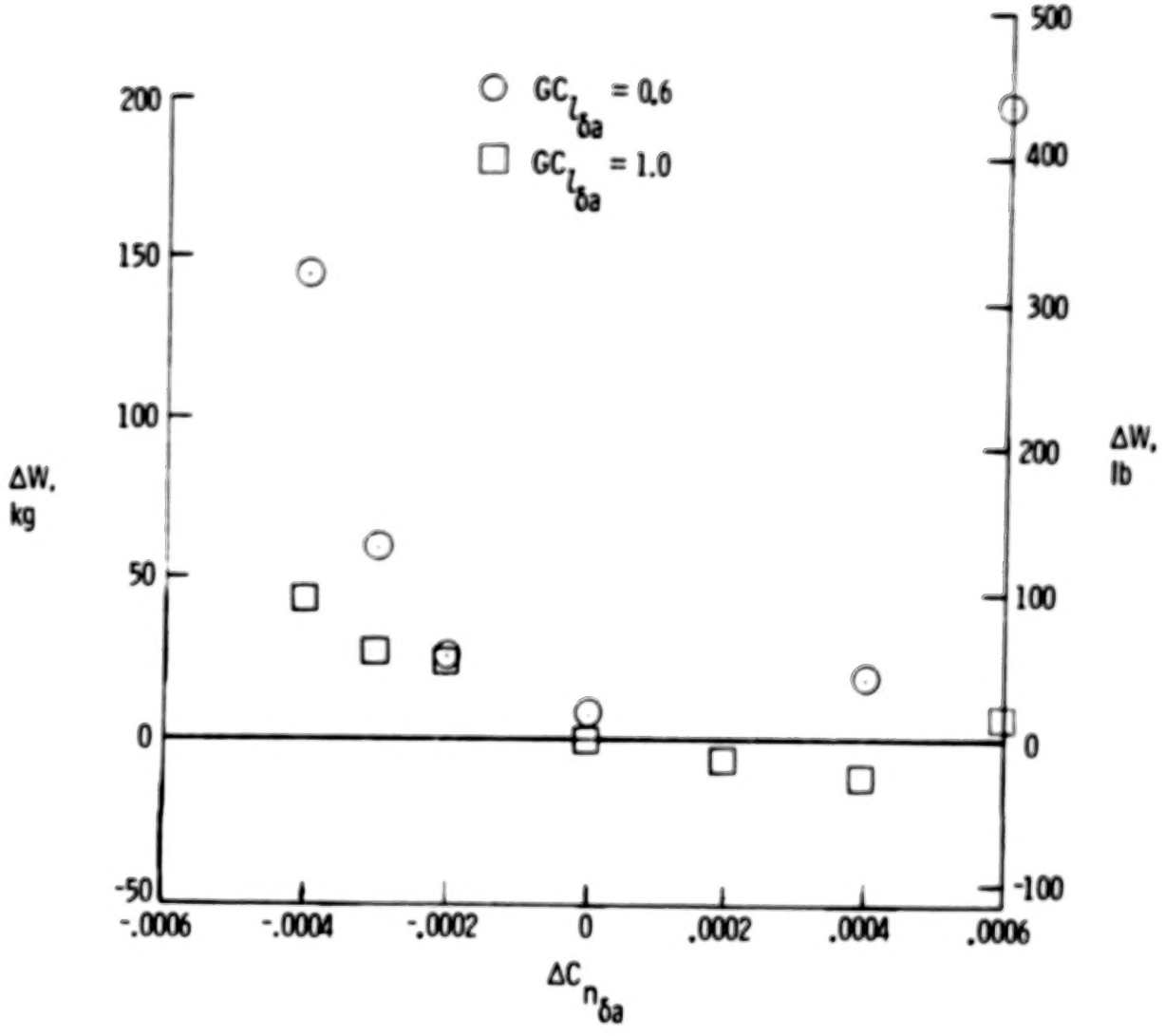

(b) Function of yaw due to aileron deflection $C_{n_{\delta a}}$.

Figure 19.- Concluded.

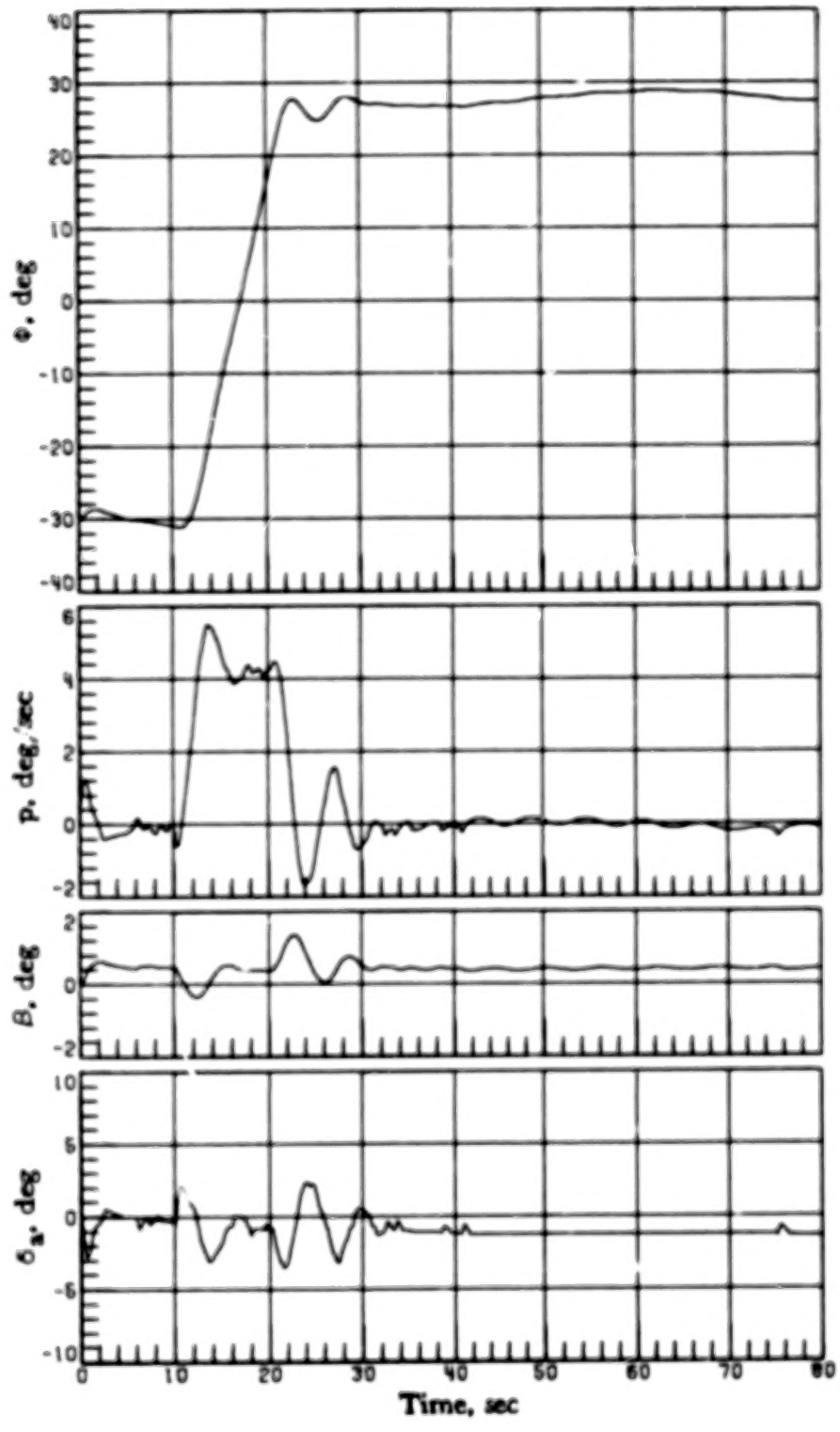

(a) $M_i = 8$; $\alpha_c = 30^\circ$.

Figure 20.- Vehicle-response simulations with $GC_{l_{\delta_a}} = 0.4$ and $\Delta C_{n_{\delta_a}} = -0.0002$. $\Phi_c = -30^\circ$ for time < 10 sec; $\Phi_c = 30^\circ$ for time ≥ 10 sec.

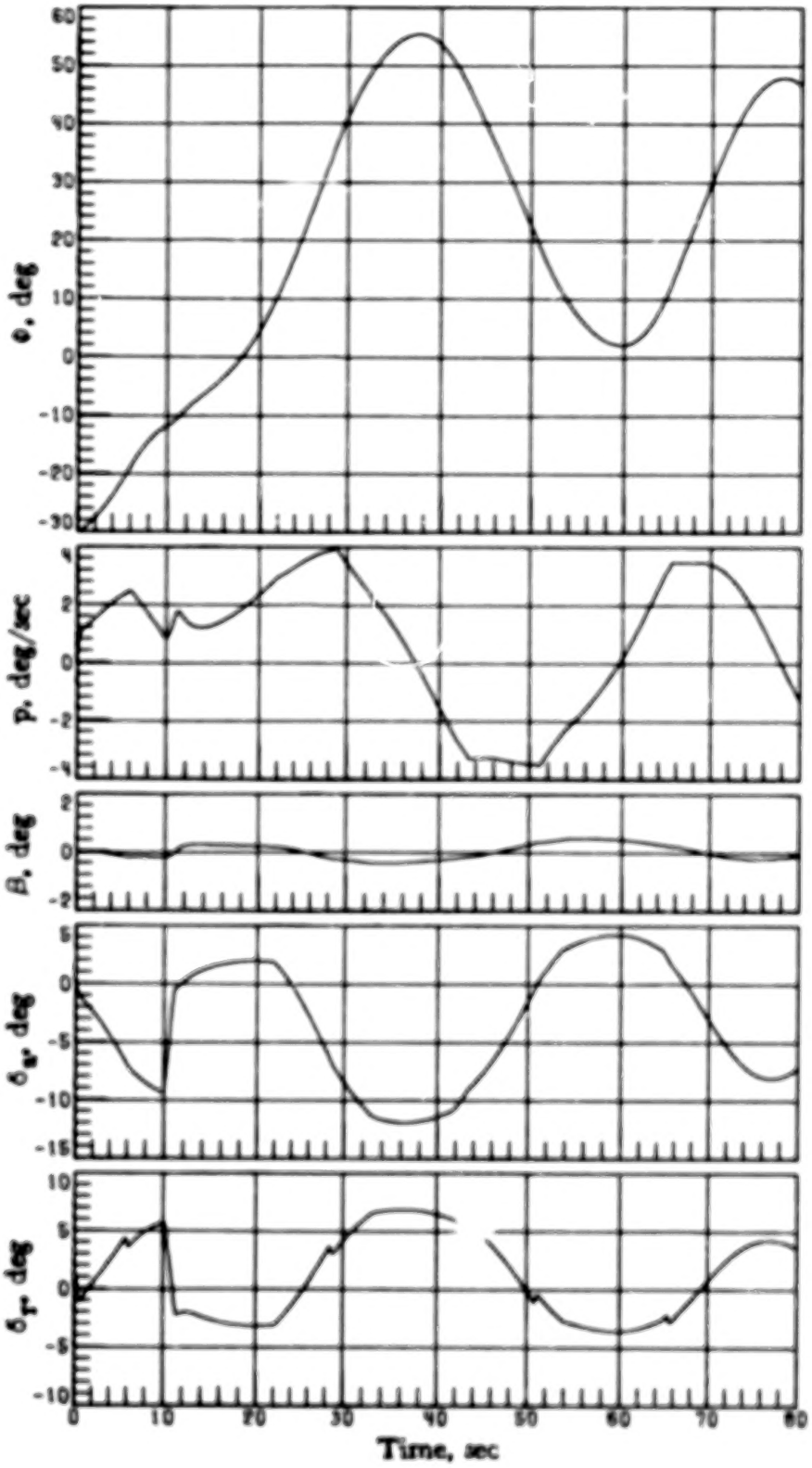

(b) $M_1 = 4$; $\alpha_c = 17.6^\circ$.

Figure 20.- Concluded.

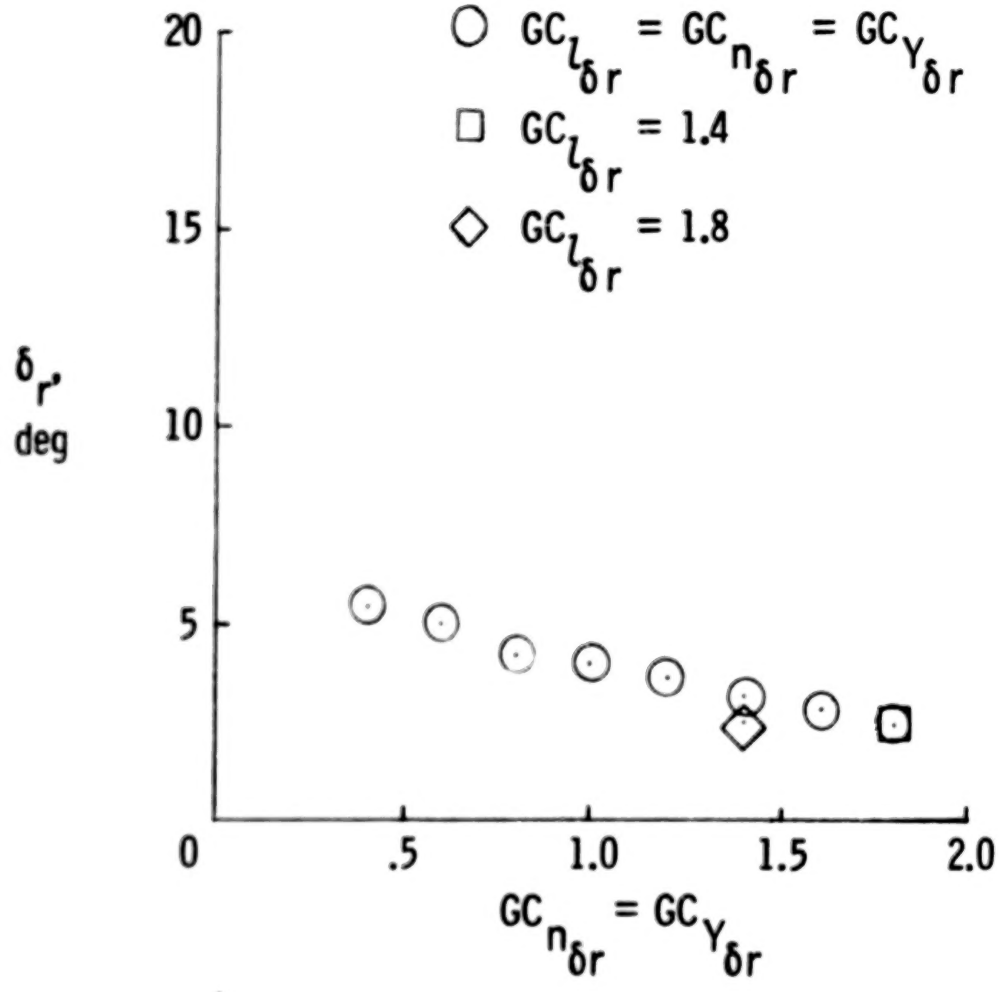

Figure 21.- Maximum rudder deflection δ_r as a function of rudder-control-parameter variation $C_{n_{\delta r}}$, $C_{l_{\delta r}}$, and $C_{Y_{\delta r}}$ for a commanded roll-angle reversal at 853 m/sec (2800 ft/sec).

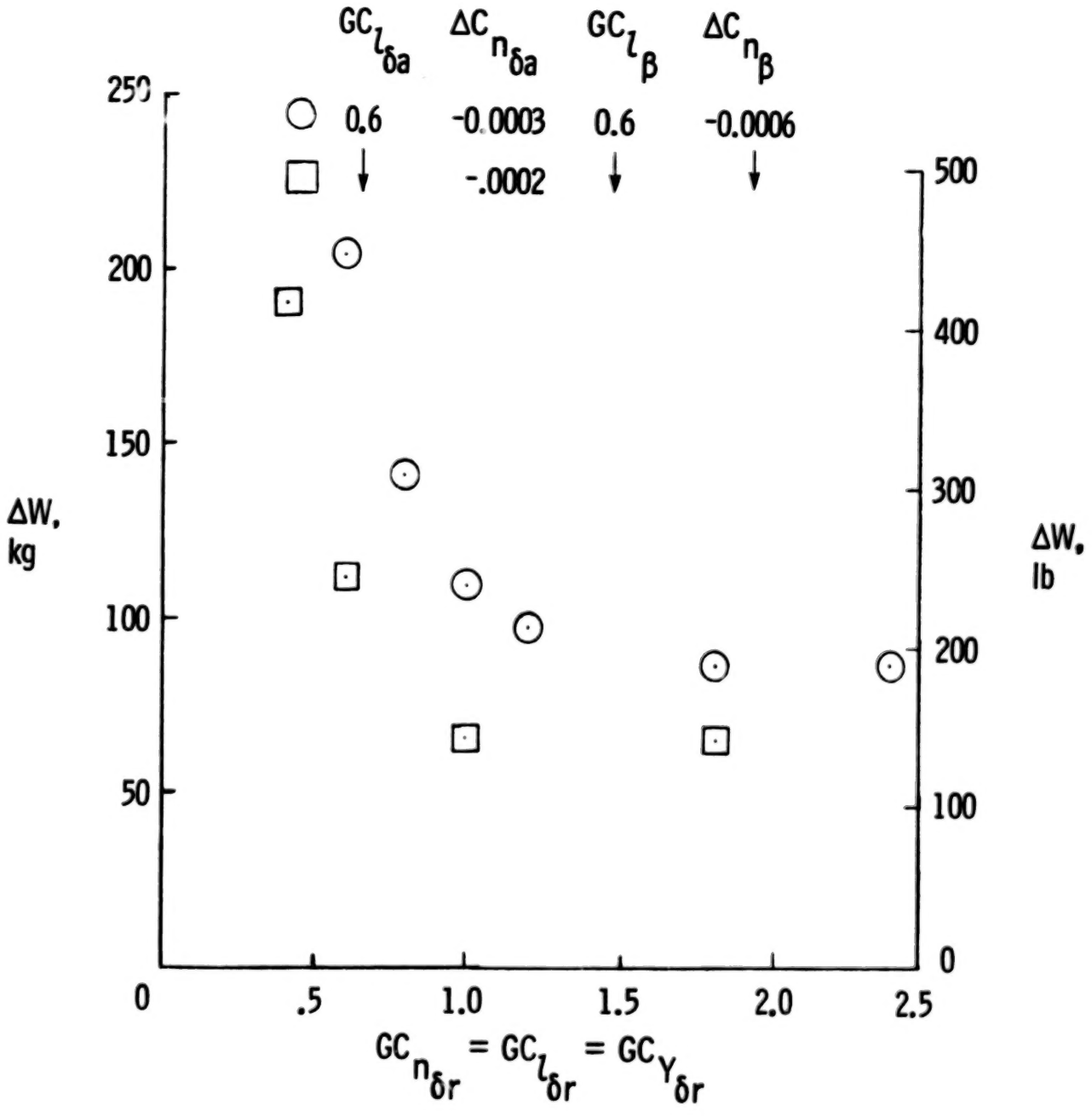

Figure 22.- Effect of rudder-control-parameter variation $C_{n_{\delta r}}$, $C_{l_{\delta r}}$, and $C_{Y_{\delta r}}$ with varied aileron-control parameters $C_{l_{\delta a}}$ and $C_{n_{\delta a}}$ and lateral-directional stability parameters C_{l_β} and C_{n_β} on RCS fuel consumption W.

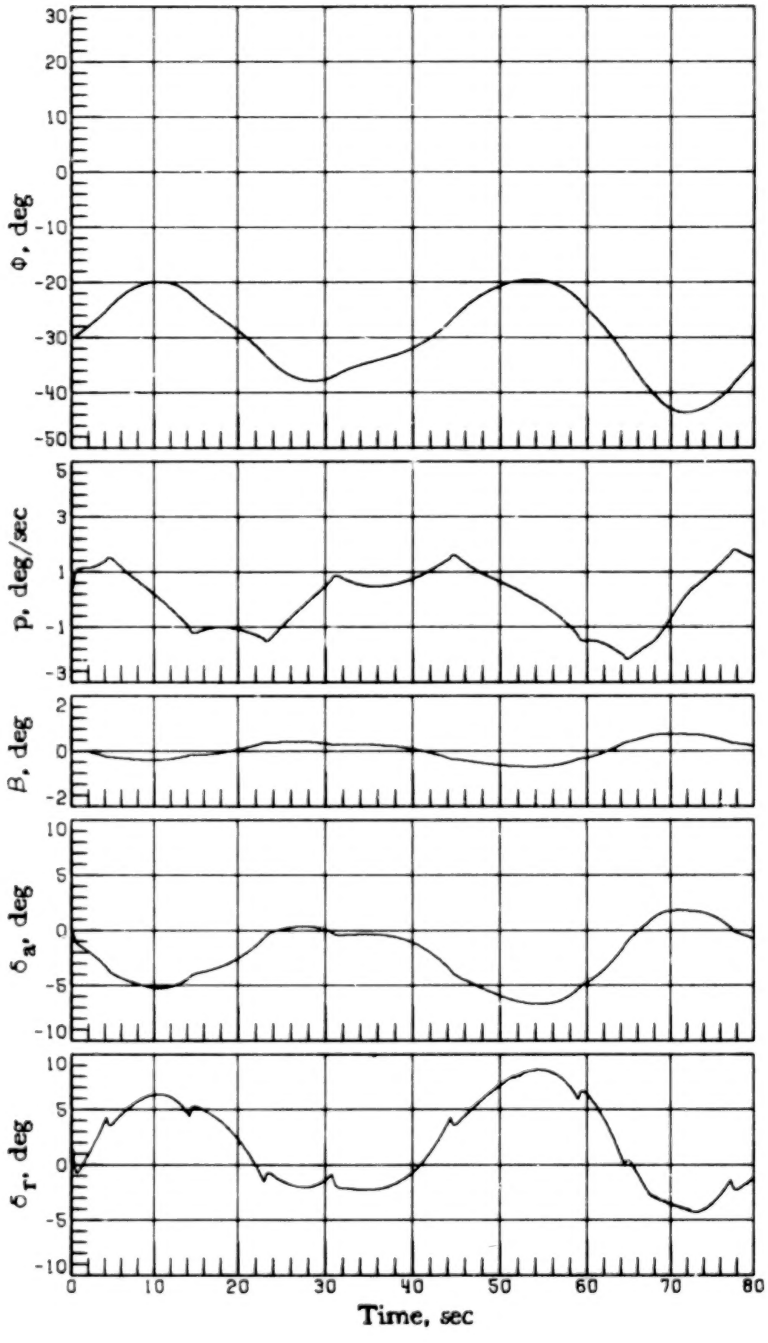

(a) $\phi_c = -30^\circ$.

Figure 23.- Vehicle-response simulations at $M_i = 4$ with $\alpha_c = 17.6^\circ$, $GC_{l_\beta} = 0.6$, $\Delta C_{n_\beta} = -0.0006$, $GC_{l_{\delta a}} = 0.6$, $\Delta C_{n_{\delta a}} = -0.0002$, and $GC_{n_{\delta r}} = GC_{l_{\delta r}} = GC_{Y_{\delta r}} = 0.6$.

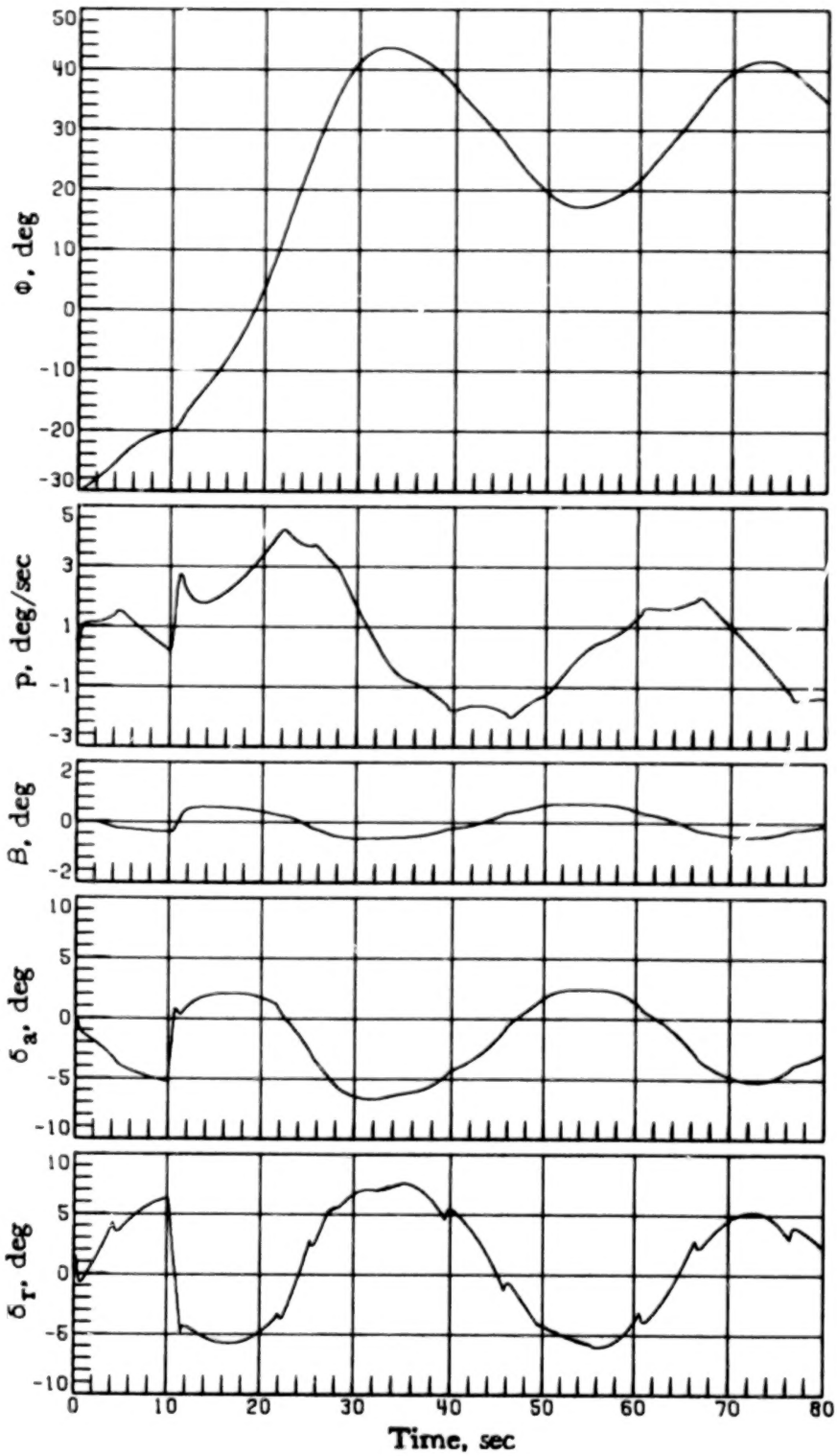

(b) $\phi_c = -30^\circ$ for time < 10 sec; $\phi_c = 30^\circ$ for time ≥ 10 sec.

Figure 23.- Concluded.

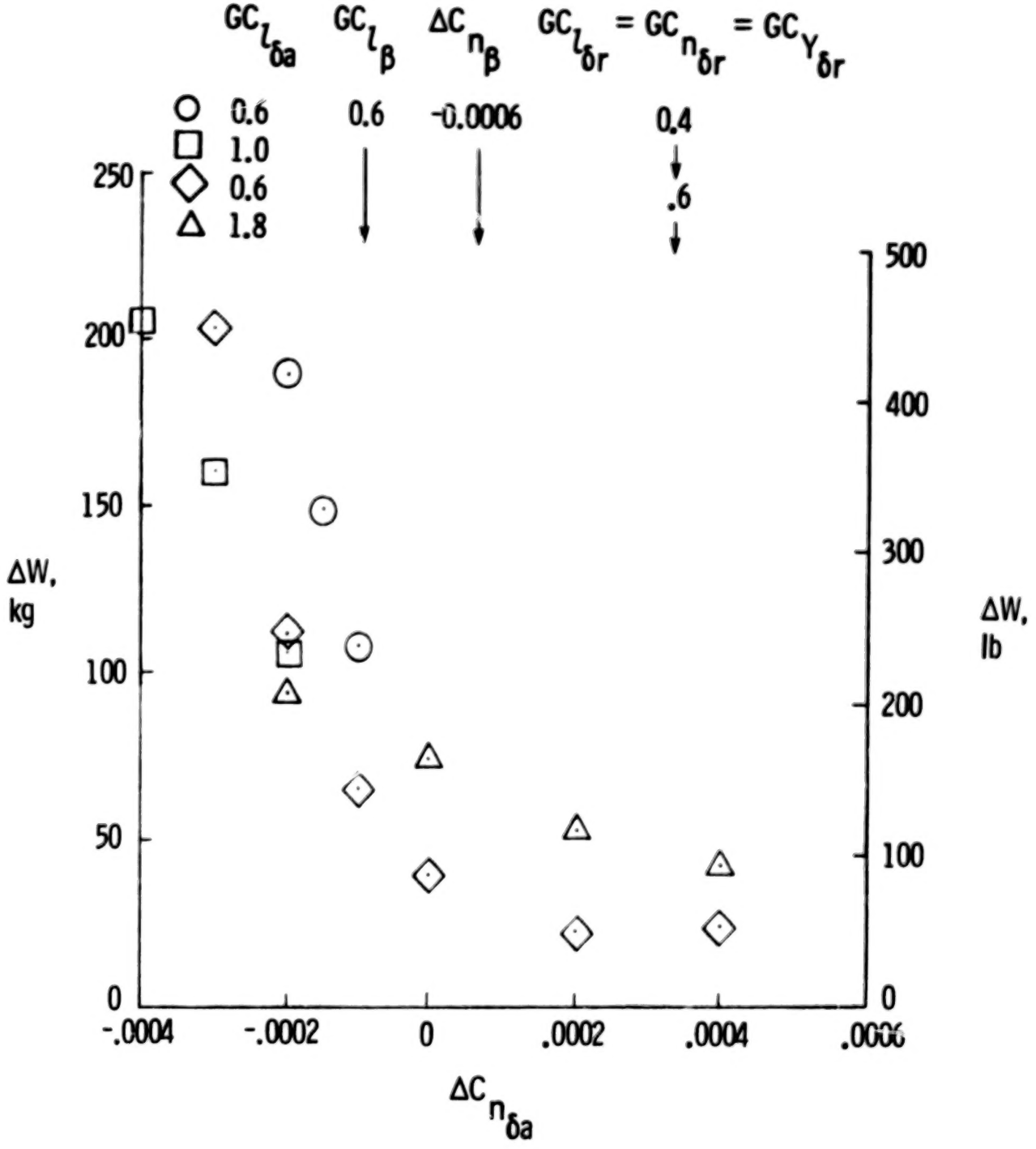

Figure 24.- Effect of yaw due to aileron deflection $C_{n_{\delta a}}$ with varied roll due to aileron deflection $C_{l_{\delta a}}$, rudder-control parameters $C_{n_{\delta r}}$, $C_{l_{\delta r}}$, and $C_{Y_{\delta r}}$, and lateral-directional stability parameters C_{l_β} and C_{n_β} on RCS fuel consumption W.

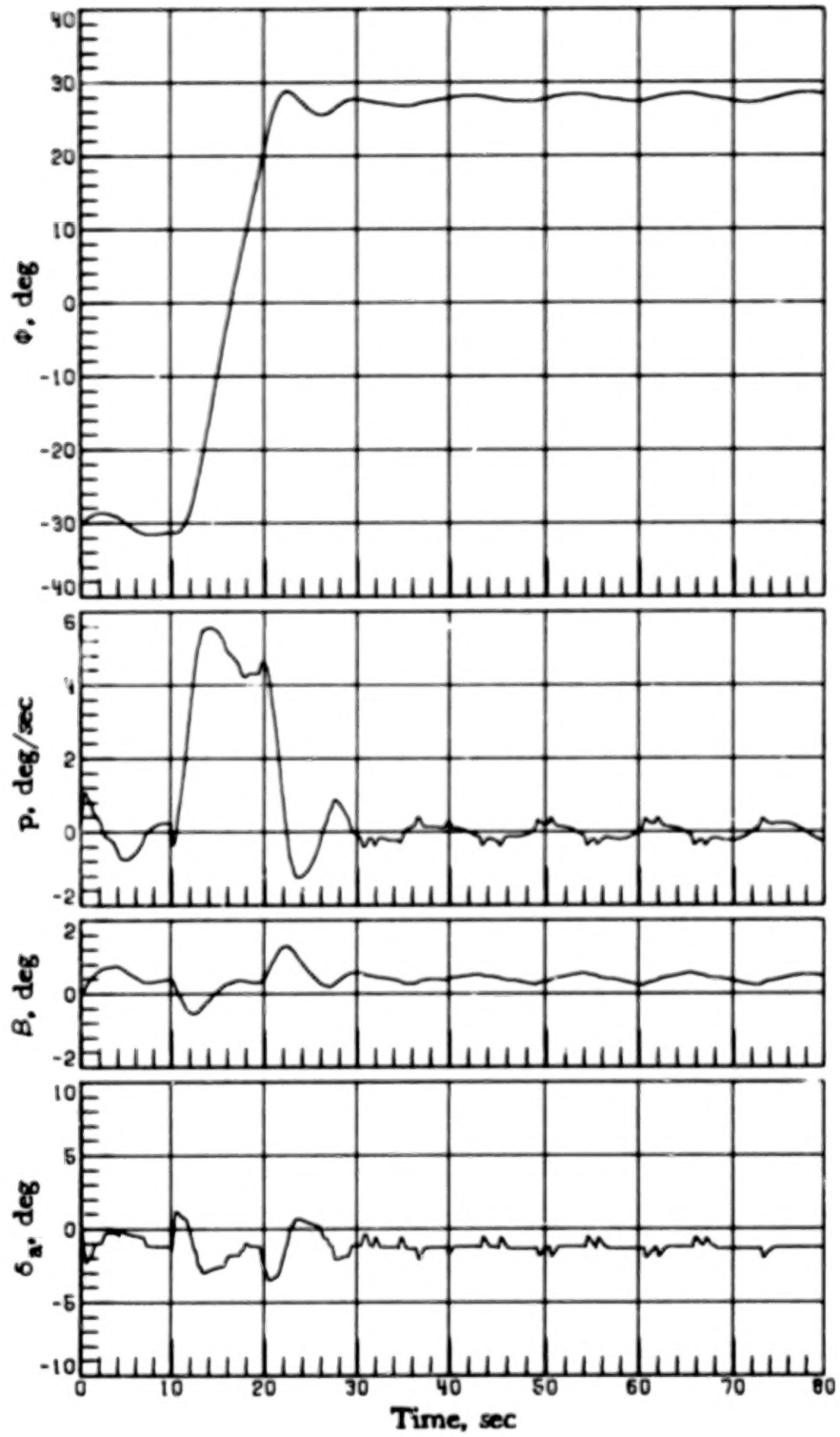

Figure 25.- Vehicle-response simulations at $M_i = 8$ with $GC_{l_\beta} = 0.6$, $\Delta C_{n_\beta} = -0.0006$, $GC_{l_{\delta a}} = 0.6$, and $\Delta C_{n_{\delta a}} = -0.0004$. $\alpha_c = 30^\circ$; $\phi_c = -30^\circ$ for time < 10 sec; $\phi_c = 30^\circ$ for time ≥ 10 sec.

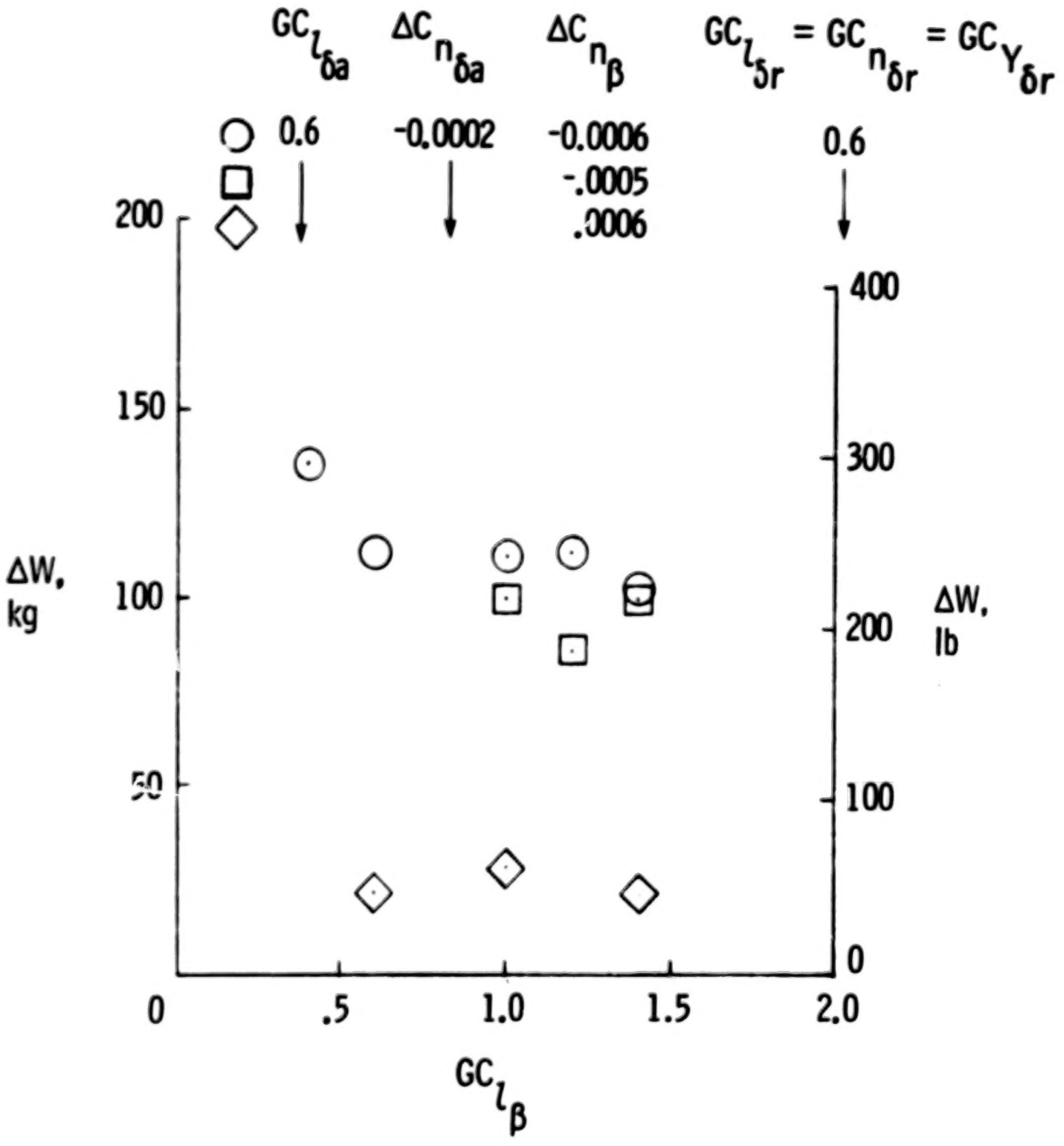

Figure 26.- Result of variation of effective dihedral C_{l_β} with varied directional stability C_{n_β}, aileron-control parameters $C_{l_{\delta a}}$ and $C_{n_{\delta a}}$, and rudder-control parameters $C_{n_{\delta r}}$, $C_{l_{\delta r}}$, and $C_{Y_{\delta r}}$ on RCS fuel consumption W.

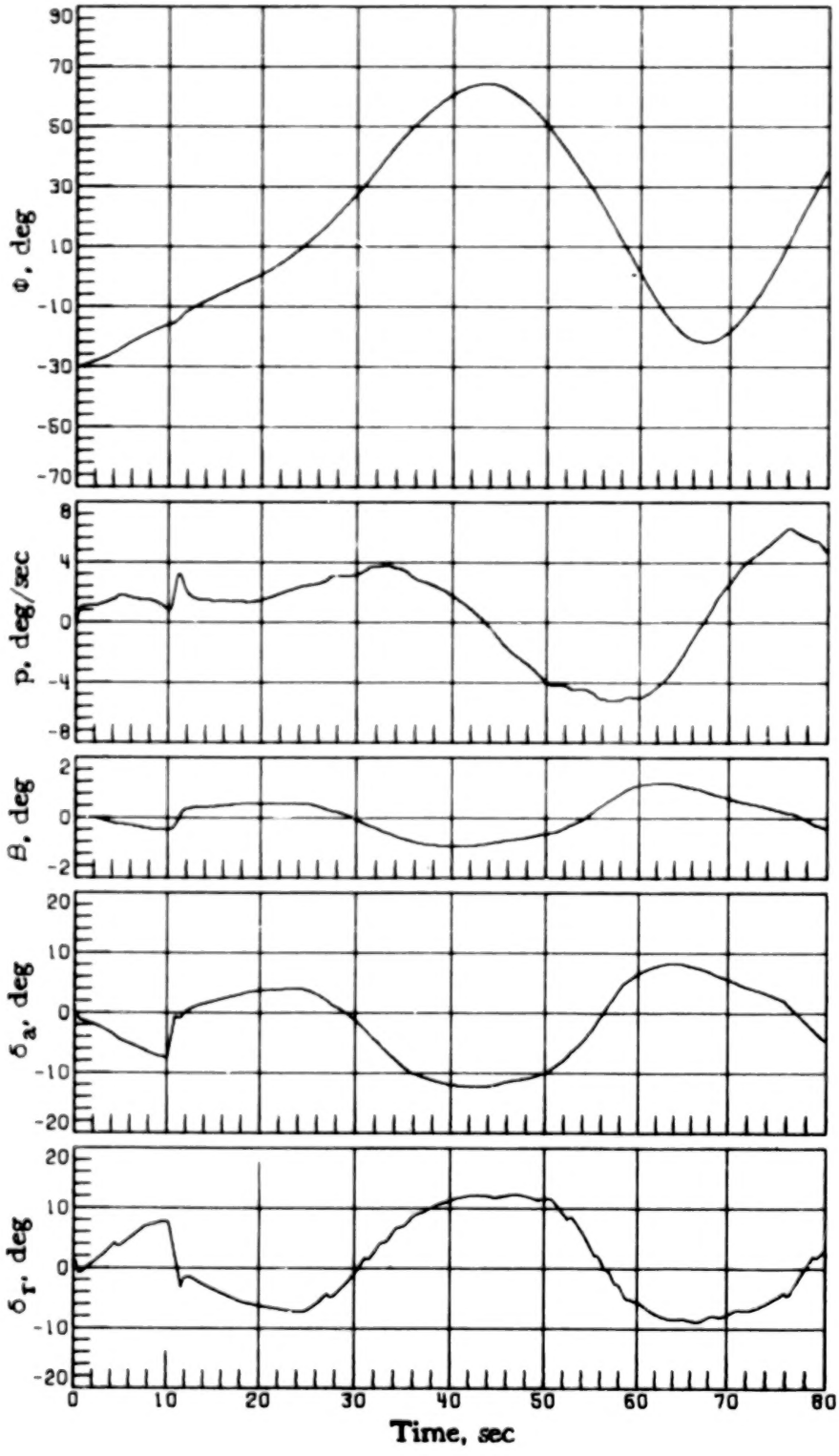

(a) $M_i = 4$; $\alpha_c = 17.6^o$; $\phi_c = -30^o$ for time < 10 sec;
$\phi_c = 30^o$ for time ≥ 10 sec.

Figure 27.- Vehicle-response simulations with $GC_{l_\beta} = 1.4$, $\Delta C_{n_\beta} = -0.0006$, $GC_{l_{\delta a}} = 0.6$, $\Delta C_{n_{\delta a}} = -0.0002$, and $GC_{n_{\delta r}} = GC_{l_{\delta r}} = GC_{Y_{\delta r}} = 0.6$.

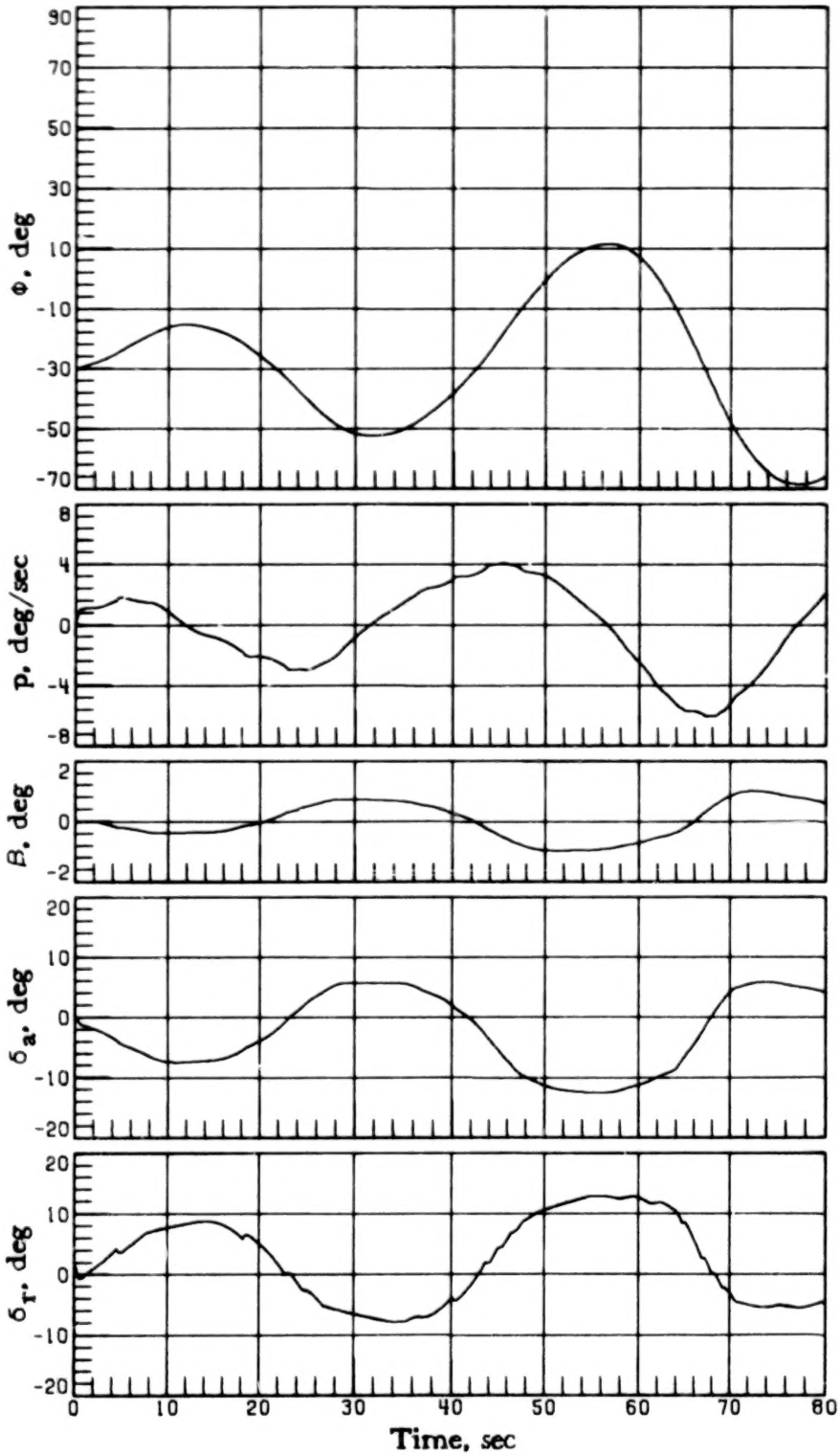

(b) $M_i = 4$; $\alpha_c = 17.6^o$; $\phi_c = -30^o$.

Figure 27.- Continued.

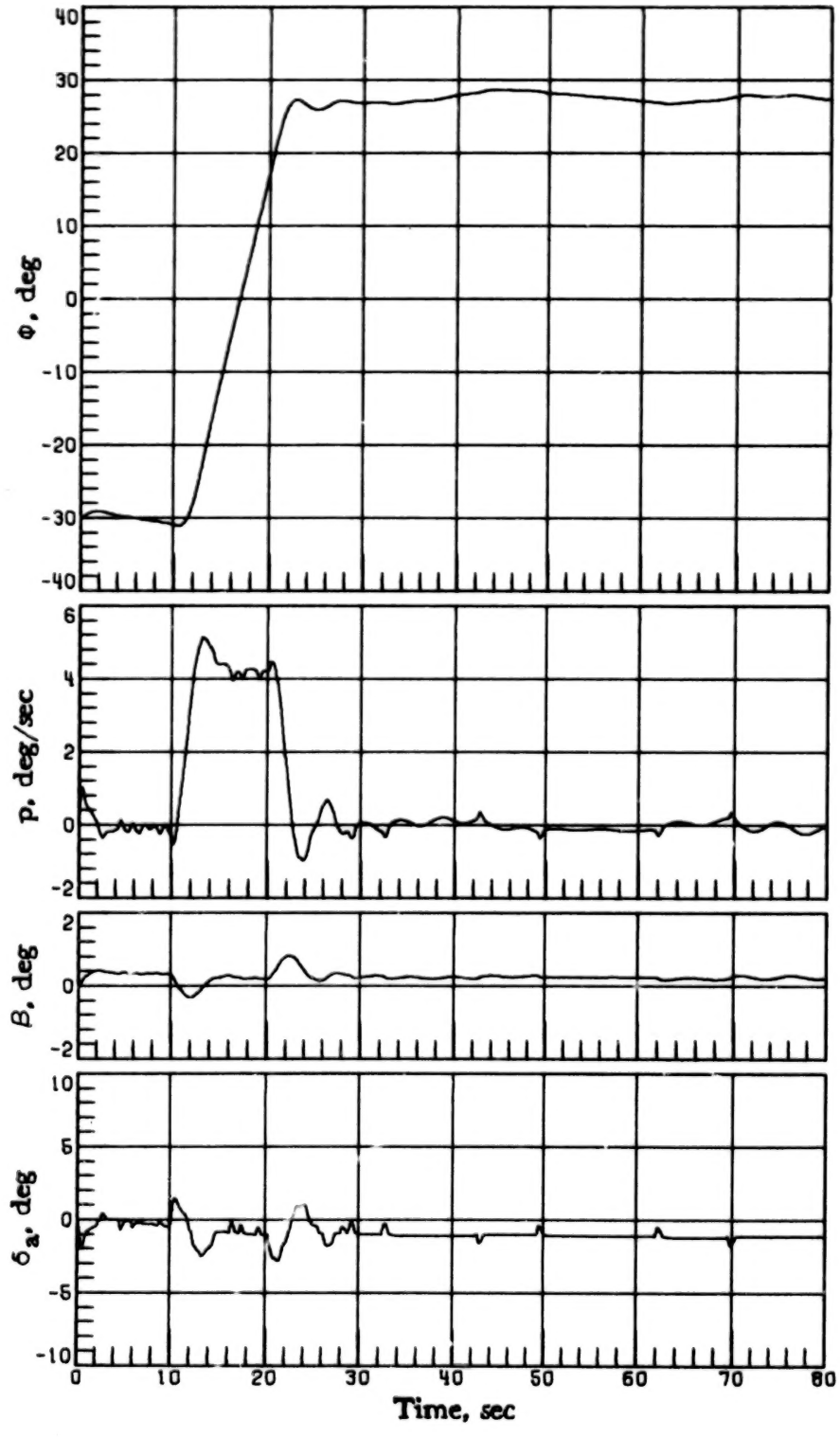

(c) $M_i = 8$; $\alpha_c = 30^o$; $\phi_c = -30^o$ for time < 10 sec; $\phi_c = 30^o$ for time ≥ 10 sec.

Figure 27.- Concluded.

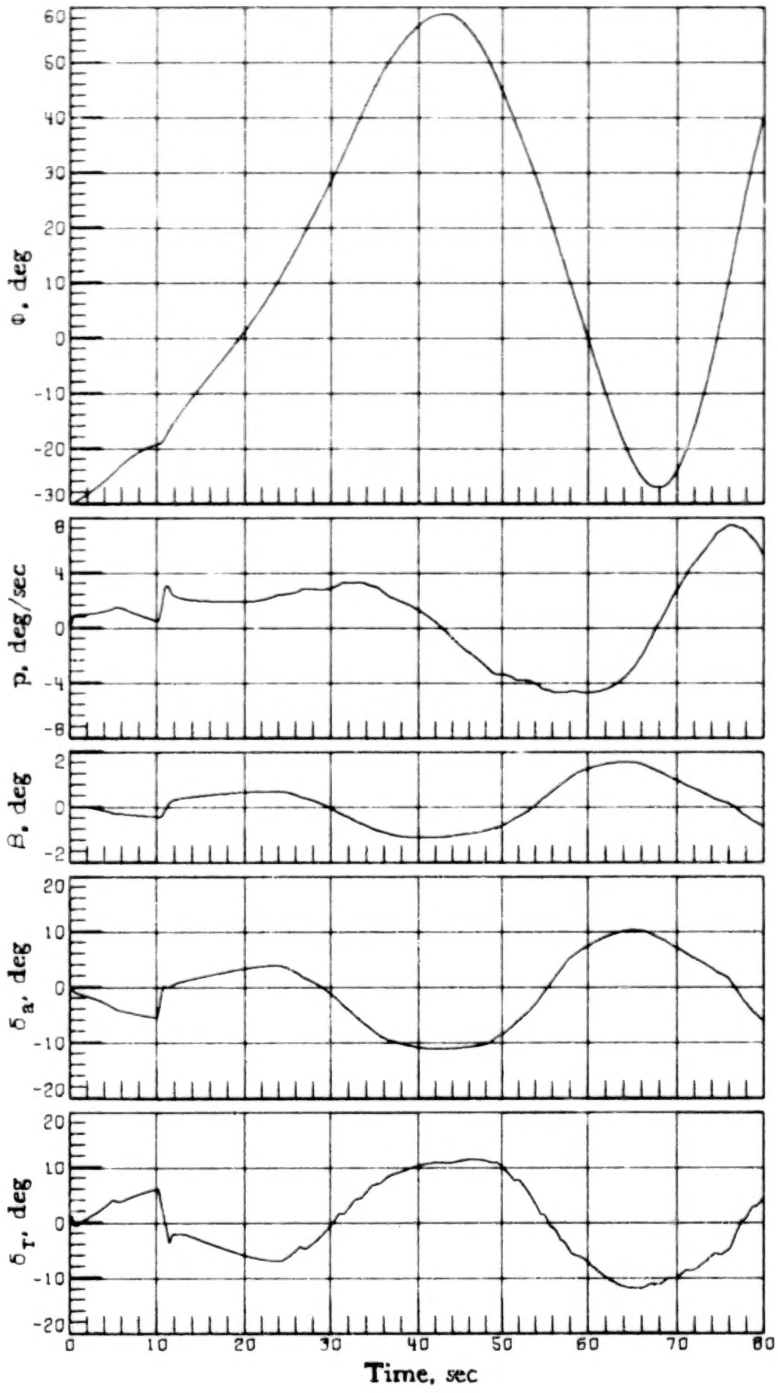

(a) $M_i = 4$; $GC_{l_\beta} = 1.3$; $\alpha_c = 17.6^\circ$.

Figure 28.- Vehicle-response simulations with varying dihedral effect GC_{l_β}, $\Delta C_{n_\beta} = -0.0006$, $GC_{Y_\beta} = 0.7$, $GC_{l_{\delta a}} = 0.7$, $\Delta C_{n_{\delta a}} = -0.0002$, and $GC_{n_{\delta r}} = GC_{l_{\delta r}} = GC_{Y_{\delta r}} = 0.7$. $\phi_c = -30^\circ$ for time < 10 sec; $\phi_c = 30^\circ$ for time ≥ 10 sec.

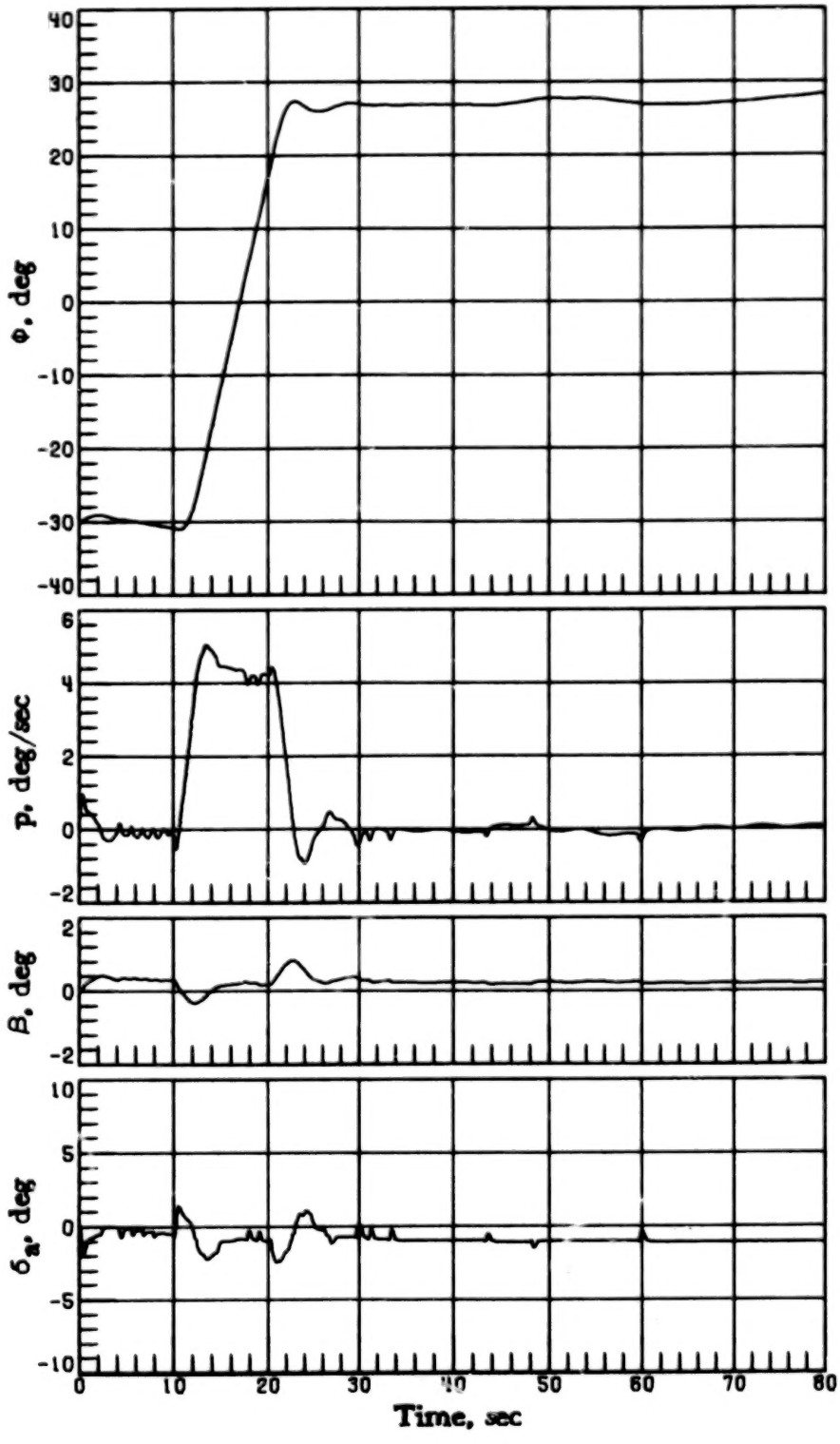

(b) $M_i = 8$; $GC_{l_\beta} = 1.3$; $\alpha_c = 30^\circ$.

Figure 28.- Continued.

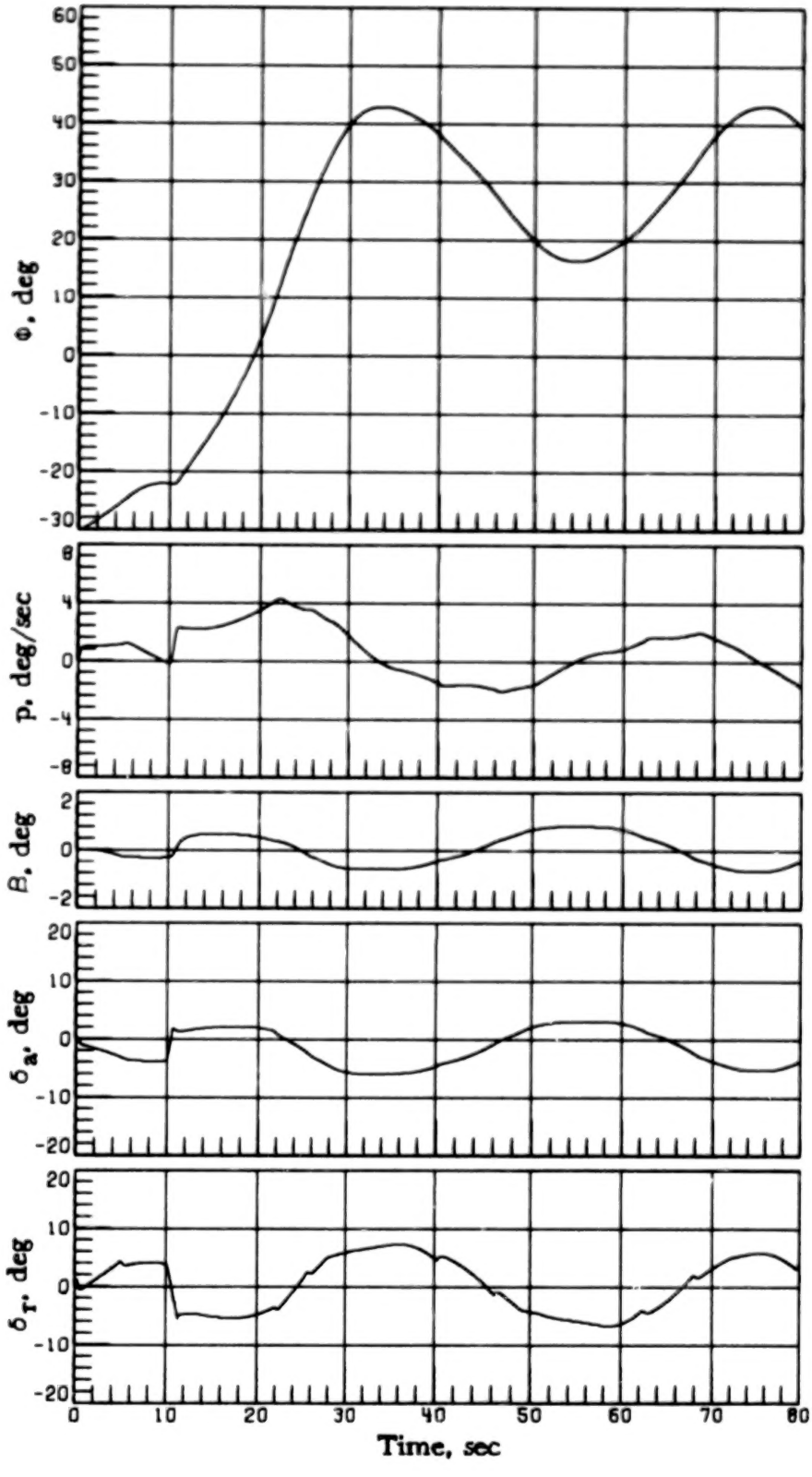

(c) $M_i = 4$; $GC_{l_\beta} = 0.6$; $\alpha_c = 17.6^\circ$.

Figure 28.- Continued.

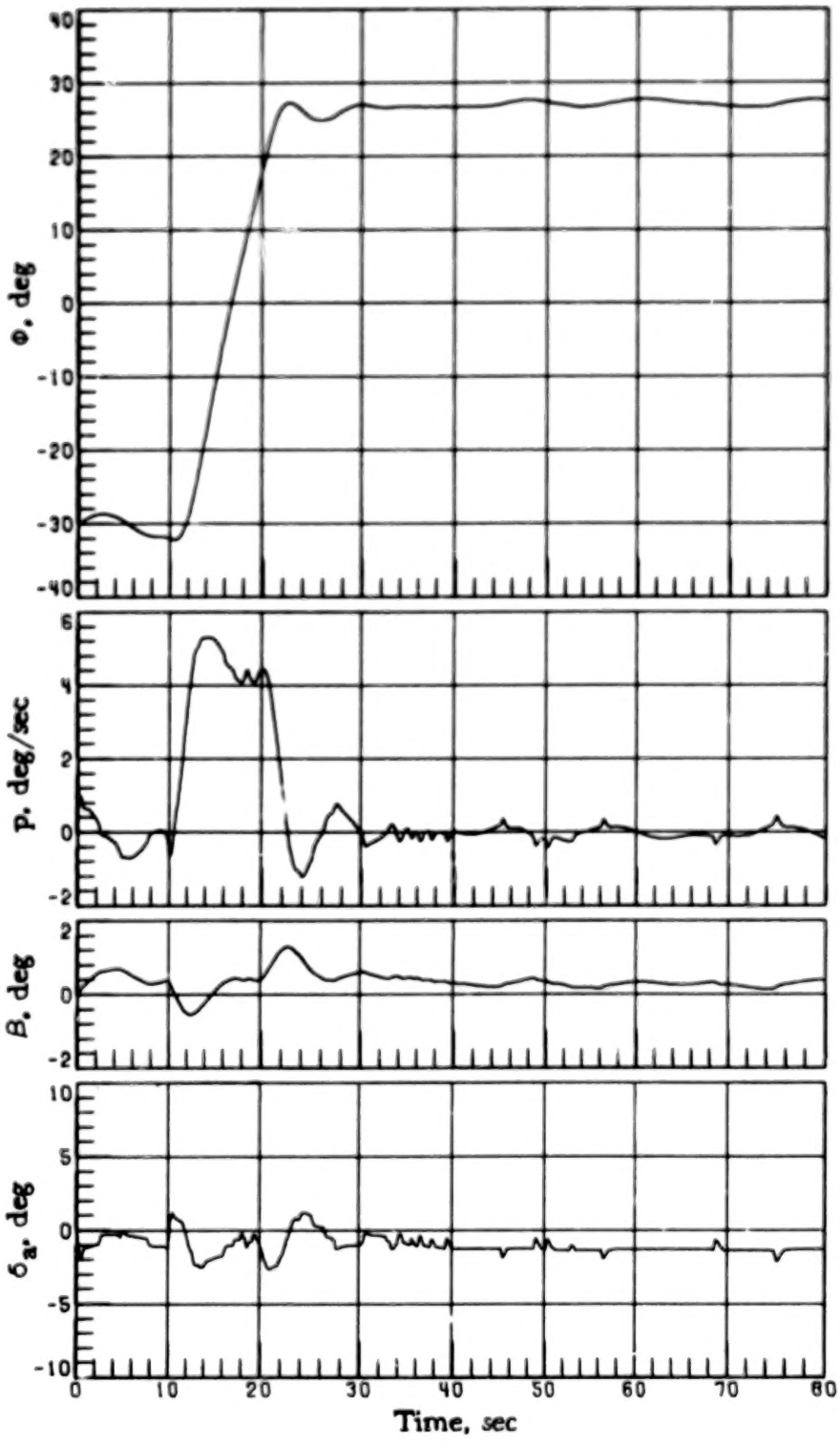

(d) $M_i = 8$; $GC_{l_\beta} = 0.6$; $\alpha_c = 30^\circ$.

Figure 28.- Concluded.

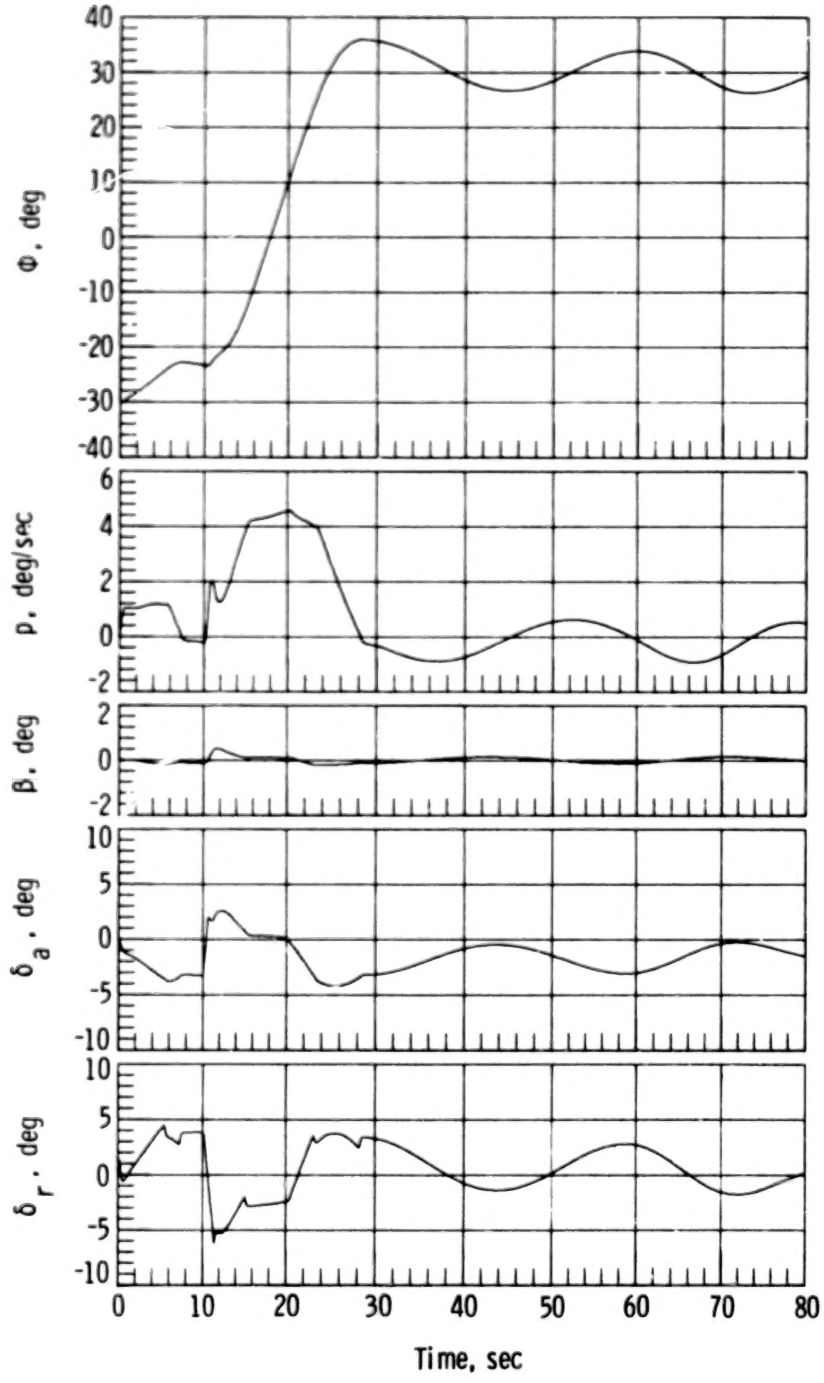

(a) $M_i = 4$; $\alpha_c = 17.6^\circ$.

Figure 29.- Vehicle-response simulations with $GC_{l_\beta} = 1.3$, $\Delta C_{n_\beta} = -0.0006$, $GC_{Y_\beta} = 1.8$, $GC_{l_{\delta a}} = 0.7$, $\Delta C_{n_{\delta a}} = -0.0002$, and $GC_{n_{\delta r}} = GC_{l_{\delta r}} = GC_{Y_{\delta r}} = 0.7$. $\phi_c = -30^\circ$ for time < 10 sec; $\phi_c = 30^\circ$ for time ≥ 10 sec.

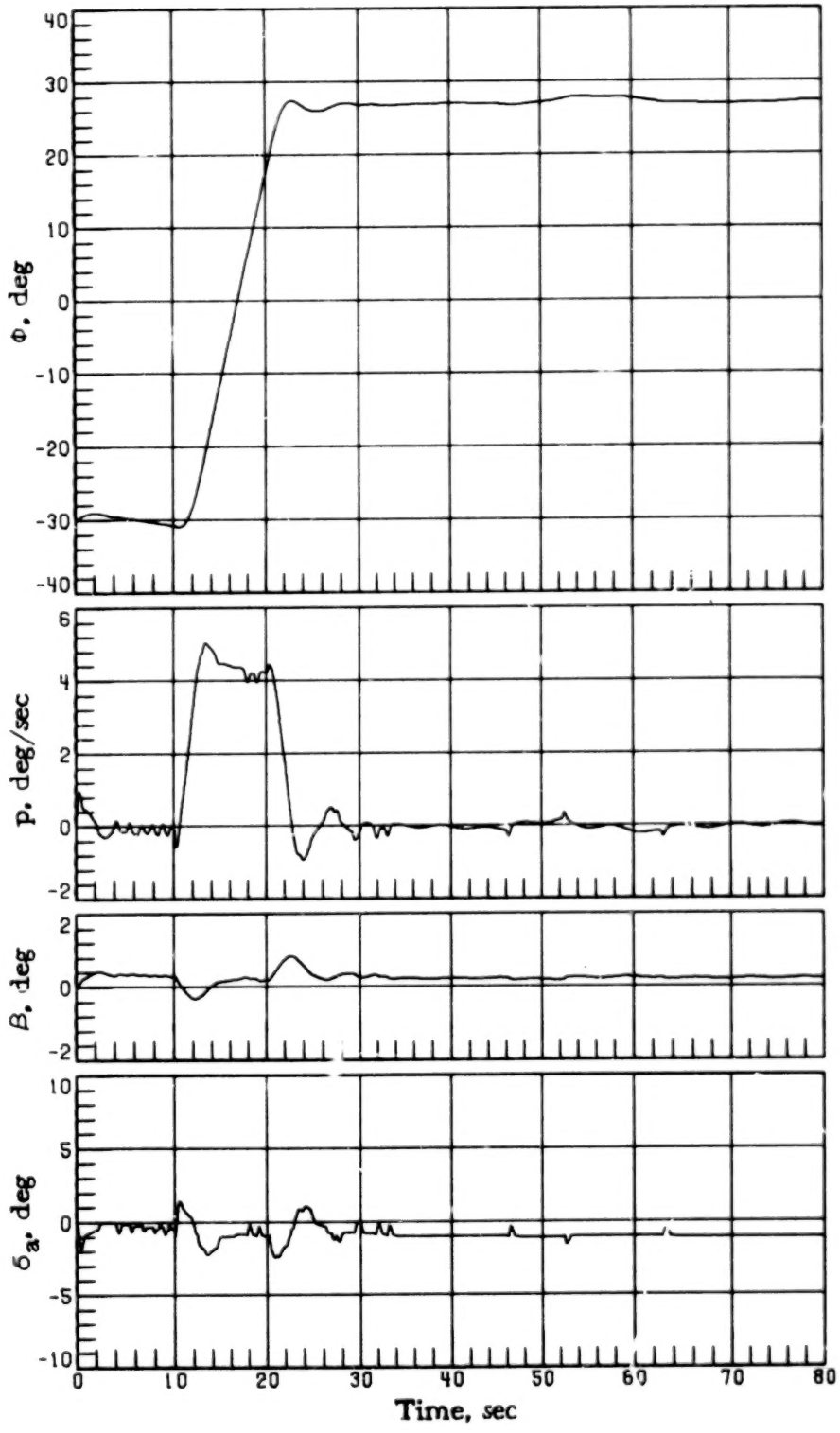

(b) $M_i = 8$; $\alpha_c = 30^o$.

Figure 29.- Concluded.

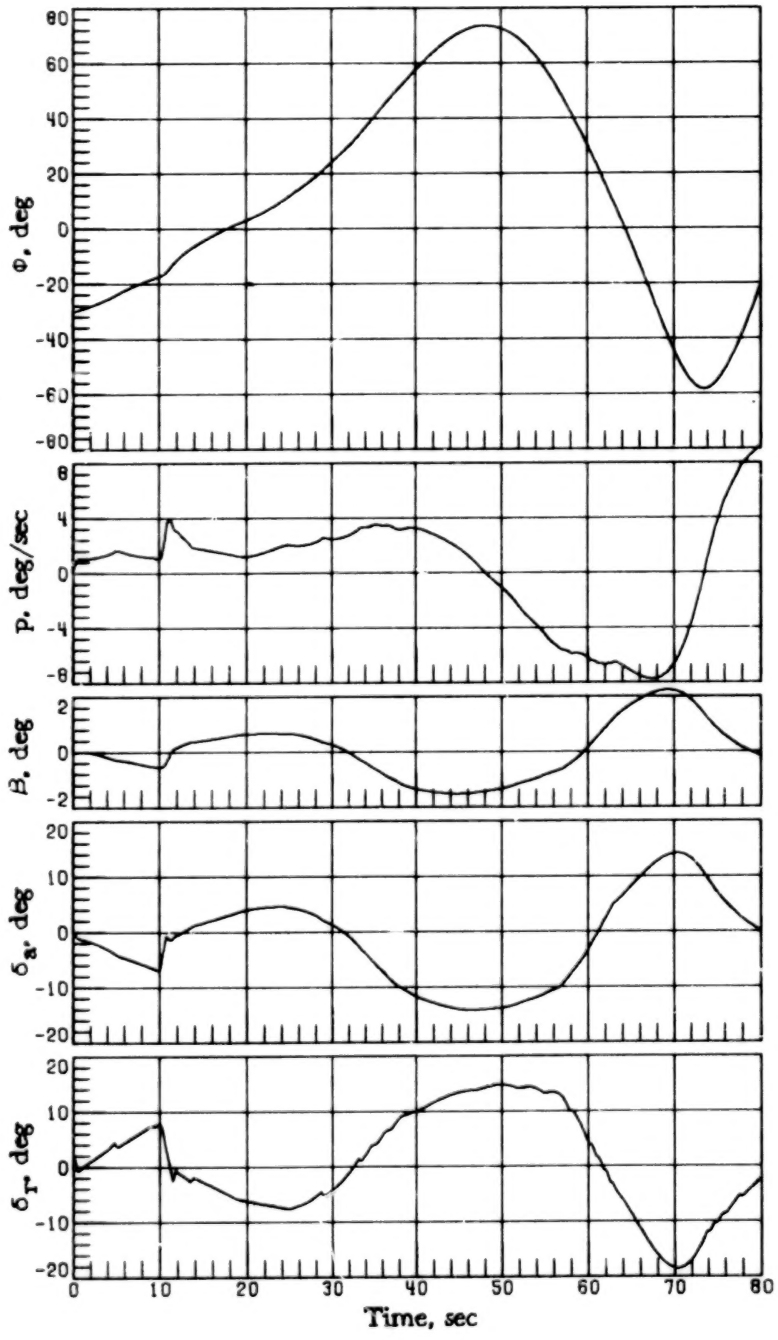

(a) $GC_{l_\beta} = 1.3$; $\Delta C_{Y_{\delta a}} = 0.0001$.

Figure 30.- Vehicle-response simulations at $M_i = 4$ with varying effective dihedral GC_{l_β} and $\Delta C_{Y_{\delta a}}$ with $\Delta C_{n_\beta} = -0.0006$, $GC_{Y_\beta} = 0.7$, $GC_{l_{\delta a}} = 0.7$, $\Delta C_{n_{\delta a}} = -0.0002$, and $GC_{n_{\delta r}} = GC_{l_{\delta r}} = GC_{Y_{\delta r}} = 0.7$. $\alpha_c = 17.6^\circ$; $\phi_c = -30^\circ$ for time < 10 sec; $\phi_c = 30^\circ$ for time ≥ 10 sec.

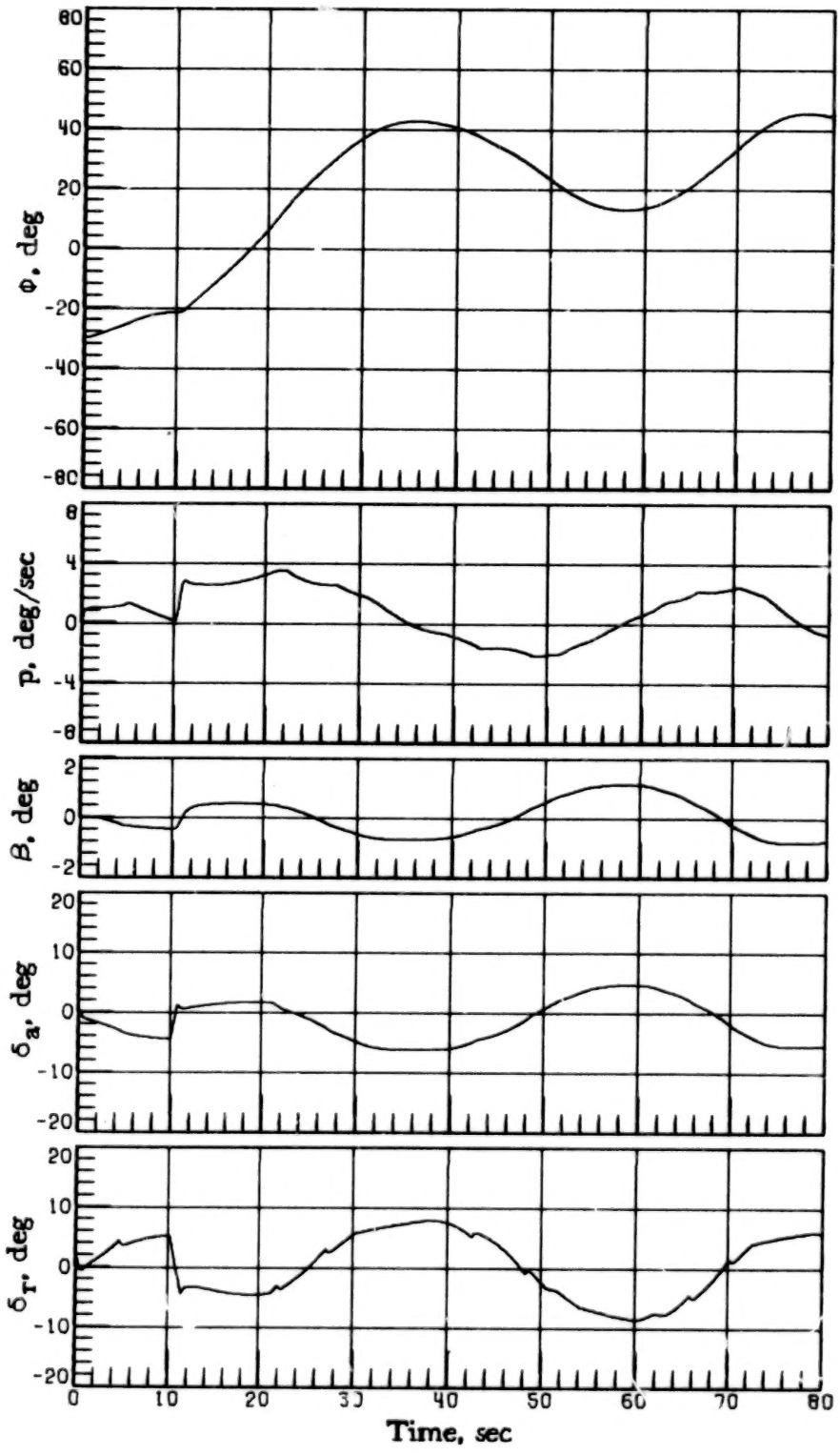

(b) $GC_{l_\beta} = 0.6$; $\Delta C_{Y_{\delta a}} = 0.0001$.

Figure 30.- Continued.

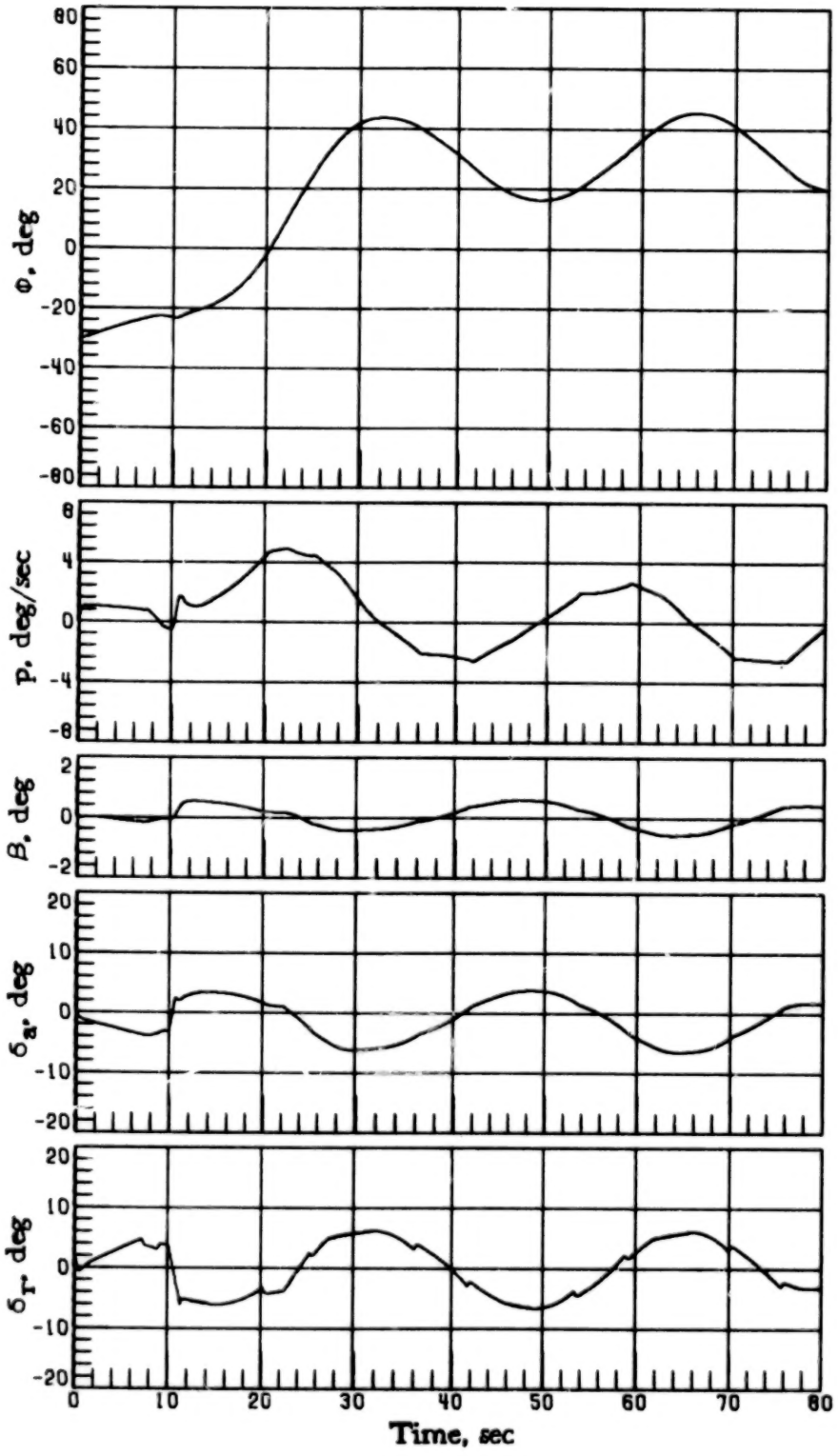

(c) $GC_{l_\beta} = 1.3$; $\Delta Cy_{\delta a} = -0.0004$.

Figure 30.- Continued.

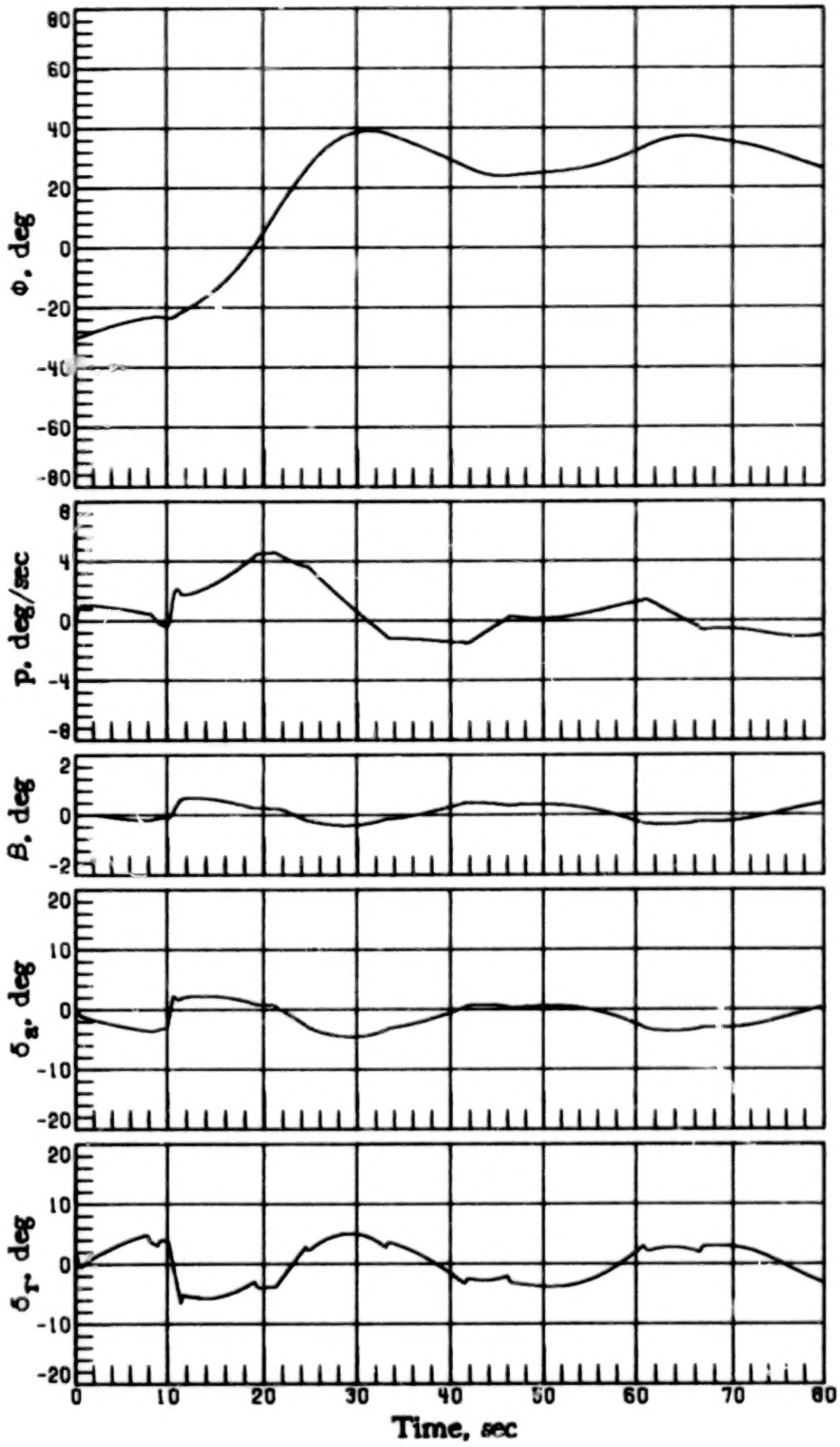

(d) $GC_{l_\beta} = 0.6$; $\Delta C_{Y_{\delta a}} = -0.0004$.

Figure 30.- Concluded.

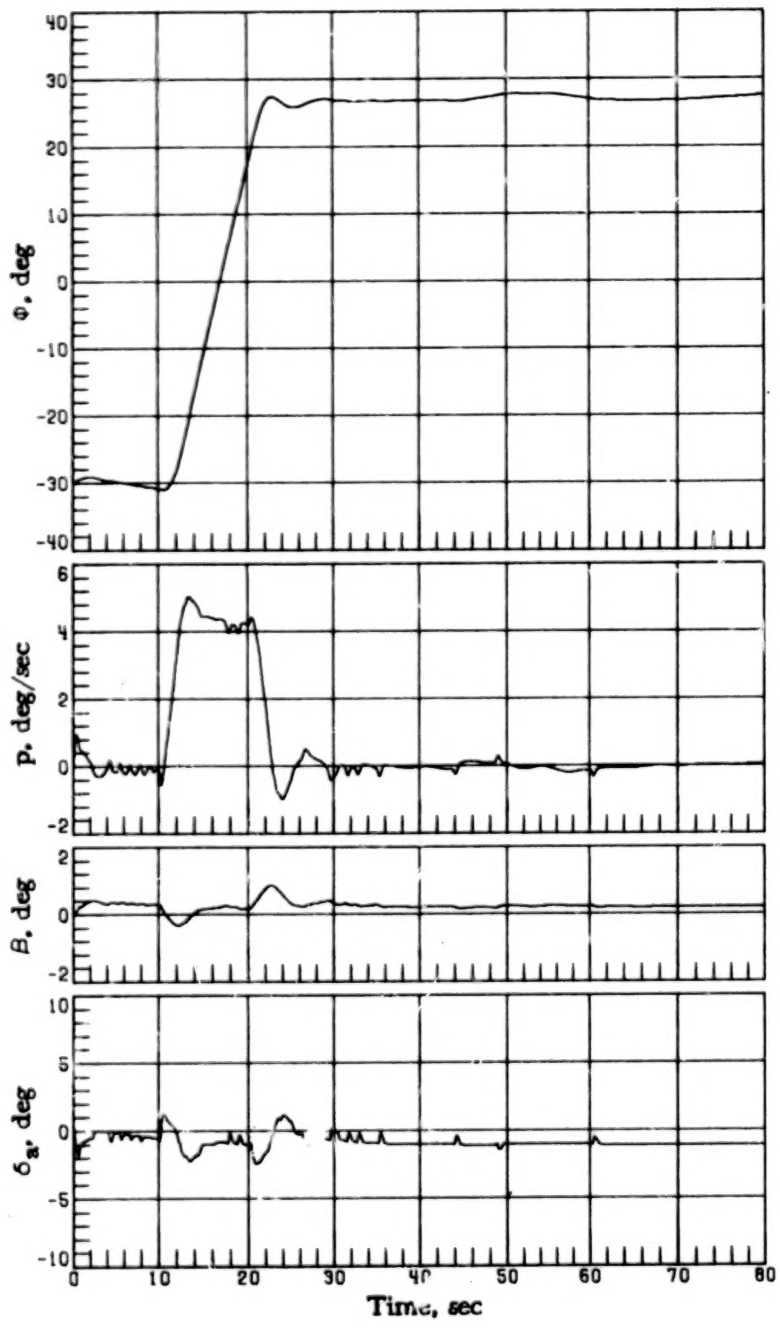

(a) $\Delta C_{Y_{\delta a}} = 0.0006$; $GC_{l_\beta} = 1.3$.

Figure 31.- Vehicle-response simulations with varying $\Delta C_{Y_{\delta a}}$ and effective dihedral GC_{l_β} at $M_i = 8$ with $\Delta C_{n_\beta} = -0.0006$, $GC_{Y_\beta} = 0.7$, $GC_{l_{\delta a}} = 0.7$, and $\Delta C_{n_{\delta a}} = -0.0002$. $\alpha_c = 30^o$; $\phi_c = -30^o$ for time < 10 sec; $\phi_c = 30^o$ for time ≥ 10 sec.

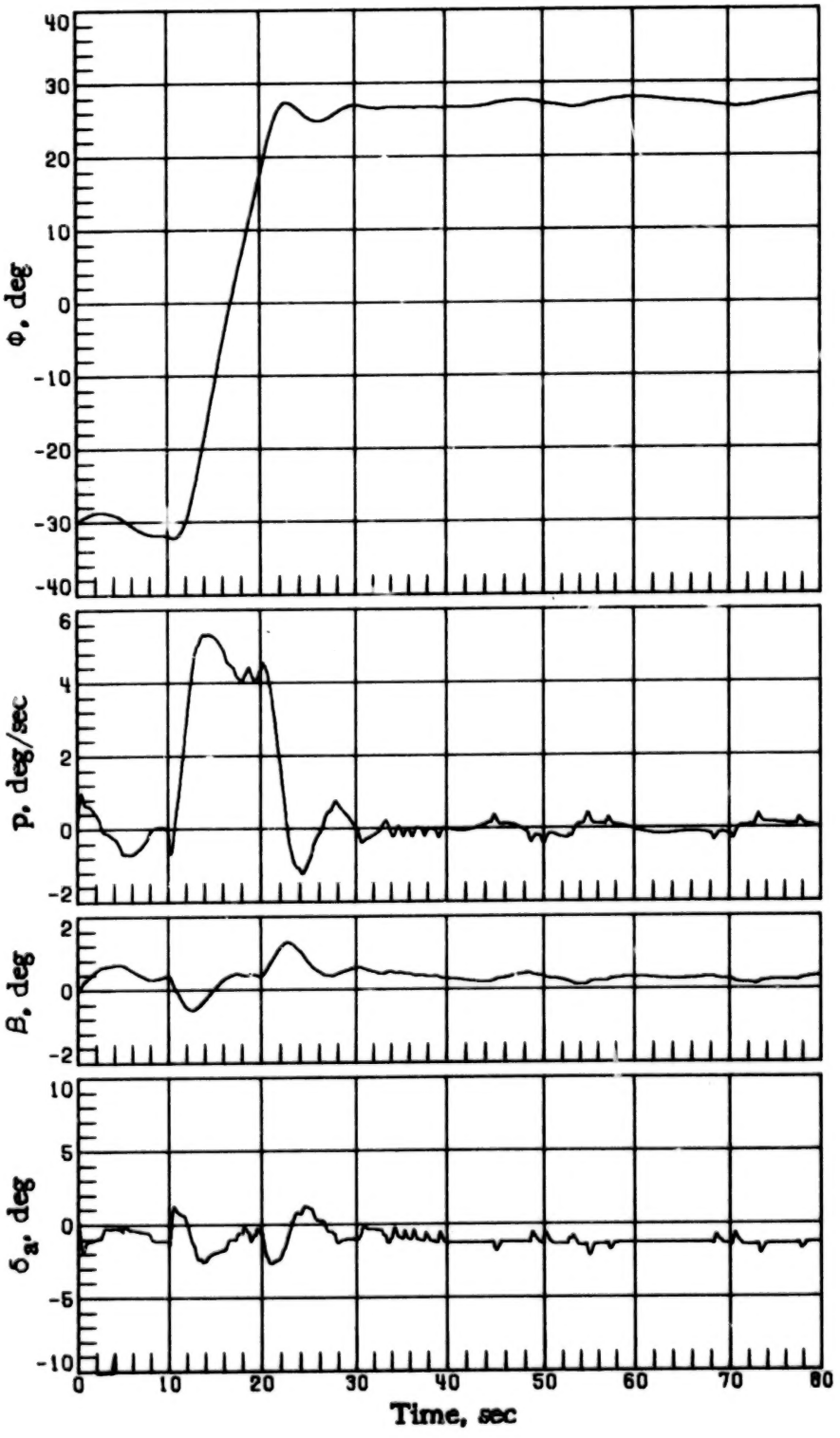

(b) $\Delta C_{Y_{\delta a}} = 0.0006$; $GC_{l_\beta} = 0.6$.

Figure 31.- Continued.

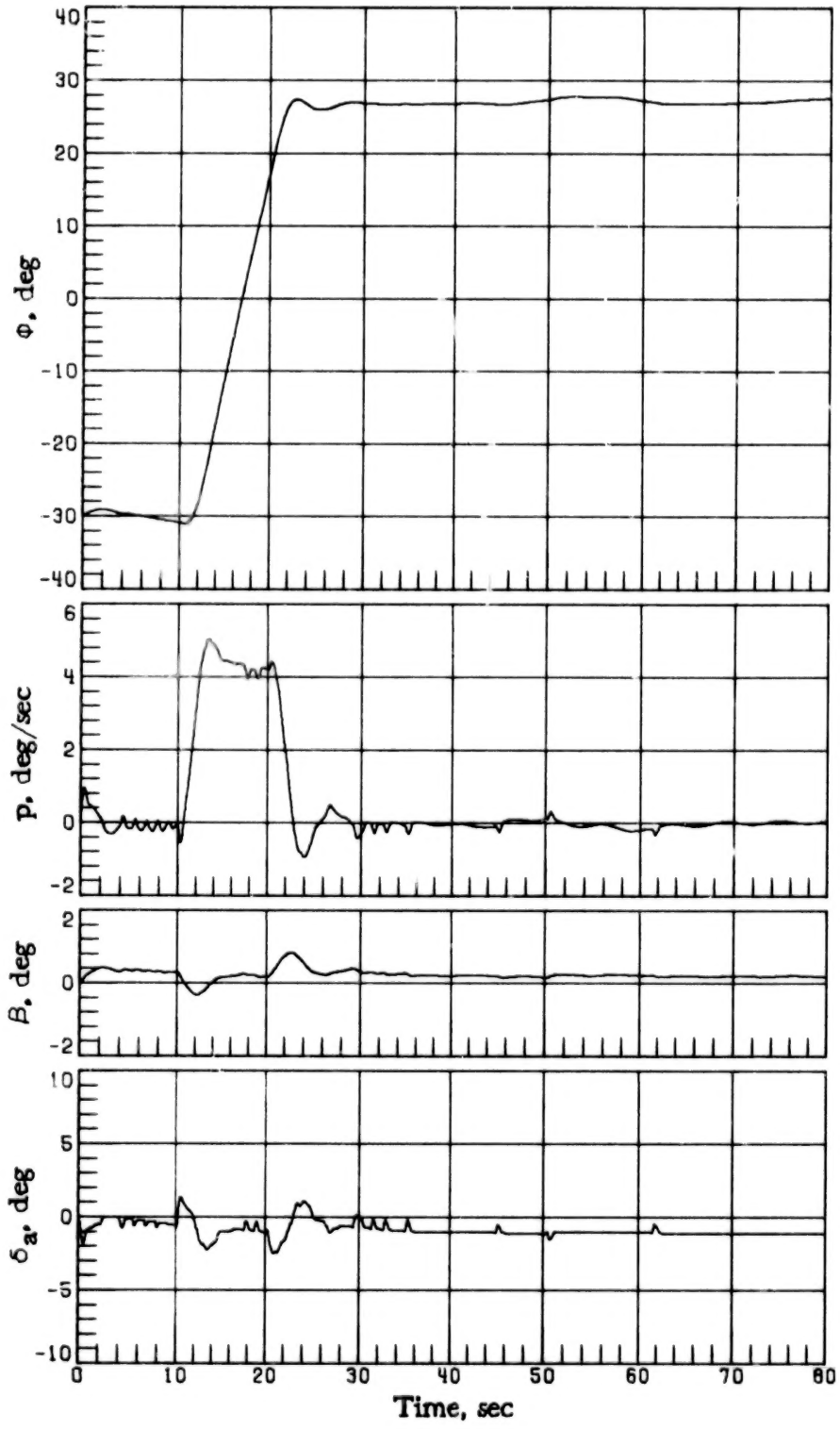

(c) $\Delta C_{Y_{\delta a}} = -0.0004$; $GC_{l_\beta} = 1.3$.

Figure 31.- Continued.

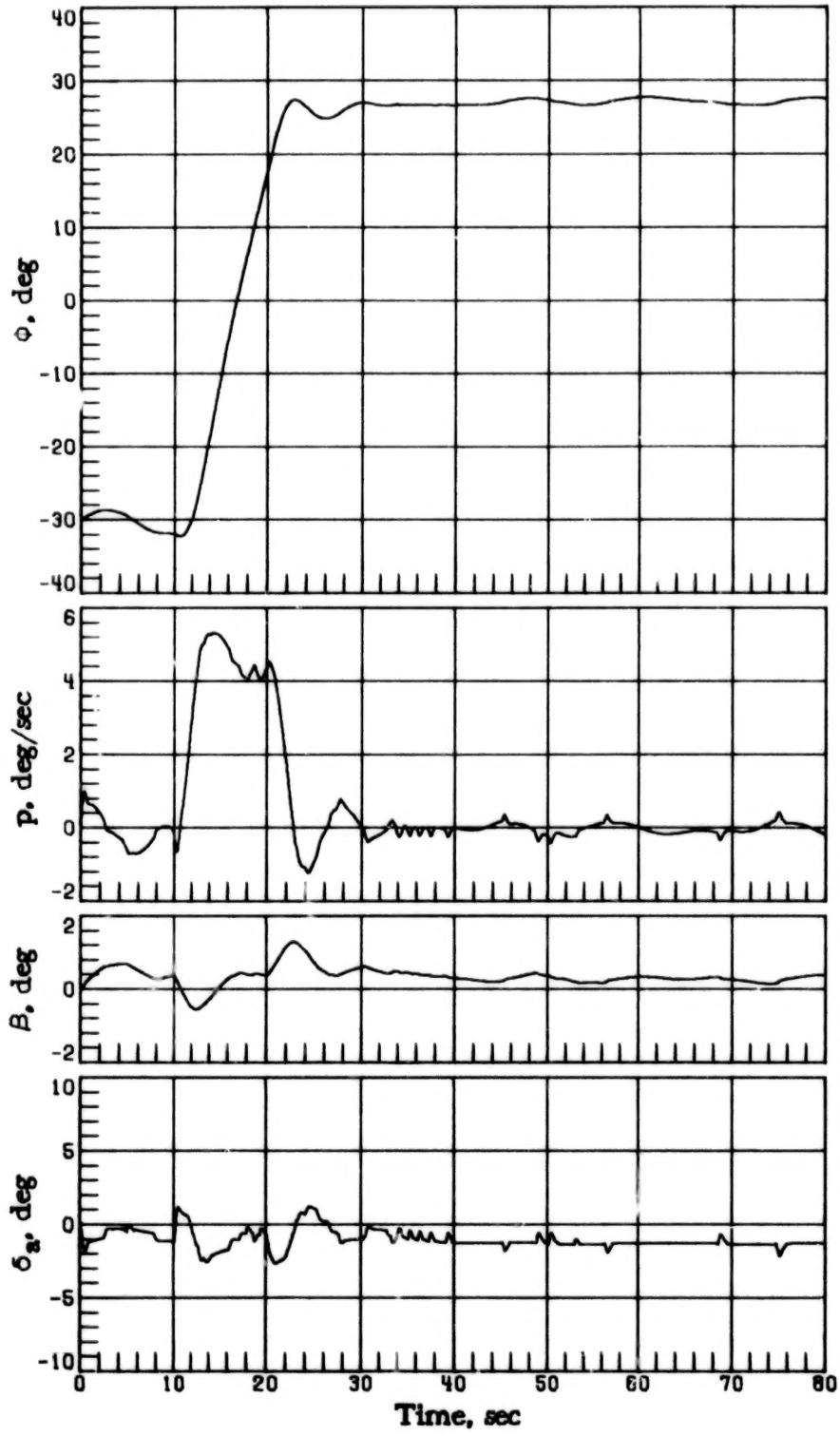

(d) $\Delta C_{Y_{\delta a}} = -0.0004$; $GC_{l_\beta} = 0.6$.

Figure 31.- Concluded.

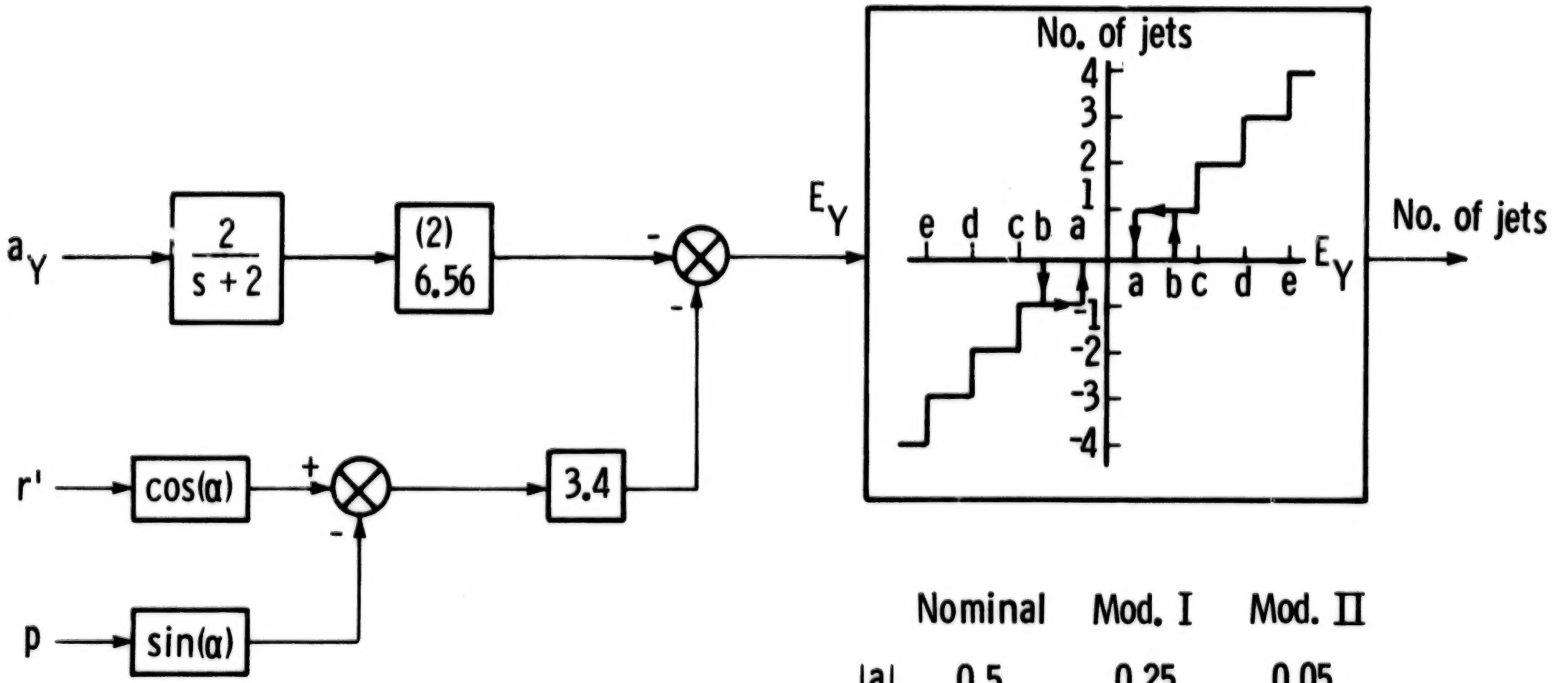

	Nominal	Mod. I	Mod. II
|a|	0.5	0.25	0.05
|b|	1.0	.5	.2
|c|	1.5	1.0	.5
|d|	2.0	1.5	1.0
|e|	2.5	2.0	1.5

Figure 32.- Yaw RCS block diagram for augmenting the rudder.

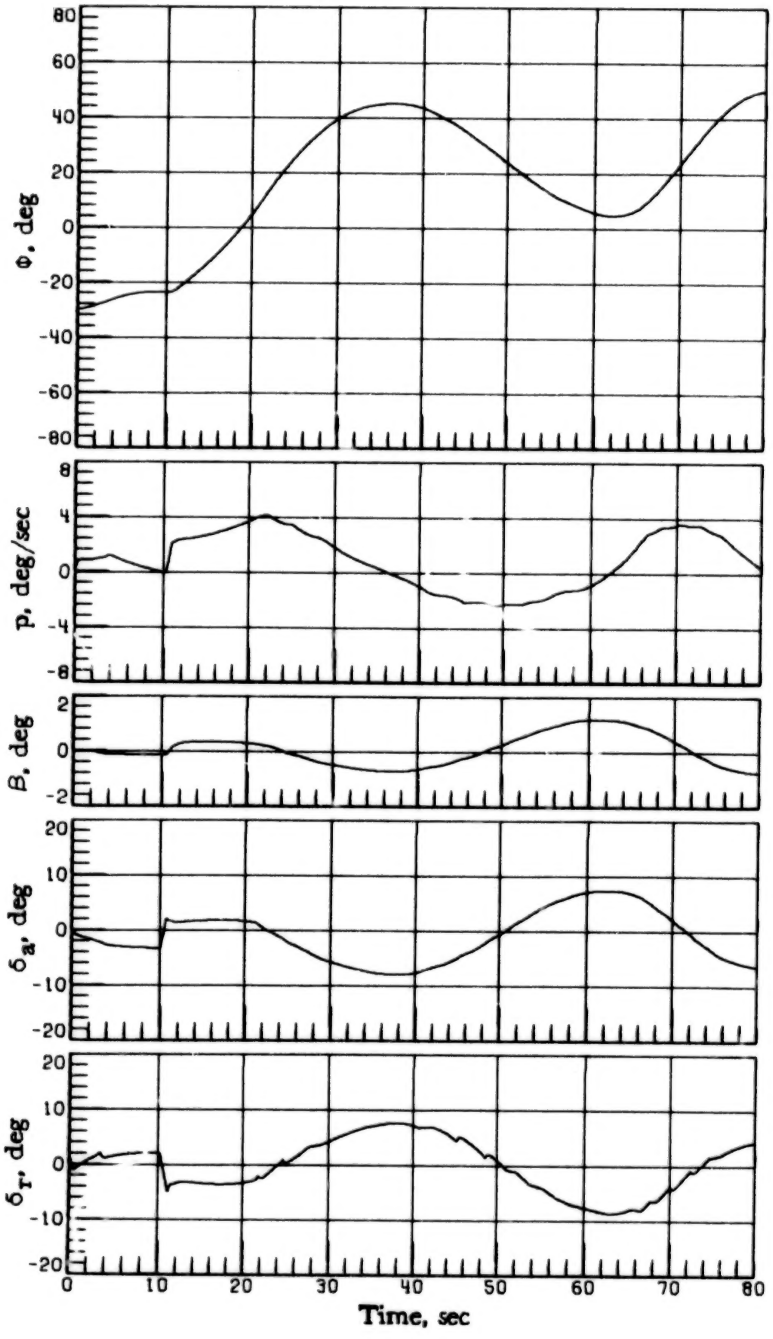

(a) Modification I.

Figure 33.- Vehicle-response simulations at $M_i = 4$ with increased yaw-jet augmentation for $GC_{l_\beta} = 1.3$, $\Delta C_{n_\beta} = -0.0006$, $GC_{Y_\beta} = 0.7$, $GC_{l_{\delta a}} = 0.7$, $\Delta C_{n_{\delta a}} = -0.0002$, $\Delta C_{Y_{\delta a}} = 0.0001$, and $GC_{n_{\delta r}} = GC_{l_{\delta r}} = GC_{Y_{\delta r}} = 0.7$. $\alpha_c = 17.6^o$, $\phi_c = -30^o$ for time < 10 sec; $\phi_c = 30^o$ for time ≥ 10 sec.

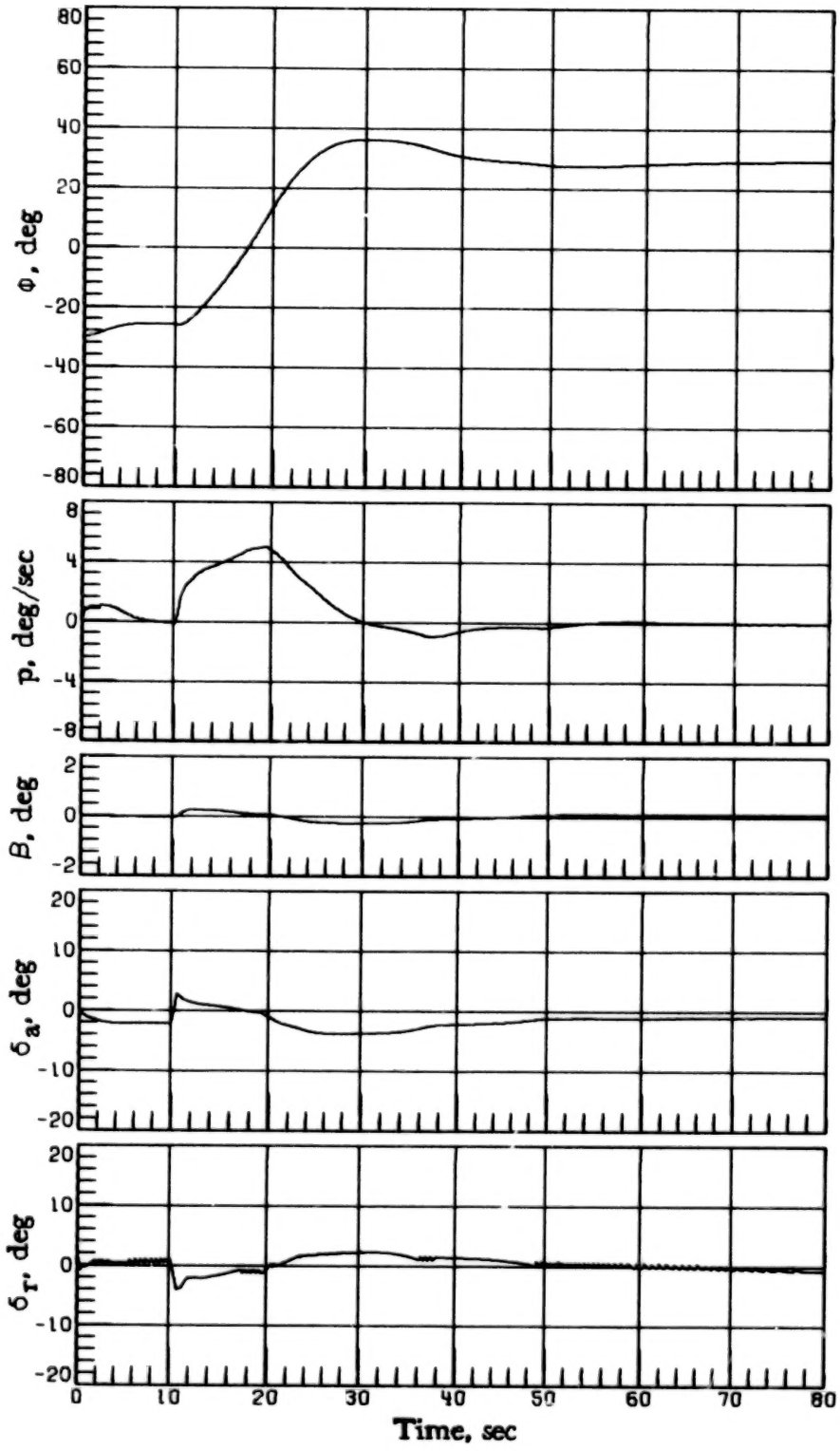

(b) Modification II.

Figure 33.- Concluded.

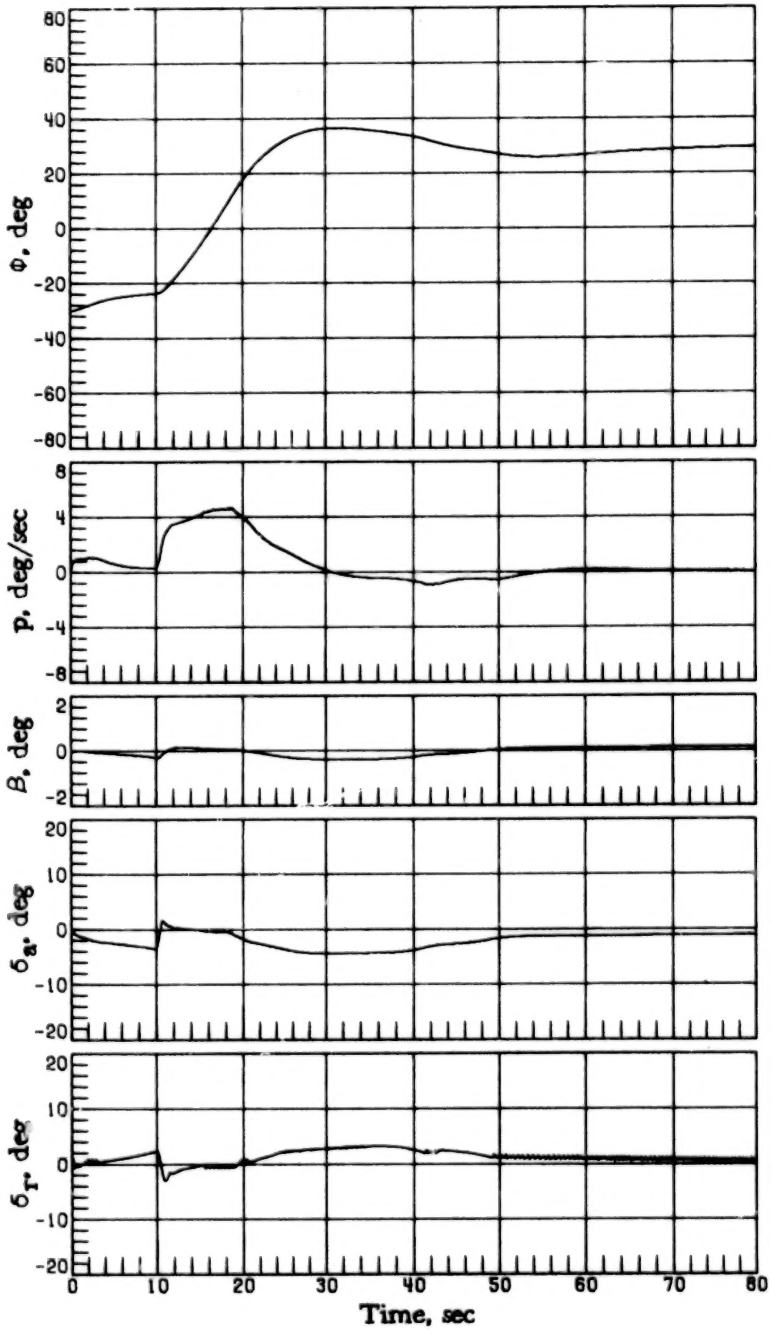

Figure 34.- Vehicle-response simulation results with modification II at $M_i = 4$ with $GC_{l_\beta} = 1.3$, $\Delta C_{n_\beta} = -0.0006$, $GC_{Y_\beta} = 0.7$, $GC_{l_{\delta a}} = 0.7$, $\Delta C_{n_{\delta a}} = -0.0002$, $\Delta C_{Y_{\delta a}} = 0.0003$, and $GC_{n_{\delta r}} = GC_{l_{\delta r}} = GC_{Y_{\delta r}} = 0.7$. $\alpha_c = 17.6^\circ$; $\phi_c = -30^\circ$ for time < 10 sec; $\phi_c = 30^\circ$ for time ≥ 10 sec.

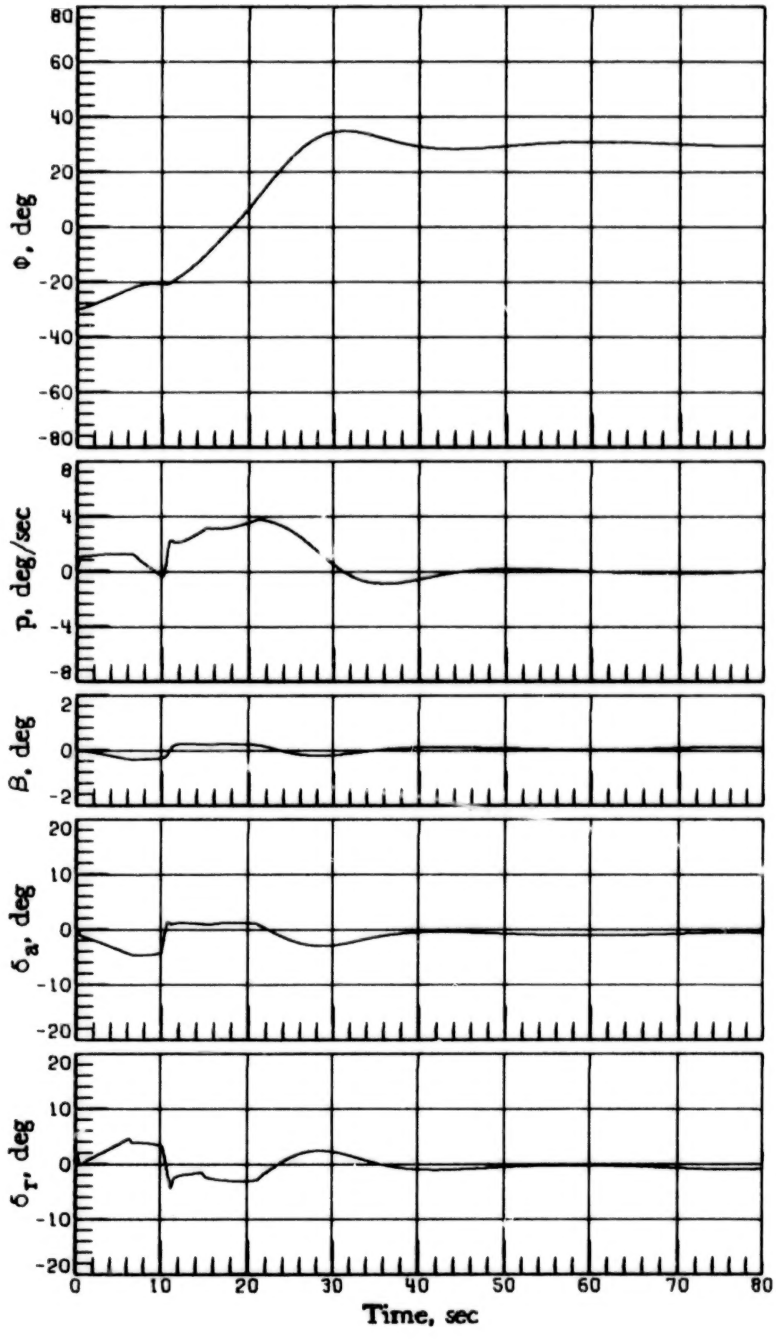

(a) $\Delta C_{Y_{\delta a}} = 0.0001$.

Figure 35.- Vehicle-response simulation results at $M_i = 3.1$ with varying $\Delta C_{n_{\delta a}}$ for $GC_{l_\beta} = 1.3$, $\Delta C_{n_\beta} = -0.0006$, $GC_{Y_\beta} = 0.7$, $GC_{l_{\delta a}} = 0.7$, $\Delta C_{n_{\delta a}} = -0.0002$, and $GC_{n_{\delta r}} = GC_{l_{\delta r}} = GC_{Y_{\delta r}} = 0.7$. $\alpha_c = 17.6^\circ$; $\phi_c = -30^\circ$ for time < 10 sec; $\phi_c = 30^\circ$ for time ≥ 10 sec.

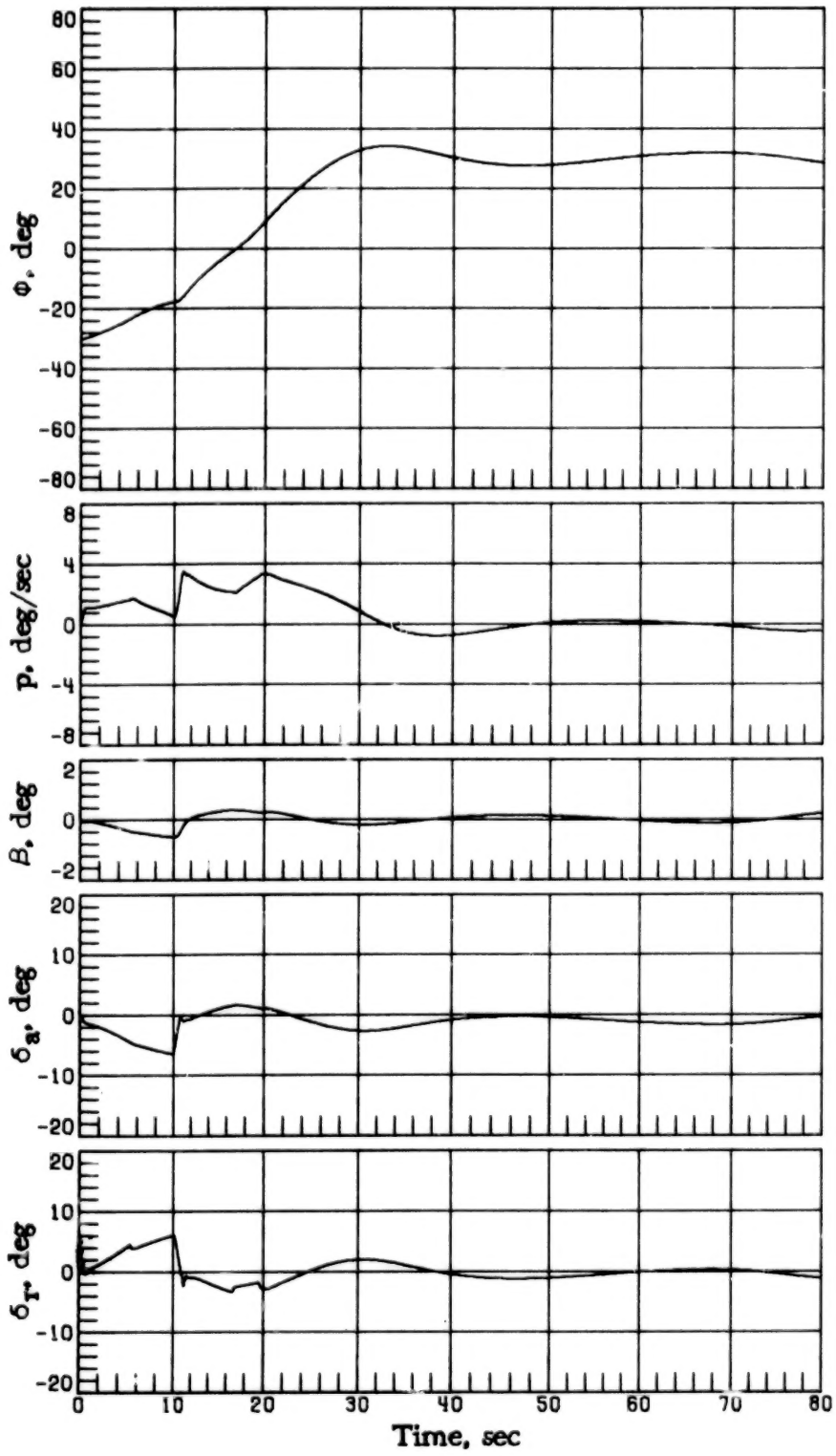

(b) $\Delta C_{Y_{\delta a}} = 0.0003$.

Figure 35.- Concluded.

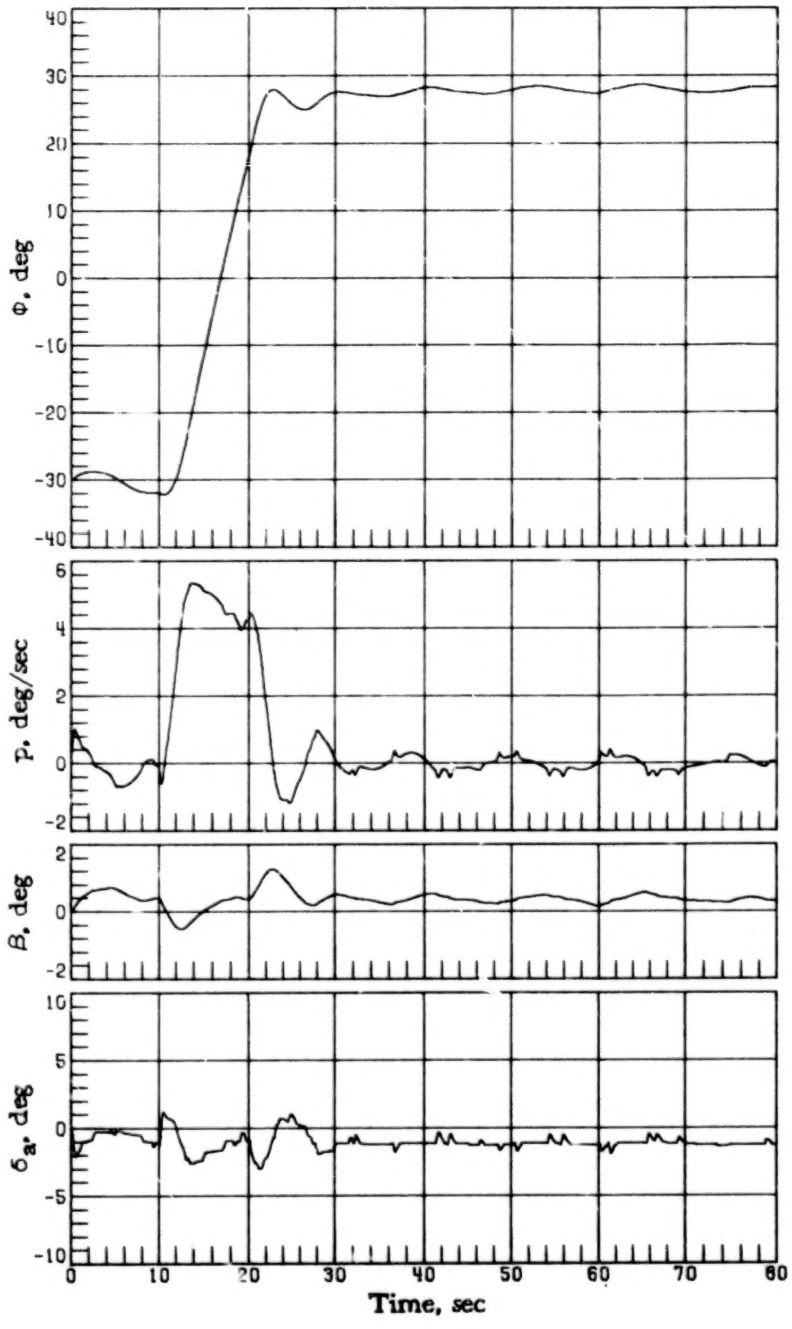

Figure 36.- Vehicle-response simulation results at $M_i = 8$ for $GC_{l_{\delta a}} = 0.7$, $\Delta C_{n_{\delta a}} = -0.0004$, $\Delta C_{Y_{\delta a}} = 0.0006$, $GC_{l_\beta} = 0.6$, $\Delta C_{n_\beta} = -0.0006$, and $GC_{Y_\beta} = 0.7$. $\alpha_c = 30°$; $\phi_c = -30°$ for time < 10 sec; $\phi_c = 30°$ for time ≥ 10 sec.

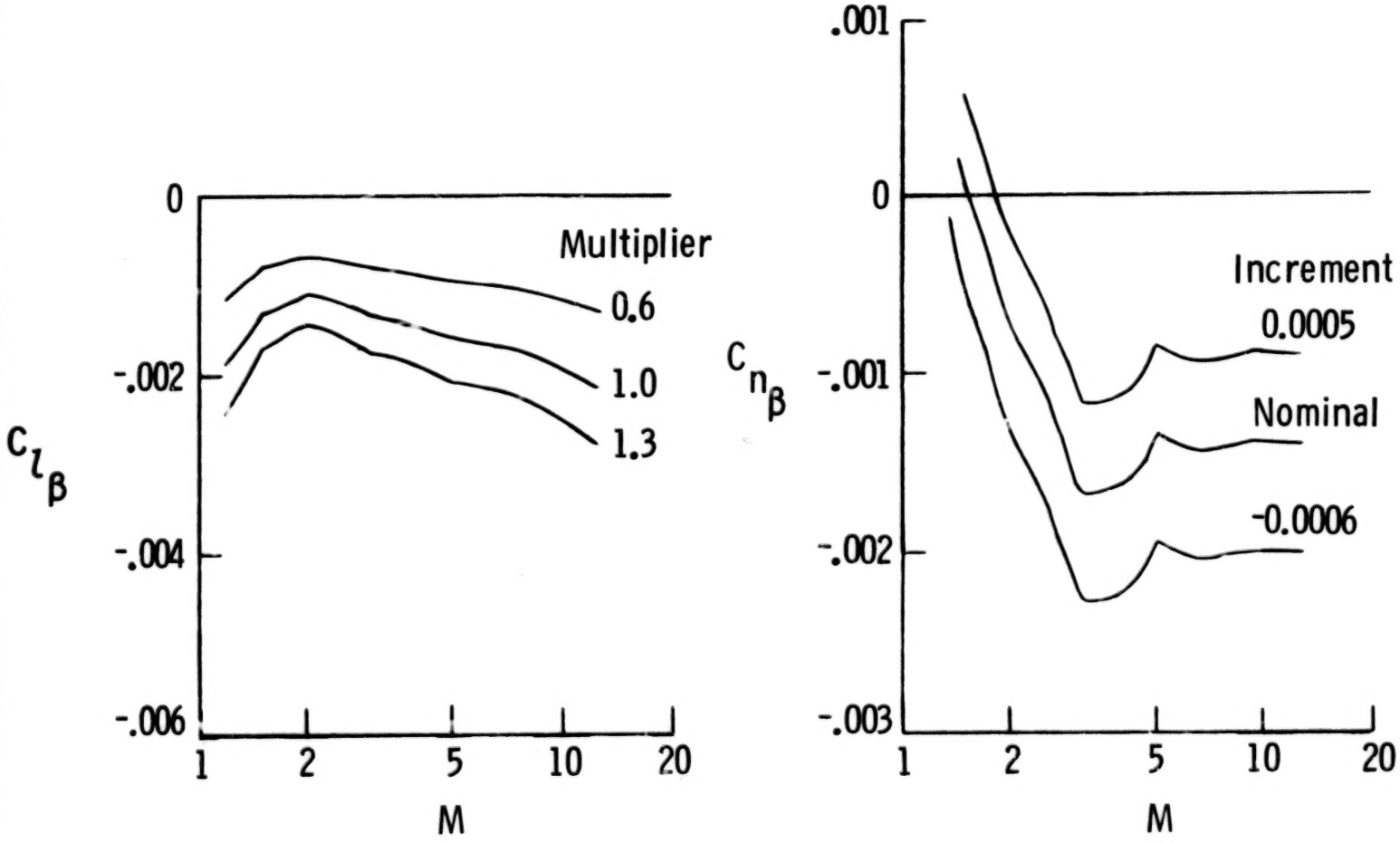

Figure 37.- Lateral-directional stability boundaries.

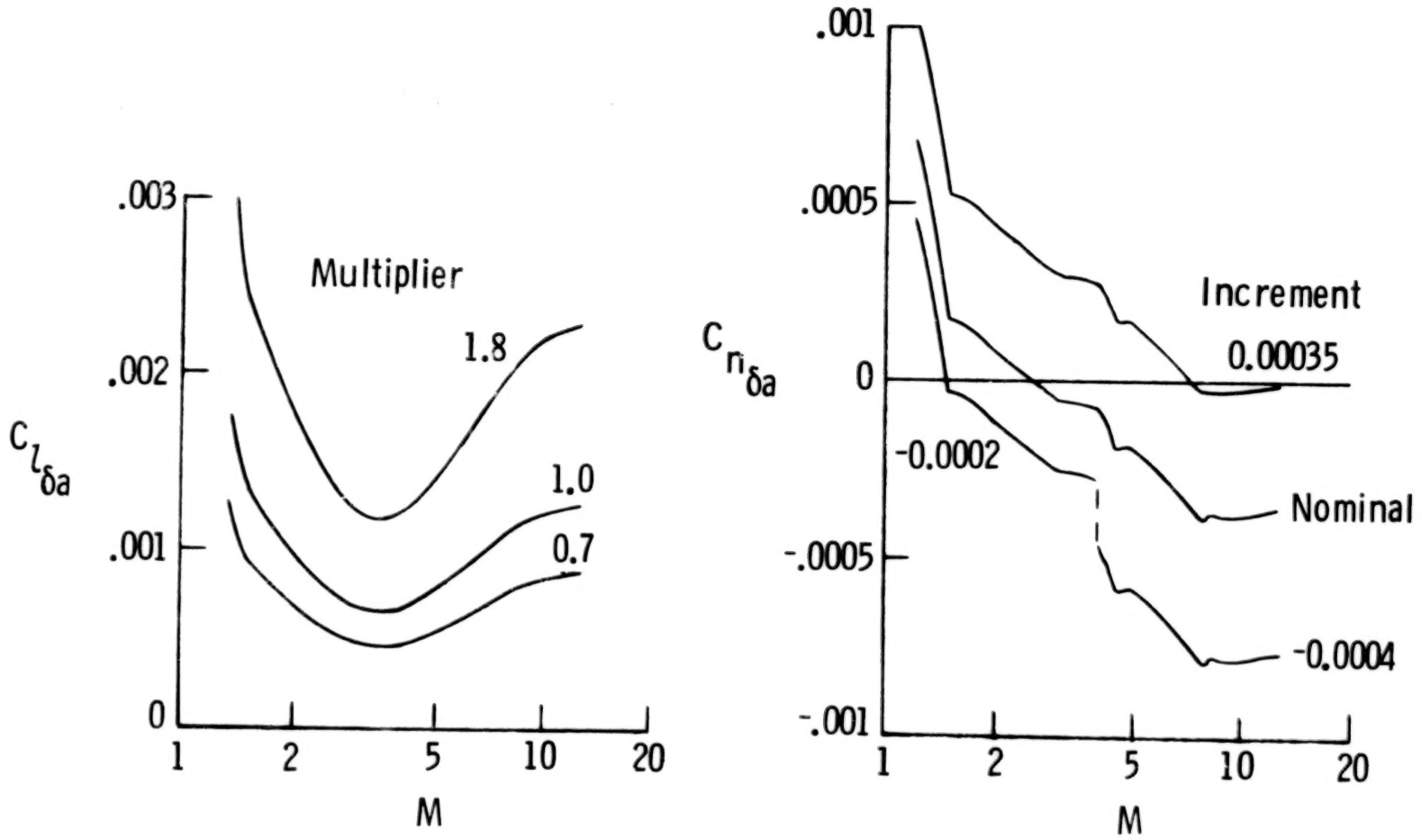

Figure 38.- Aileron-effectiveness boundaries.

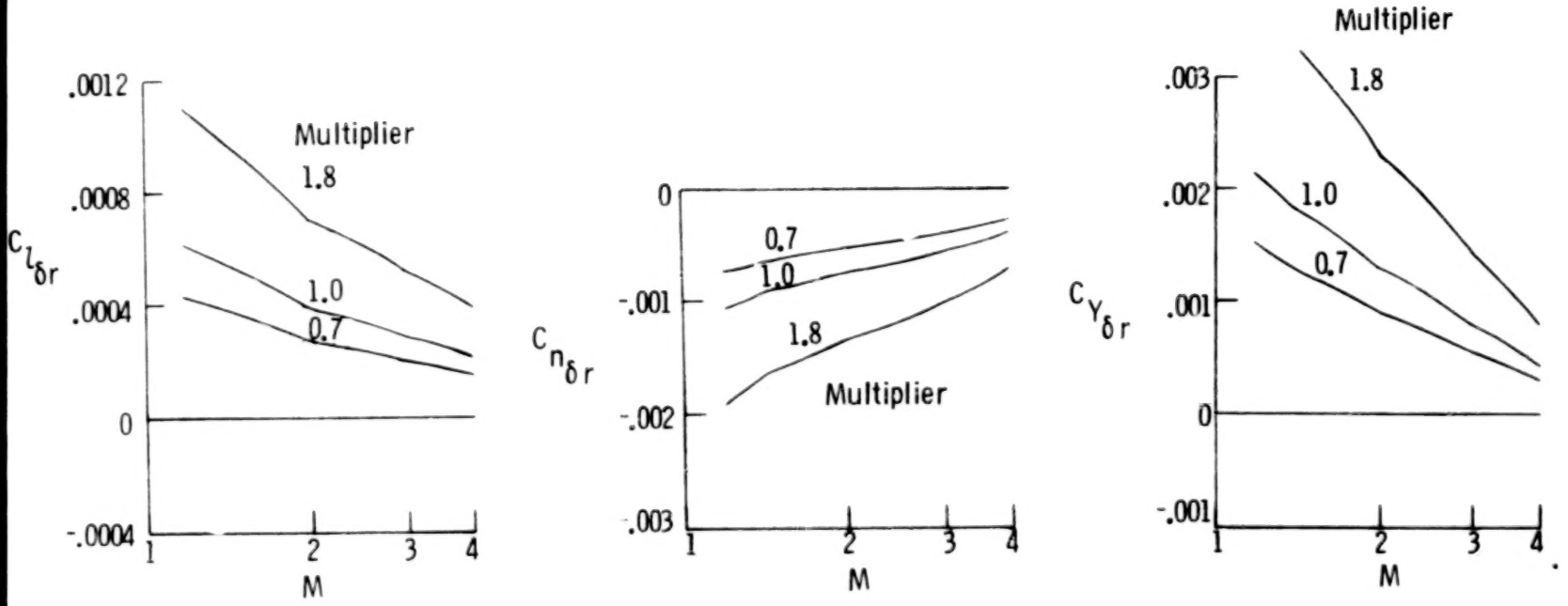

Figure 39.- Rudder-effectiveness boundaries.

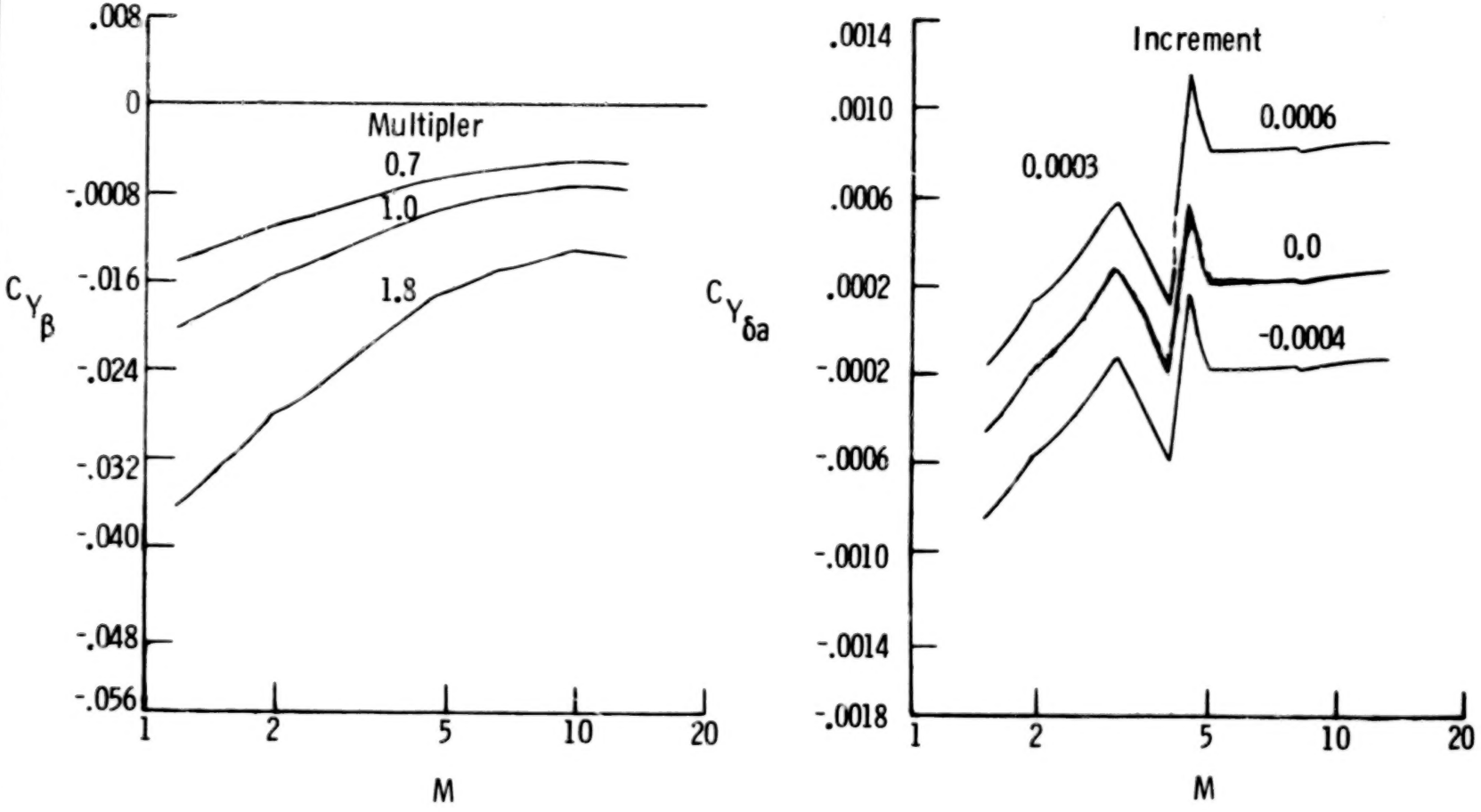

Figure 40.- Side-force derivative boundaries.

1. Report No.	2. Government Accession No.	3. Recipient's Catalog No.
NASA TP-1011		

4. Title and Subtitle	5. Report Date
ENTRY DYNAMICS OF SPACE SHUTTLE ORBITER WITH LATERAL-DIRECTIONAL STABILITY AND CONTROL UNCERTAINTIES AT SUPERSONIC AND HYPERSONIC SPEEDS	December 1977
	6. Performing Organization Code
7. Author(s)	8. Performing Organization Report No.
Howard W. Stone and Richard W. Powell	L-11112
	10. Work Unit No. 506-26-30-04
9. Performing Organization Name and Address NASA Langley Research Center Hampton, VA 23665	11. Contract or Grant No.
	13. Type of Report and Period Covered Technical Paper
12. Sponsoring Agency Name and Address National Aeronautics and Space Administration Washington, DC 20546	14. Sponsoring Agency Code

15. Supplementary Notes

16. Abstract

A six-degree-of-freedom simulation analysis was conducted to examine the effects of the lateral-directional static aerodynamic stability and control uncertainties on the performance of the automatic (no manual inputs) entry-guidance and control systems of the space shuttle orbiter. To establish the acceptable boundaries of the uncertainties, the static aerodynamic characteristics were varied either by applying a multiplier to the aerodynamic parameter or by adding an increment. Two control-system modifications were identified that decrease the sensitivity to off-nominal aerodynamics. With these modifications, the acceptable aerodynamic boundaries were determined.

17. Key Words (Suggested by Author(s))	18. Distribution Statement
Space shuttle orbiter Entry-control system Aerodynamic uncertainties	Unclassified - Unlimited Subject Category 18

19. Security Classif. (of this report)	20. Security Classif. (of this page)	21. No. of Pages	22. Price*
Unclassified	Unclassified	101	$5.50

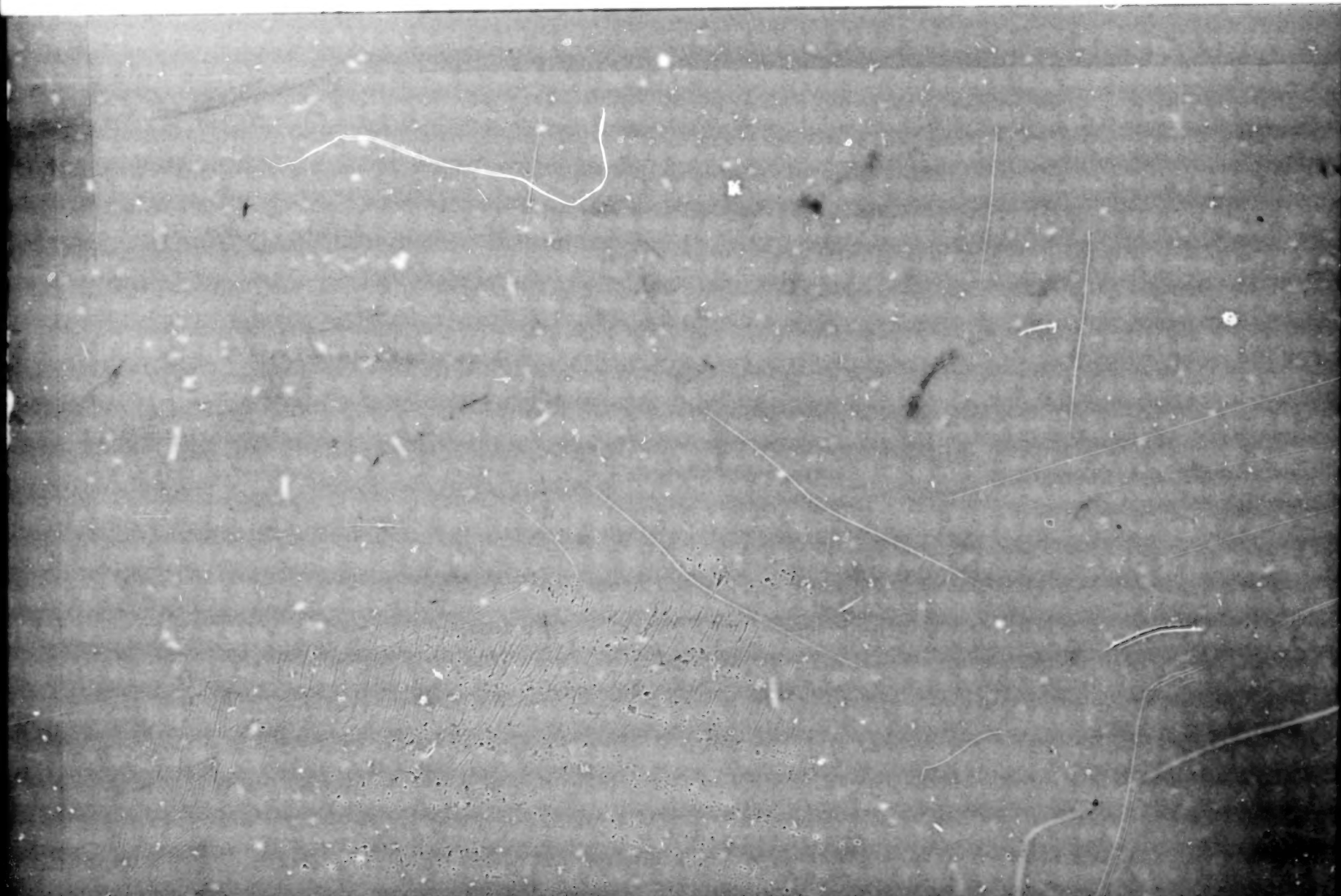

END

4.18.78